Master's thesis

NTNU
Norwegian University of Science and Technology
Faculty of Information Technology and Electrical Engineering
Department of Energy and Process Engineering

Vegard Skinnes

Validation of dynamic models of the thermal systems of swimming pools

Master's thesis in Energy and Environmental Engineering
Supervisor: Laurent Georges
June 2020

NTNU
Norwegian University of Science and Technology

Vegard Skinnes

Validation of dynamic models of the thermal systems of swimming pools

Master's thesis in Energy and Environmental Engineering
Supervisor: Laurent Georges
June 2020

Norwegian University of Science and Technology
Faculty of Information Technology and Electrical Engineering
Department of Energy and Process Engineering

NTNU
Norwegian University of
Science and Technology

Preface

This master thesis represents the final work of my master's degree at the Norwegian University of Science and Technology (NTNU). The work is carried out at the department of Energy and Process Engineering, constituting 30 ECTS credits.

The master period has been a special and memorable time in many terms. The work on the thesis has been challenging, but also very educational. Much of the knowledge and experience I have gained will be useful to carry with me in life. The lockdown of society due to the COVID 19 virus in March made the last months here at NTNU very different from what I had imagined, but fortunately the work on the thesis has not been affected to any great extent.

There are several people worth thanking for helpful contributions to the work. First, I would like to thank my supervisor Laurent Georges and co-supervisor Ole Smedegård for valuable inputs on the work. Special thanks to you Ole for all the guidance throughout the semester, and the commitment you have shown in the discussions with me. I would also like to thank Linda Stæhli and the management at Dalgård School and Resource Center for free access to the swimming pool and its technical rooms, in addition to Thomas Hjertenes and Hallvard Haukenes at Menerga for useful information on the air handling unit.

Abstract

Swimming pools are complex buildings that place high demands on both building bodies and technical systems. A well-functioning air handling unit with optimum control of temperature and humidity control is very important to create a good indoor climate and to avoid moisture damage in the building structure. Energy consumption is very high compared to other building categories, as large volumes of air and water are to be heated to comfortable temperatures. In addition, the process of dehumidifying the indoor air is a very energy-intensive process that requires large volumes of air. This requires good solutions to make a swimming pool system as energy efficient as possible. In this master thesis, a model has been developed of the swimming pool at Dalgård School and Resource Center, where the aim has been to validate the model with regard to evaporation rates and the thermal energy needs for various posts in the facility. The model is further used to investigate possible measures of improvement, which may reduce the energy consumption of the swimming pool.

Dalgård swimming pool is an old facility from 1978, which went through a partial rehabilitation in 2014. The swimming pool is mostly used by the school's students, as well as some associations in the evening. Measurements were carried out between February 25 and March 11, where there was still activity in the pool before the facility was closed. Measurements of temperature and relative humidity have been carried out at several locations in the plant, and energy consumption is measured in the heating coil of the air handling unit and in the primary heat exchanger for the pool water. These measurements are further used in calculations of evaporation rates and energy consumption. The model of the swimming pool is developed in the simulation tool IDA ICE, based on the technical documentation of the ventilation unit and observations within the facility.

Compliant results were found between simulations in the model and calculations based on measurements for several posts. Simulated evaporation rate was found to be 8.5% higher than the calculated and the energy consumption for heating of pool water was 10% higher than that measured. Regarding the heat transfer in the heating coil within the air handling unit, the simulations gave a 4.7% lower average power than the measurements showed.

Unfortunately, the integrated heat pump in the air handling unit was out of order during the measurement period. Therefore, simulations were conducted both with and without heat pump, to see what effect this had on the energy performance of the facility. For the analyzed measurement period, the energy consumption for heating of air and water was reduced by 50.6 and 30.4% respectively. A one-year simulation showed that the heat pump could reduce the total energy consumption of the swimming pool facility by 26%.

Sammendrag

Svømmehaller er komplekse bygg som stiller høye krav til både bygningskropp og tekniske systemer. Et velfungerende ventilasjonsaggregat med optimal styring av temperatur- og fuktkontroll er svært viktig for å skape et godt inneklima og for å unngå fuktskader i bygningskonstruksjonen. Energibruken er svært høy sammenlignet med andre bygningskategorier, da store luftvolumer og vannmengder skal varmes opp til komfortable temperaturer. I tillegg er prosessen med avfukting av inneluften en svært energikrevende prosess som krever store luftmengder. Dette krever gode løsninger for å gjøre et svømmehallanlegg så energieffektivt som mulig. I denne masteroppgaven er det utviklet en modell av svømmehallen ved Dalgård skole og ressurssenter, hvor målet har vært å validere modellen med tanke på fordampning og det termiske energibehovet ved ulike poster i anlegget. Modellen er videre brukt til å se på hvilke løsninger som kan forbedres, for å redusere energibruken til svømmehallen.

Dalgård svømmehall er et gammelt anlegg fra 1978, som gikk gjennom en delvis rehabilitering i 2014. Svømmehallen blir stort sett brukt av skolens elever, samt noen foreninger på kveldstid. Målinger ble gjennomført i perioden 25. februar til 11. mars, hvor det fortsatt var aktivitet i bassenget før anlegget ble stengt. Målinger av temperatur og relativ luftighet er gjennomført på flere steder i anlegget, og effektforbruk er målt i varmebatteriet til ventilasjonsaggregatet og i primærvarmeveksleren til bassengvannet. Disse målingene er videre brukt i beregninger av fordampningsrate og energibruk. Modellen av svømmehallen er utviklet i simuleringsverktøyet IDA ICE, basert på den tekniske dokumentasjonen til ventilasjonsaggregatet og observasjoner i anlegget.

Resultatene viser et godt samsvar mellom simuleringer i modellen og beregninger gjort ut ifra målinger på flere punkter. Simulert fordampningsrate viste seg å være 8.5% høyere enn den som ble beregnet, og energibruken til oppvarming av bassengvann var 10% høyere enn det som ble målt. Når det gjelder varmeoverføringen i varmebatteriet i ventilasjonsaggregatet, ga simuleringene en 4.7% lavere gjennomsnittlig effekt enn det målingene viste.

Den integrerte varmepumpen i ventilasjonsaggregatet var dessverre ute av drift i perioden målingene ble gjennomført. Det ble derfor gjennomført simuleringer både med og uten varmepumpe, for å se på hvilken effekt dette hadde på energiytelsen til anlegget. For den analyserte måleperioden ble energibruken til oppvarming av luft og vann redusert med henholdsvis 50.6 og 30.4%. En årssimulering viste at varmepumpen kunne redusere det totale energiforbruket til svømmehallen med 26%.

Table of Contents

List of Figures

List of Tables

Abbreviations

AHU	Air handling unit
ASHRAE	American Society of Heating, Refrigerating and Air-Conditioning Engineers
BCVTB	Building Control Virtual Test Bed
BPS	Building Performance Simulation
CFC	Chlorofluorocarbon
GWP	Global warming potential
HCFC	Hydrochlorofluorocarbon
HFC	Hydrofluorocarbon
IDA ICE	IDA Indoor Climate and Energy
NTU	Number of transfer units
RH	Relative humidity [%]
SPH	Swimming pool hall
TEK	Norwegian building code (Byggteknisk forskrift)
TRNSYS	Transient Simulation Tool

Introduction

1.1 Background and motivation

Swimming pools are buildings with very high energy consumption compared to other building categories. Large amounts of energy are required for heating of pool water and air. In addition, the process of dehumidifying the air is very energy intensive and requires large airflows. In a Norwegian study from 2008 [1], the total energy consumption was found to be 300 kWh/m^2 for the investigated facilities. Other studies [2] have found even higher values, and statistics vary a lot. Through the Climate Change Act [3], the Norwegian Government aims for a 40% reduction of greenhouse gas emissions by 2030 compared to the reference year 1990, and a 80-95% reduction by 2050. To achieve these targets, all sectors of the society must contribute, also the building sector. A deeper understanding of feasible energy saving measures is therefore essential.

Despite the intensive energy use, swimming pools are not categorized as an own building type in the building code (TEK) [4] and the most crucial aspects of the energy performance are neglected. The extent of energy efficient solutions for this building category is therefore strongly dependent on high ambitions among the building managers. A detailed dynamic model of these facilities will enable an understanding of which parameters are crucial for the best possible energy performance. With such a model, one can initiate an optimization process in terms of energy, contributing to the achievement of the climate goals set in the Paris Agreement.

Building performance simulation (BPS) is an important tool in the design phase of most building projects and should be especially important for complex buildings like swimming facilities. However, due to lack of requirements in the building codes, the motivation has been small. In addition, the difficulty of modeling all the complex systems and components of the plant has reduced the willingness to utilize BPS. This master thesis aims at further validating detailed dynamic models for swimming pool facilities, using the BPS package IDA ICE.

1.2 Objectives

The present thesis is a continuation of the work carried out by Henrik Alvestad [5]. The purpose is to further analyze the thermal energy needs and characteristics at various posts in a swimming pool facility. A good understanding of these needs and characteristics is essential in order to improve the current buildings and their technical installations, as well as to improve their design procedure. Understanding of the energy needs is also a necessary background to start an optimization process for such buildings.

The main objective of the thesis is to validate a detailed dynamic model of a swimming pool facility, in this case the swimming pool at Dalgård in Trondheim. It should be developed in IDA ICE, a main building performance simulation (BPS) package, and contain the main thermal systems of the facility, including the air handling unit and pool water circuit. The objective is to determine how accurate the model can predict evaporation rates and heating needs and, therefore, how simulations can support the swimming pool design.

The following tasks are to be considered:

1. Literature review on thermal and physical characteristics of swimming pools, and previous dynamic models of such buildings.
2. Perform measurements relevant for a comparison with the IDA ICE model. This includes measurements within the swimming pool hall, air handling unit, and pool water circuit.
3. Comparison of simulations and measurements in terms of evaporation rates, thermal energy needs and ventilation losses.
4. State suggestions for improvements of the thermal systems within the swimming pool facility.

2 Theory and literature review

This chapter discovers the underlying theory on the building physics and energy performance of swimming pools. Different requirements, norms and recommendations are presented, and various issues are discussed. Finally, a review of the existing literature on thermal performance of swimming pools using detailed dynamic simulations is included.

2.1 Indoor climate and building physics

The indoor air of swimming pool facilities is characterized by a significantly higher temperature and humidity than other building categories. In addition, the water temperature should be high enough to ensure thermal comfort of the swimmers. Consequently, swimming pool facilities face many challenges regarding the building physics, energy performance and indoor environment. These challenges and other fundamental aspects of the swimming pools are discussed in the following sections.

2.1.1 Humid air

When describing the indoor climate in terms of humidity, the relative humidity, RH, is commonly used. It affects the thermal comfort, and is defined as the ratio of water vapor partial pressure (p_v) to saturation pressure (p_{sat}) at a given temperature (T). The RH is commonly given as a percentage, as expressed in equation 5.1.

$$\boldsymbol{\phi = \frac{p_v(T)}{p_{sat}(T)} \cdot 100\%} \tag{2.1}$$

At an RH of 100%, the air is saturated, and further humidification of the air will cause water droplets to condense. The saturation pressure can be found in different tables, but in this context the equation suggested by Buck [6] will be used (p_{sat} given in kPa, T in °C):

$$\boldsymbol{p_{sat}(T) = 0.61121e^{\left(18.678 - \frac{T}{234.5}\right)\left(\frac{T}{257.14+T}\right)}} \tag{2.2}$$

For the humid air inside a swimming pool facility, the properties are within the range where both the vapor and dry air component can be treated as ideal gas [7]. The partial pressures is therefore given by the mass (m), ideal gas constant ($R = 8314\,J/kmolK$), molar mass ($M = 28.97\frac{kg}{kmol}(dry\ air), M = 18.02\frac{kg}{kmol}(vapor)$), temperature ($T$) and volume ($V$) of the given component, as shown in equation 5.1.

$$p = \frac{mRT}{MV} \tag{2.3}$$

Equation 5.1 can be used to find the absolute humidity (x), which is another measure of the humid air. It is defined as the ratio of mass of vapor to mass of dry air, and by combining equation 2.1 and 5.1, and using the fact that $p_{tot} = p_a + p_v$, the relationship given in equation 5.1 can be found. The absolute humidity will be used to find the vapor content when estimating the evaporation rate from the swimming pool.

$$x = \frac{m_v}{m_a} = 0.622\left(\frac{p_v}{p_{tot} - p_v}\right) \qquad 2.4$$

A frequently used tool in humid air calculations is the Mollier chart shown in Figure 2-1. Similar to a psychrometric chart, it relates the temperature, humidity, and enthalpy of the moist air at a given total pressure. An important term in the humid air calculations of swimming pools is the dew point temperature of the ambient air. It is defined as the temperature at which the air must be cooled, under constant pressure, to achieve saturation[8]. For example, air at 31°C and 50% RH will have a dew point temperature of 19.4°C at a total air pressure of 1 atm. In the Mollier chart, the dew point temperature is found by following a vertical line from T = 31°C, ϕ = 50% until the saturation line (ϕ = 100%) is reached.

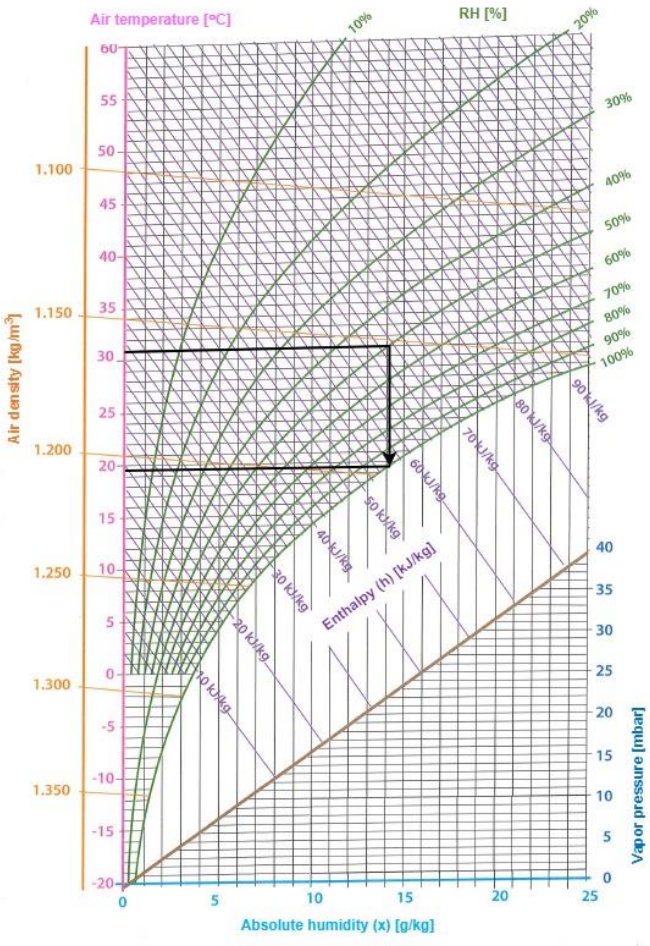

Figure 2-1: Mollier chart

2.1.2 Water treatment and air quality

Water treatment is an important part of the swimming pool operation, and consists of water exchange, disinfection, filtration, heating and pH control[9]. Today, chlorine is used as disinfectant in all Norwegian swimming facilities[10]. As a strong oxidizing agent, it both kill bacteria and destruct organic matter from the swimmers. In the chemical reactions between the chlorine and the organic matter, undesired by-products as chloramines and trihalomethanes are formed[11]. Trichloramine is toxic, causes irritated mucous membranes and respiratory tract, and is very volatile. This causes the compound to go into vapor form and is released into the air over the water. Nitter et al. [12] found that the compounds will accumulate in a lower layer above the water surface due to a higher density compared to the ambient air. This is just within the breathing zone of the swimmers, and frequent air exchange in combination with good hygiene is therefore necessary to achieve a satisfactory air quality for the swimmers.

The air quality is also affected by the RH of the ambient air. Arundel et al. [13] found that the optimum range for the relative humidity, in terms of human health, was 40-60%. While a low relative humidity creates favorable conditions for different types of viruses, the growth of bacteria, fungi and mold increases at higher relative humidity. Exposure to the presence of these substances over a longer period of time might result in respiratory issues. A low relative humidity will also affect the thermal comfort of the occupants. Due to higher evaporation rates from the surface of the skin at low RH's, the swimmers will feel a cooling sensation when they leave the pools. The recommendation given in the ASHRAE Handbook is 50-60% RH for all type of pools[9].

2.1.3 Building physics

With air temperatures around 30°C and RH of 50%, swimming pool facilities face great challenges with respect to the building physics. As illustrated in the Mollier chart in section 2.1.1, air with such properties has a high dew point temperature. If the air is cooled to a temperature lower than the dew point, it will be saturated, and condensation occurs. It is therefore important that the inner surfaces of the facility maintain a temperature higher than the dew point temperature of the air. In cold northern climates, this requires that the outer constructions have a high insulating quality (low U-value) and that thermal bridges are avoided. In 2006, ¾ of all the Norwegian swimming pool facilities were older than 25 years[14], which illustrates that condensation issues might be present in many facilities.

Condensation can also occur inside the constructions if the humid indoor air penetrates the walls. This happens if the vapor pressure inside the swimming pool hall is higher than in the adjoining rooms or outdoor, or if the indoor air pressure is higher than the outdoor air pressure. As the air moves through the construction layers it will be cooled, and

condensation might occur[8]. An excess vapor pressure is commonly observed inside the swimming pool hall due to evaporation from the water surface.

The pressure difference between indoor and outdoor air varies with the height due to buoyancy forces. If leakages are evenly distributed over the wall height, the neutral plane, where the indoor and outdoor pressure are equal, will be located halfway up the wall [8]. Away from the neutral plane, the pressure will increase towards the roof and decrease towards the floor, as indicated by equation 2.5. This effect is higher inside the swimming pool hall than outdoor due to a higher air temperature and density. The resulting pressure distribution across the wall is illustrated in Figure 2-2, where an overpressure is established beneath the ceiling and an under pressure at the floor.

$$\Delta p = \rho g \Delta h \qquad 2.5$$

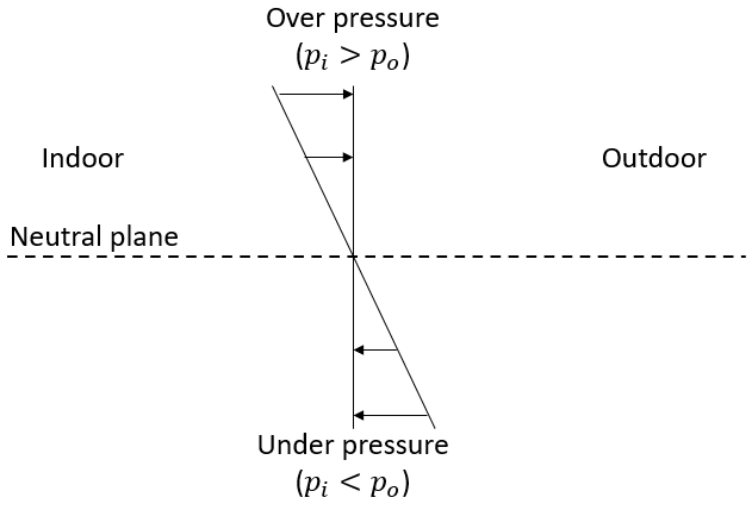

Figure 2-2: Pressure distribution over a wall with evenly distributed leakages

The characteristic pressure difference across the wall is commonly known as the *stack effect*, where outdoor air infiltrates the building envelope close to the floor and indoor air exfiltrates near the ceiling [8]. Swimming pools do typically have high ceilings, and the overpressure beneath the ceiling can be significant. The Norwegian Swimming Federation has established requirements for the least free ceiling height in swimming pools. Without any diving facility, it should be at least 5 meters for the 25 meter pool facilities and 7.5 meters for the 50 meter pool facilities[15]. Larger facilities and aquatic center houses attractions like slides and diving facilities which requires an even higher ceiling.

To eliminate or reduce the overpressure, it is common to use the ventilation system to establish an under pressure of 10-20 Pa [16]. Due to the stack effect, this under pressure has to be higher for facilities with a high ceiling to keep the under pressure over the entire wall. This might result in an unacceptable large under pressure at the floor. Doors could be hard to open, and emergency exits blocked. An overpressure close to the ceiling is

therefore in many cases unavoidable. To avoid vapor penetrating the construction and increase the risk for moisture damages a tight vapor barrier should always be installed.

2.1.4 Evaporation

A natatorium design guide from 2013[17] describes three different sources of moisture considered in swimming facilities: internal loads, occupants and outdoor air loads. Internal loads are evaporation from wet surfaces, which contributes to the greatest part of the moisture added to the ambient air of the swimming pool. The major part of the wet surface is the swimming pool surface, but phenomena like waves, sprays, wet deck, wet bodies, and water slides will increase the contact area between water and air. As a result, the total evaporation will increase.

In order to maintain an acceptable indoor air quality and avoid moisture problems on the building construction, the vaporized water should be removed from the ambient air of the swimming pool. A good estimation of the evaporation rates is thus important to size the HVAC system correctly. An undersized system not capable of keeping the humidity at an optimal level is unfortunate for the indoor environment and the life span of the building constructions, while an oversized system can lead to unnecessarily high energy costs [18].

Both natural convection and forced convection are driving mechanisms of the evaporation, where the former dominates for small air velocities above the water surface. As the air in a thin layer just above the water surface is saturated, it will have the same temperature as the water surface. Due to the fact that moist air has a lower density than dry air, the water vapor in this layer will start to rise. If the relative humidity inside the room is held constant, a lower air temperature results in a higher evaporation rate. This can be observed from the Mollier chart in Figure 2-1 and equation 2.6. The saturation pressure at room air dew point ($p_{sat,dp}$) decreases, resulting in an increased $(p_{sat,w} - p_{sat,dp})$ factor and therefore a higher $\dot{m}_{evap}$. The same is observed if the RH is decreased at a constant air temperature. As a measure against this evaporation issue, Byggforsk and ASHRAE recommends to keep the air temperature at 2 and 1-2°C above the water temperature, respectively[10][9].

Estimating evaporation from indoor water surfaces has a long history, and one of the most widespread correlations was formed by Carrier back in 1918 [19]. The correlation is shown in equation 2.6 and several of the correlations made in recent times are based on this equation. Equation 2.6 is an empirical correlation which is, according to Shah [20], based on experiments performed on an unoccupied pool where air was blown along the water surface. The equation says that the evaporation rate ($\dot{m}_{evap}$) in kg/s is a function of the pool surface area (A) in m^2, latent heat of vaporization (Y) in kJ/kg, saturation vapor pressure at surface water temperature ($p_{sat,w}$) in kPa, saturation pressure at the room air dew point ($p_{sat,dp}$) in kPa, and the air velocity (u) over the water surface in m/s.

$$\dot{m}_{evap} = \frac{A}{Y}(p_{sat,w} - p_{sat,dp})(0.089 + 0.0782u) \quad 2.6$$

According to ASHRAE [9], the Carrier correlation is valid for pools with normal activity levels, involving splashing and limited are of wetted deck. As of today, a modified version of equation 2.6 provided by ASHRAE [9] is among the most used. This correlation includes an activity factor (F_a) to alter the evaporation rate at different activity levels. The correlation is given in equation 5.1 and is valid for air velocities between 0.05 and 0.15 m/s and a latent heat of vaporization around 2400 kJ/kg.

$$\dot{m}_{evap} = 4 \cdot 10^{-5} A(p_{sat,w} - p_{sat,dp})F_a \quad 2.7$$

F_a depends on the activity level in the water and is a measure of the water agitation. Phenomena like waves, sprays, wet deck, and wet bodies should be implemented into this variable. For that reason, the number of bathing people is, in addition to their activity level, an important variable that should be considered when estimating the activity factor. The typical activity factor for an unoccupied pool is 0.5, while for public and school pools it is set to 1. An overview of typical activity factors for various types of pools, retrieved from the ASHRAE 2007 Handbook [9], are given in appendix B. Seen from equation 5.1, the evaporation rate is proportional to the activity factor, and it is therefore of great importance what value is chosen to insert into the equation. It does not exist any instrument that measure the activity factor, but it is totally based on observations of the activity in the swimming pool, which to a large extent is of subjective perception.

Many studies deal with the evaporation from indoor swimming pools, and the authors have come up with different correlations for both unoccupied and occupied pools. Most of these correlations are based on experimental data obtained within the respective study, and as the conditions in the different swimming pools or test objects vary, the correlations do the same. On the other hand, there are analytical formulas based entirely on theory of heat and mass transfer. The method suggested by Shah [20][21][22], given in Appendix A, is a combination of heat and mass transfer theory and empirical considerations. It is based on data collected from several external sources and takes both natural convection and forced convection into account. The latter might be significant when the air currents from the ventilation system is directed along the water surface.

Empirical correlations are based on measurements of the real evaporation rates. There are several methods to do this, where measurements of the condensate collected at the air handling unit dehumidifier and energy balance on the pool water are two common approaches. The latter was utilized by Smith *et al.* [23] to determine the evaporation rate from an indoor swimming pool. With this approach, it was found that the Carrier correlation (equation 2.6) corresponded well with measurements with a small number of people in the

pool. For an unoccupied pool, he found that the Carrier correlation overpredicted and suggested a multiplication factor of 0.74, while for fully occupied pools, a multiplication factor of 1.26 was suggested due to underprediction.

Both the condensate method and the energy balance method involve some simplifications in determining the evaporation rate. When measuring the condensate, it is not accounted for any infiltration or exfiltration of water vapor through the building construction. Instead it is assumed that all the condensate can be attributed to the evaporation from wet surfaces inside the swimming pool hall. The energy balance on the other hand does not include evaporation from wetted decks. Summing all the heat gains and losses of the pool water, the evaporation rate could be estimated by equation 2.8. Somewhat simplified the gains include the primary heat ($\dot{Q}_{heat}$), pump work ($\dot{Q}_{pump}$) and eventually solar gain ($\dot{Q}_{solar\ gain}$), while the losses include the water exchange in terms of makeup water ($\dot{Q}_{mw}$), heat losses in the pipes ($\dot{Q}_{pipe\ loss}$), as well as evaporative ($\dot{Q}_{evap}$), convective ($\dot{Q}_{conv}$) and radiative ($\dot{Q}_{rad}$) heat loss from the pool water surface.

$$\dot{m}_{evap} = \frac{\dot{Q}_{evap}}{Y} = \frac{\dot{Q}_{heat} + \dot{Q}_{pump} + \dot{Q}_{solar\ gain} - \dot{Q}_{mw} - \dot{Q}_{pipe\ loss} - \dot{Q}_{conv} - \dot{Q}_{rad}}{Y} \qquad 2.8$$

Another approach for estimating the evaporation rate is to apply a water vapor mass balance on the swimming pool hall. The water vapor entering the hall through evaporation ($\dot{m}_{evap}$), ventilation ($\dot{m}_{v,supply}$) and infiltration ($\dot{m}_{v,inf}$) should equal the amount leaving the hall through ventilation ($\dot{m}_{v,return}$) and the change in water vapor content in the hall air per time unit ($\frac{dm_{v,room}}{dt}$). Figure 2-3 illustrates the water vapor mass balance of the swimming pool hall, and the evaporation rate is given by equation 2.9.

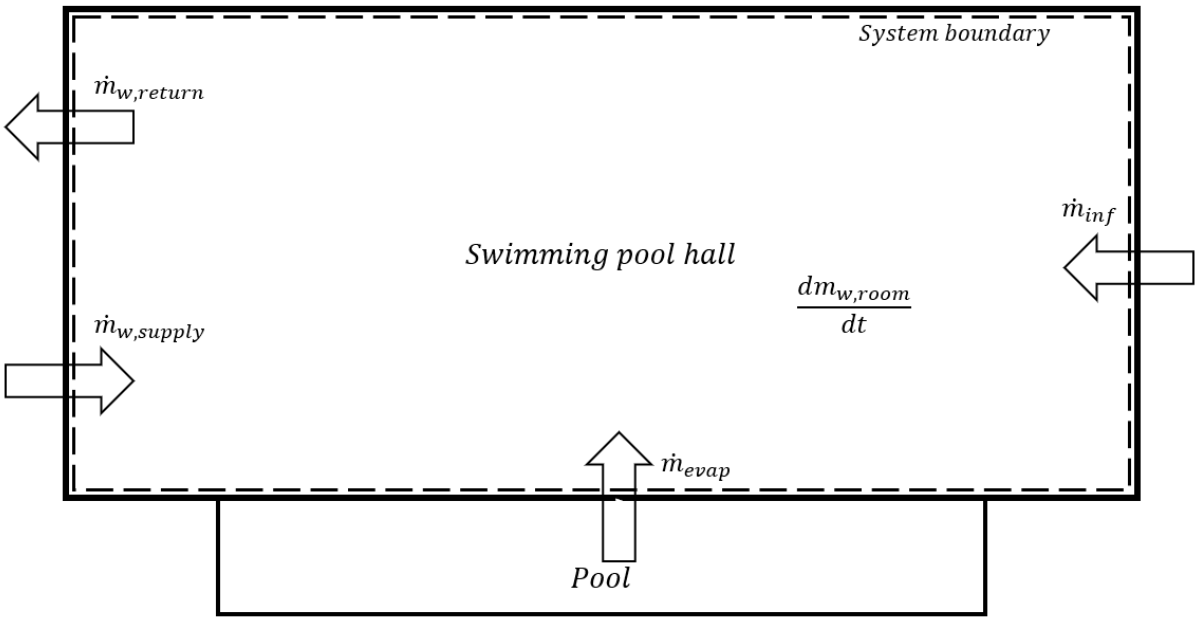

Figure 2-3: Water vapor mass balance

$$\dot{m}_{evap} = \dot{m}_{v,return} - \dot{m}_{v,supply} - \dot{m}_{v,inf} + \frac{dm_{v,room}}{dt} \quad 2.9$$

The water vapor flow rates can be found by equation 2.4 with dry air mass flow rate and absolute humidity as input variables. In many cases it is more convenient to measure the volume flow rate, such as over the supply air and exhaust fan. By assuming ideal gas properties and combining equation 2.1 - 2.4, the water vapor mass flow rates can be expressed as

$$\dot{m}_v = \rho_a \dot{V} x = \frac{p_a}{\frac{R}{M}T} \dot{V} \frac{0.622 p_v}{p - p_v} \quad 2.10$$

In the same way, the change in room air vapor content is given by

$$\frac{dm_{v,room}}{dt} = \frac{V}{\frac{R}{M}} \left(\frac{p_v}{T}\right) \frac{d}{dt} \quad 2.11$$

Based on experience, Byggforsk has tabulated evaporation rates for different types of pools, as a function of typical water temperatures. As expected, these values increase with the water agitation, water temperature and activity level of the occupants[10]:

Table 2-1: Evaporation rates for different types of pool

Type of pool	Typical water temperature [°C]	Evaporation rate [kg/m²h]
Night mode/unoccupied	28	0.10
Residential pool	27-28	0.10

Therapy	32-36	0.35-0.50
Hotel	27	0.18
Public, schools	28	0.25
Whirlpools	36-38	0.9-1.0
Water slides	31	0.5 kg/h per m slide

2.1.5 Energy balance

Due to the high demands for water heating and air treatment, swimming pool facilities typically have a large energy consumption. In a study from Statistics Norway from 2008 [1], the average energy use of Norwegian swimming pool facilities was found to be 300 kWh/m^2 total area. Kampel *et. al* [2] chose to investigate the energy use in terms of kWh/m^2 water surface area, as a great part of the energy use is related to the pools. Based on data from 41 different Norwegian swimming pool facilities, they found a variation in consumed energy from 1000 to 11 000 kWh/m^2 water surface. When designing a swimming pool facility, it is of high interest to predict the overall energy needs. If the needs of the various posts in the thermal system are known, it will be easier to implement energy saving measures and improve the design.

Figure 2-4 shows the heat gains and losses over a control volume enclosing the swimming pool hall, water treatment system and AHU. Electricity consumption is not considered in this heat balance. The losses include the transmission losses through the building envelope ($\dot{Q}_{trans}$), ventilation losses ($\dot{Q}_{vent,loss}$) and losses associated with the water exchange in the pool water circuit ($\dot{Q}_{water\ ex}$). In addition, there will be losses through the pool construction, pipes, and ventilation ducts, but these are considered negligible compared to the other losses due to typical high air temperatures in the technical rooms of the facility. The gains include pool water heating ($\dot{Q}_{water,heat}$), heating of ventilation air ($\dot{Q}_{vent,heat}$), heat from pumps ($\dot{Q}_{pump}$), UV irradiation ($\dot{Q}_{UV}$), solar gains ($\dot{Q}_{solar}$) and internal gains from people and lighting ($\dot{Q}_{int}$).

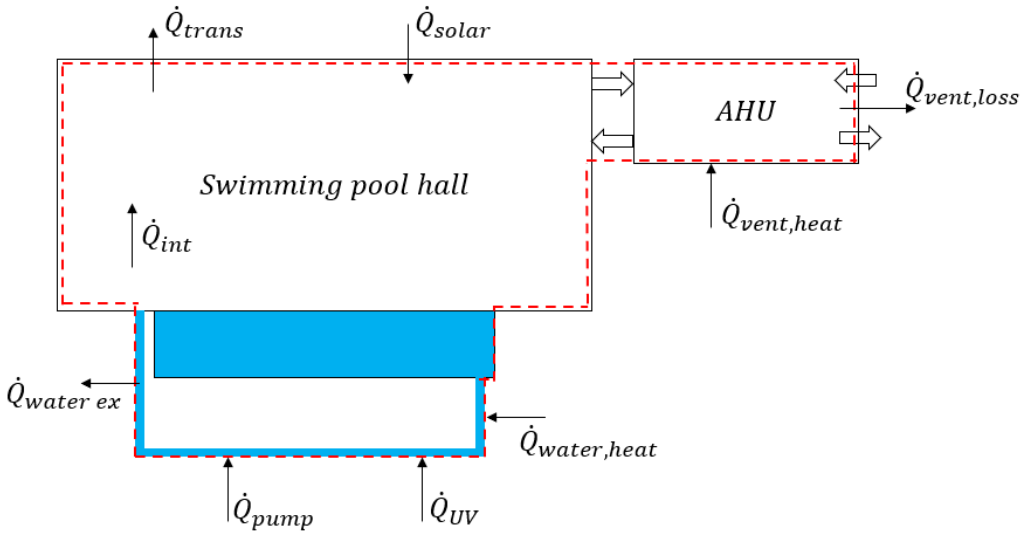

Figure 2-4: Energy balance of the thermal system in a swimming pool facility

2.2 Ventilation principles

The ventilation principle of a swimming facility should always aim to fulfill thermal comfort and healthy conditions for the occupants. Historically this has not always been the full truth. In this section, two different approaches which emphasizes different parts of the purpose of ventilation are described.

Aas et al. [24] describes four important tasks of the ventilation system in a swimming pool. As in other building categories, the main purpose of the ventilation system should be to provide thermal comfort and fresh air to the users. A satisfying indoor environment is important for users to revisit the facility. Secondly, the system should be able to remove pollutants and contaminants from the space, to keep the desired indoor climate. Further, to deal with the humidity challenges described in section 2.1.1, the ventilation system should have a high dehumidifying capacity. Lastly, the system should be optimized regarding energy performance, to reduce economic costs and climate impact. As the humidity level and pollution concentration in the room strongly affects the indoor air climate, there is a great relationship between the former purposes.

The ventilation air has commonly been used as a preventive measure to avoid condensation at the outer surfaces[24]. Dry air is typically supplied through slits beneath grates in the floor along the outer construction, typically beneath windows due to the high U-values compared to other construction parts. The air will stick to the window surface and prevent condensation. This principle, shown in Figure 2-5, limits the possibility of optimizing the ventilation system with respect to the air quality in the occupied zone, which should have been its main function.

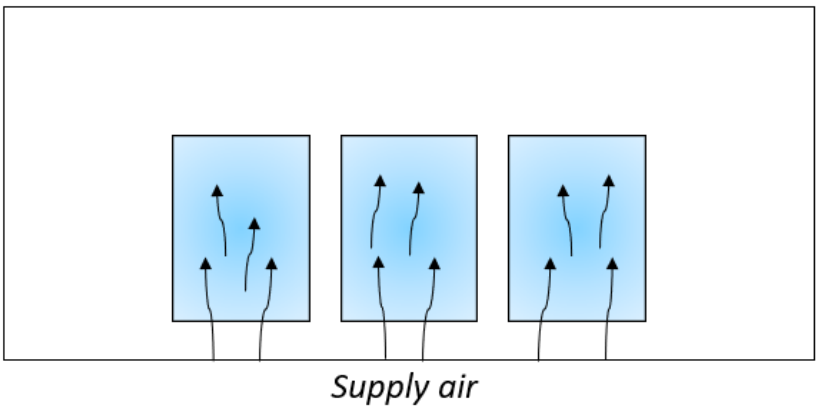

Figure 2-5: Ventilation air supplied beneath the external windows

A German study from 2018 [11] looked at how one should rethink the on the possible ventilation solutions in swimming pools, as buildings become of ever higher energy standards. The U-value of exterior walls and windows decreases, and the temperature inside these surfaces will approach the temperature of the indoor air. This opens up the possibility to optimize ventilation to a greater extent with regard to air quality, as condensation on external surfaces will no longer be a problem. Exterior constructions of higher energy quality will in themselves lead to lower energy consumption but can also indirectly influence energy consumption in several positive ways.

A ventilation system with a full focus on air quality and a good indoor climate for the users may require less energy, than if it additionally should protect against condensation on the outer structures. A tighter outer construction may also allow a higher RH inside the hall, which will cause less evaporation from the wet surfaces. This in turn will result in a lower dehumidification requirement and a lower heat loss from the pools. Energy consumption for both the ventilation system and pool water heating will decrease. However, it is important that the RH in the hall is not higher than what is comfortable for users, and special attention must be paid to those parts of the hall volume where overpressure occurs. Figure 2-6 illustrates how the supply air can be directed towards the pool water surface and remove contaminants and chlorination by-products from the breathing zone of the swimmers.

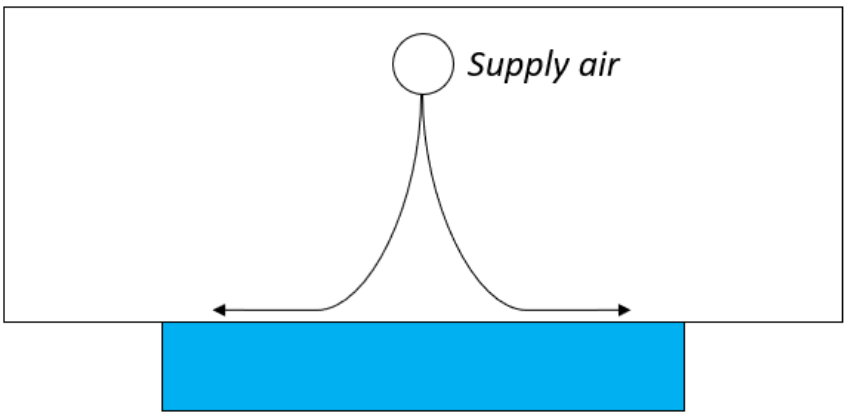

Figure 2-6: Ventilation air directed towards the pool water surface

2.3 Air handling unit

Air treatment in terms of pool hall space heating, dehumidification and control of volume flow rates is handled by the swimming pool AHU. This section gives a brief introduction to the thermal processes occurring in this unit.

2.3.1 Layout

An illustration of an typical AHU used in swimming pool facilities is shown in Figure 2-7. The figure is based on the layout of the real unit analyzed in this thesis and is reused in chapter 3.

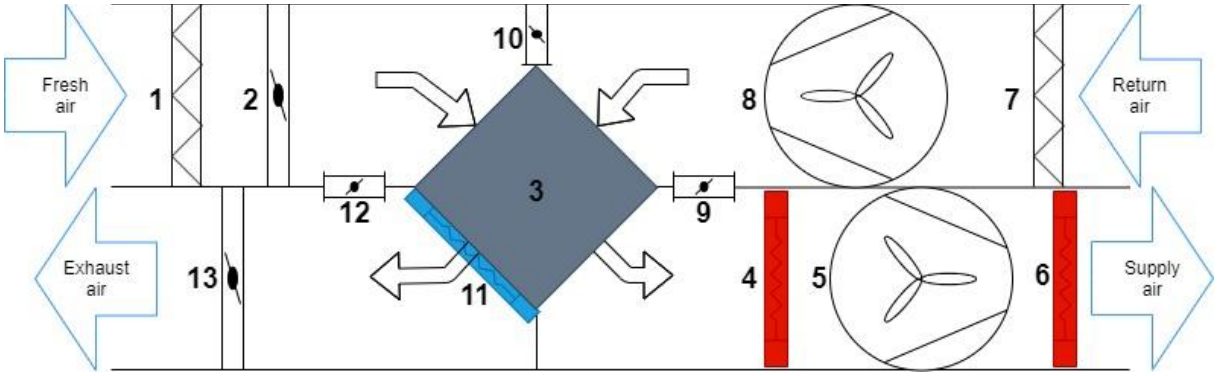

Figure 2-7: Principle sketch of the AHU

Inside the unit, dampers (labeled 2, 9, 10, 12 and 13 in Figure 2-7) are used to adjust the composition of the supply air. Due to the high energy consumption observed in swimming pool facilities, recirculation of return air (through damper 9 and 12) is essential. Without recirculation, large amounts of heat would be lost through the exhaust air. To utilize the heat in the return when the fresh air demand inside the hall is large, and there is little or no recirculation, a cross flow heat exchanger (labeled 3 in Figure 2-7) should be installed [25]. The recuperative heat exchanger (the airflows are not in contact with each other) prevents transmission of humidity and potential harmful contaminants from exhaust air to

supply air [26]. Due to harsh conditions, the heat exchanger must be corrosion-free, and is typically made of polypropylene[27]. The temperature efficiency of the unit is expressed in equation 5.1 and illustrated in Figure 2-8.

$$\eta_t = \frac{t_{c,out} - t_{c,in}}{t_{h,in} - t_{c,in}} \qquad 2.12$$

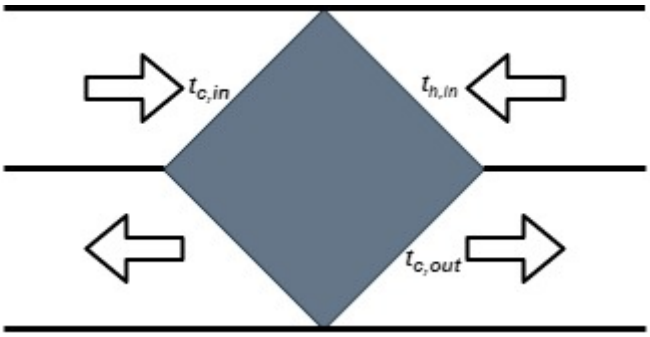

Figure 2-8: Cross-flow heat exchanger temperature efficiency

2.3.2 Heat pump

In modern swimming pool air handling units, it is common to utilize a heat pump solution for both dehumidification of the return air and heating of supply air [10]. The dehumidification of the return air makes it possible to extract the latent heat of vaporization stored in the humid air at the heat pump evaporator and reuse it at the air condenser. Commonly, the evaporator is referred to as the *dehumidifier* due to its purpose. A Swedish study from 2001 showed that implementation of a heat pump could reduce the annual energy demand of the facility by 14% [28].

The heat pump is a technology that moves thermal energy between two sources, with electrical energy input. The advantage with a heat pump is that the thermal energy moved is greater than the electrical energy consumed. This relationship is called the coefficient of performance (COP), and the typical thermal energy output is 3-4 times greater than the electrical input. The underlying thermodynamic process of a heat pump is the vapor compression refrigeration cycle. This cycle is illustrated in the pressure-enthalpy (Log-p-h) diagram in Figure 2-9:

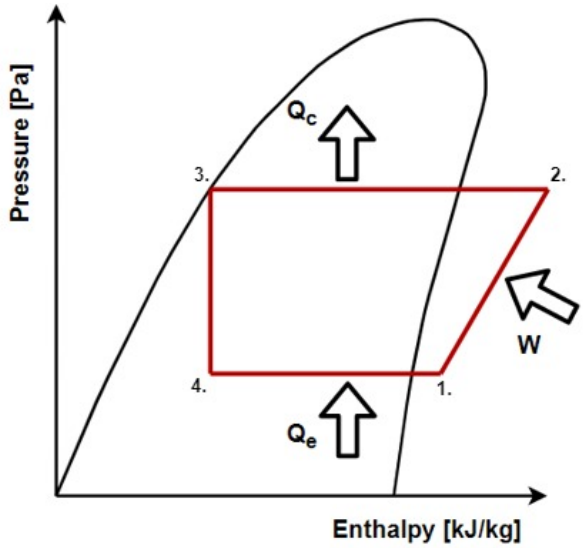

Figure 2-9: Principle heat pump cycle

- *1-2* Isentropic compression. The lossless compressor work is given by the product of refrigerant mass flow rate ($\dot{m}_R$) and enthalpy increase ($h_2 - h_1$):

$$\dot{W}_{ls} = \dot{m}_R(h_2 - h_1) \tag{2.13}$$

- *2-3* Isobaric heat rejection at the condenser, given by:

$$\dot{Q}_C = \dot{Q}_E + \dot{W} = \dot{m}_R(h_2 - h_3) \tag{2.14}$$

- *3-4* Isenthalpic expansion, constant enthalpy during expansion

$$h_3 = h_4 \tag{2.15}$$

- *4-1* Isobaric heat extraction at the evaporator, given by:

$$\dot{Q}_E = \dot{m}_R(h_1 - h_4) \tag{2.16}$$

The COP is given by the relationship between delivered heat $\dot{Q}_C$ [W] electrical input $\dot{W}$ [W]:

$$COP_{HP} = \frac{\dot{Q}_C}{\dot{W}} = \frac{T_H}{(T_H - T_L)} \tag{2.17}$$

The heat pump transports heat from the low temperature (T_L) exhaust air and delivers it to the high temperature (T_H) supply air. The circulating medium inside the heat pump transporting this heat is called working fluid, or refrigerant. The refrigerant has certain desirable thermophysical properties such as low boiling point and high heat capacity. Historically the working fluid was natural substances such as CO_2 and ammonia, used in refrigeration systems for cooling purposes. In the 1930's synthetical refrigerants was

developed and took over the marked. These fluids were chlorofluorocarbons (CFC) and hydrochlorofluorocarbons (HCFC), which had a high ozone depletion potential (ODP). This led to the Montreal Protocol in 1989, in which synthetic refrigerants containing chlorin was banned[29]. As a result, the development of hydrofluorocarbons (HFC) increased, which is still widely used today. The HFC's has zero ODP, but high global warming potential (GWP), and several regulations and restrictions has been implemented to decrease the use of HFC's with high GWP.

R407C is the common refrigerant used for heat pumps in AHU applications[27]. It is a tertiary HFC mixture of R125, R32 and R134a and will have a temperature glide in the condenser and evaporator[30]. At 1 bar it has a boiling point of -43,8°C, and the critical temperature and pressure are 86°C and 46,3 bar, respectively. The GWP is 1770, but it is neither toxic nor flammable[30]. Any leakage of the refrigerant could possibly be led to the people inside the swimming pool, either through the ventilation or into the water through the pool water condenser. The non-toxic property is thus of great importance. Figure 2-10 is a simplified sketch of how a heat pump unit is implemented in an AHU.

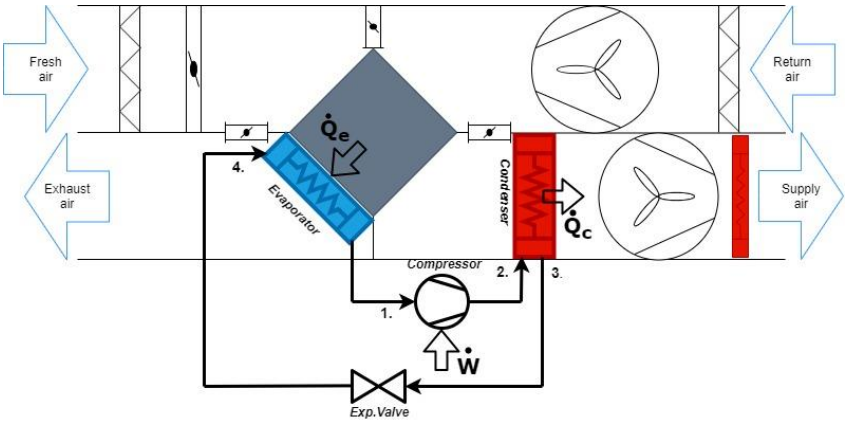

Figure 2-10: Heat pump in AHU

2.3.3 Illustration in Mollier chart

In Figure 2-11, the thermal processes (1 – 6) occurring as the air moves through the AHU is illustrated in a Mollier chart. In this case, there is some recirculation both through the dehumidification damper (labeled 12 in Figure 2-7) and heat recirculation damper (labeled 9 in Figure 2-7).

As the cold fresh air enters the AHU, it is mixed with recirculated dehumidified air (process 1). The state of the mixed air will lie on a straight line between the state of the entering fresh air and recirculated air, weighted with respect to the amount of the airflows. In process 2, the mixed air is heated through the cross flow heat exchanger represented by a vertical line in the Mollier chart. The absolute humidity remains constant, while the RH drops. A new mixing process occurs after the heat exchanger, and the absolute humidity

and temperature increases. Finally, the supply air is further heated through the air condenser and heating coil at constant absolute humidity (process 4). To be able to dehumidify and heat the air inside the swimming pool hall, the supply air should have a lower RH and higher temperature than the return air setpoint, respectively.

The return air is first cooled through the crossflow heat exchanger in process 5 at constant humidity. Depending on the properties of the airflows, it eventually reaches saturation where condensation occurs. After the heat exchanger, the return air is further cooled in the dehumidifier (process 6), where the latent heat in the humid air is recovered in the heat pump cycle.

The heat obtained and extracted in the condenser, heating coil and dehumidifier is expressed by equation 2.18 and 2.19.

Liquid side of heat exchangers:

$$\dot{Q} = \dot{m}_w \cdot c_{p,w} \cdot \Delta T \qquad 2.18$$

Air side of heat exchangers:

$$\dot{Q} = \dot{m}_{air} \cdot c_{p,air} \cdot \Delta T = \rho_{air} \cdot \dot{V}_{air} \cdot c_{p,air} \cdot \Delta T \qquad 2.19$$

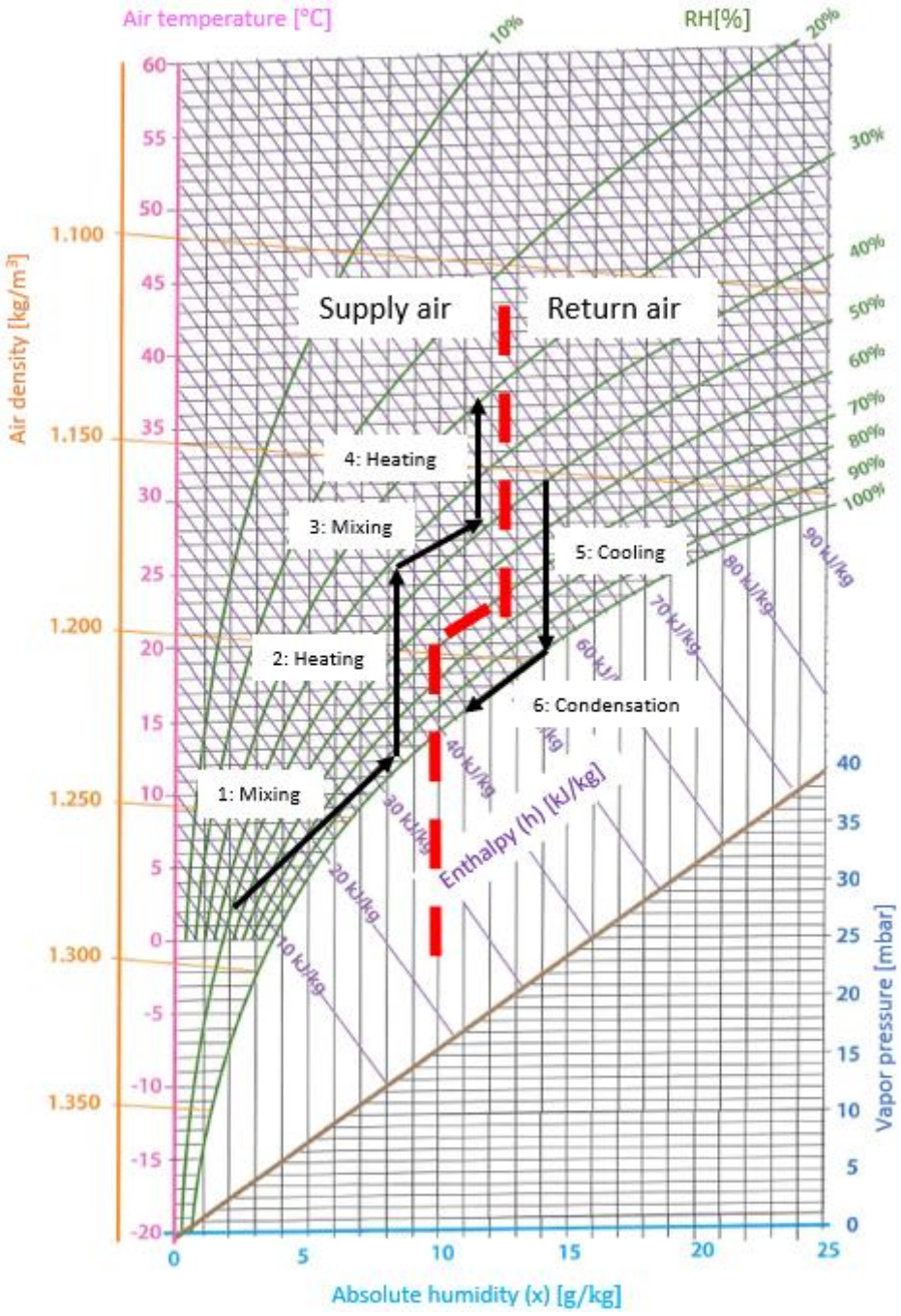

Figure 2-11: Thermal processes in the AHU

2.3.4 Control system fundementals

The operation of the AHU and the state of the air supplied to the swimming pool hall relies on a well-designed control system. This section gives a brief introduction to control theory.

If one considers a room with a given desired air temperature, y_0 (setpoint), the following control strategy can be implemented in order to keep the temperature at the setpoint.

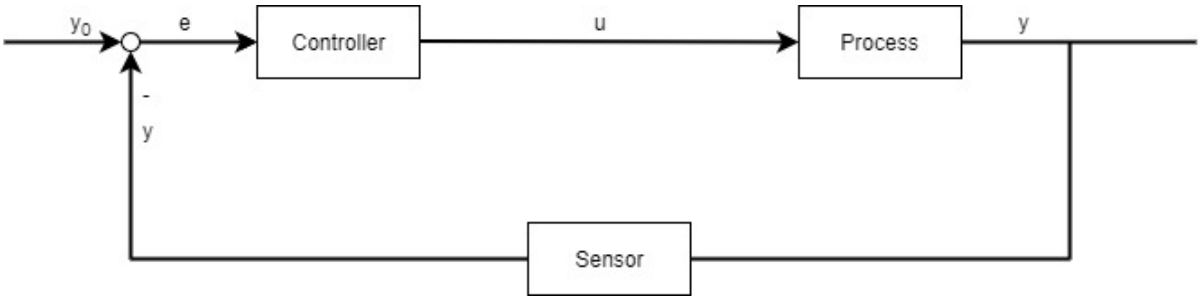

Figure 2-12: Principle control loop

A sensor inside the room measures the air temperature (y) and sends the signal to a controller. In this controller, the measured value is compared to the setpoint. Based on the calculated difference, the error (e), the controller sends an output signal (u) to an actuator (for instance the valve in a heating coil). As the performance of the actuator changes, the process of heating the air changes. In the case of a heating control, if the measured temperature is far below the setpoint, the value of u should be large; more heating is needed. Continuously, the controller attempts to minimize the error, e.

There are three commonly used controllers in modern control systems; a proportional controller (P), a proportional-integral controller (PI) and a proportional-integral-derivative controller (PID). The output of the P controller is proportional to the measured control error. An amplifier multiplies the measured difference, e, with a gain parameter, k. If any disturbances are present in the process, using a single P controller will always result in constant undesired offset from setpoint[31]. The aim of introducing an integrator term to the controller is to remove this residual deviation. It continuously integrates the control error, to compensate for the limitations of the P controller. The aim of the derivative term in a PID controller is to reduce the action of the integrator term when approaching the setpoint.

2.4 Requirements and recommendations

In the following sections, some recommendations and requirements regarding ventilation and energy performance of swimming pools are presented.

2.4.1 Ventilation requirements

For public buildings, TEK 17 says that the least required fresh air volume should be evaluated based on the following pollution sources [32]:

A – Persons

B – Materials, products, and installations

C – Activities and processes

When calculating the necessary fresh air volume, the highest value of (*A+B*) and *C* should be used. The requirements are given in Table 2-2:

Table 2-2: Ventilation requirements public buildings, TEK 17

Pollution source	Requirement
A	26 m^3/person
B (when occupied)	2.5 m^3/h per m^2 floor area
B (unoccupied)	0.7 m^3/h per m^2 floor area
C (bathrooms)	54 m^3/h per shower (extract air)

In swimming pools, there are no requirements other than that it must ensure a satisfying indoor air quality. However, the following recommendations are given by Byggforsk[10]:

- *4-7 ACH for larger facilities*
- *8-10 ACH for therapy pools*

The highest value of

- *1.4 l/s per m^2 total floor area (pool + deck)*
- *2.8 l/s per m^2 water surface (pool + spillway + shower area)*

The values differ among the international codes, and the recommendations in ASHRAE are[9]:

- *4-6 ACH for pools with no spectator areas*
- *6-8 ACH for pools with spectator areas*
- *4-6 ACH for therapeutic pools*

2.4.2 Water exchange

In order to maintain a satisfactory quality of the pool water, it should be replaced with fresh make-up water at regular intervals. The Norwegian association for technical solutions in swimming pools (*Norsk Bassengbad Teknisk Forening*) has the following guidelines for the amount of water exchange [33]:

- 30 liters per person per day (for normal public pools)
- 60 liters per person per day (for pools with a water temperature higher than 34°C)

2.4.3 Relative humidity

A higher RH inside the swimming pool hall will reduce the evaporation from the water surface since the vapor saturation at room air dew point is increased. This can be observed from equation 2.1 and the Mollier chart in Figure 2-1. However, as described in section 2.1.3, the RH should be limited to avoid moisture problems in the building construction.

The following recommendations are given in Byggforsk [25] and the ASHRAE Handbook [9]:

- Byggforsk
  - 50 - 55% RH during winter
  - → 65% RH in summer, due higher outdoor temperatures, and lower differences in vapor partial pressures
- ASHRAE Handbook
  - 50 – 60% RH

2.4.4 Energy requirements

In the Norwegian building codes (TEK), there are no specific requirements for the energy performance of swimming pool facilities. Generally, for sport facilities, TEK 17 says that the total energy demand should not exceed 145 kWh/m^2 for sport facilities[4]. This is an unattainable requirement for a swimming pool facility due to the high demands for pool water heating and ventilation. Anyway, efficient measures should be implemented to reduce the demands. Increasing the energy performance of the technical installations is one approach, but in order to reduce the demand, the insulating ability of the building envelop should be increased.

The U-value, or the thermal transmittance, is a measure of the insulating ability of the building construction. Constructions with a high U-value have a high thermal conductivity, and in an energy-saving perspective it is therefore desirable to keep this value as low as possible. Depending on the physical properties, the U-value will vary between the different parts of a building construction. The requirements for average U-values given in TEK 87, 10, 17 and Norwegian passive house standard NS 3701 are presented in Table 2-3 [34][35][4][36]:

Table 2-3: Requirements for U-values in different building codes

	U-value [W/m^{2}K] (TEK 87)	U-value [W/m^{2}K] (TEK 10)	U-value [W/m^{2}K] (TEK 17)	U-value [W/m^{2}K] (NS 3701)
External wall	≤ 0.3	≤ 0.22	≤ 0.22	≤ 0.12
External roof	≤ 0.2	≤ 0.18	≤ 0.18	≤ 0.09
External floor	≤ 0.2	≤ 0.18	≤ 0.18	≤ 0.08
Window/door including frame/sill	≤ 2.4	≤ 1.2	≤ 1.2	≤ 0.8

The normalized thermal bridge value given in NS 3701 is 0.03 W/m^{2}K [36].

2.5 Building performance simulation (BPS)

Building performance simulation is defined as *"… a computer-based mathematical model of some aspects of building performance based on fundamental physical principles and engineering models"* [37]. There are several different packages for building performance simulation, where IDA ICE is the one used in this thesis.

2.5.1 Simulation tool

According to the objective of this thesis, the examined swimming pools are modelled in IDA ICE, version 4.8. IDA ICE is an abbreviation for IDA Indoor Climate and Energy, and is a detailed dynamic simulation tool used for the study of indoor thermal climate and building energy performance [38]. It is developed by the Swedish company EQUA Simulation AB, located in Stockholm, and the aim of the simulation tool is to enable accurate simulations of buildings and their control systems in order to optimize energy performance and indoor climate. It provides the users full insight to the equations used in the models, and it is possible to log every variable, making it fully transparent. The modelling is equation based, utilizing the Neutral Model Format. This means that the predefined models and components available in the IDA ICE library are general and standardized, widening the possible use.

2.5.2 Existing swimming pool models

This thesis is a continuation of the work carried out in the master thesis of Henrik Alvestad[5]. In that thesis, the swimming pool hall and the corresponding AHU unit was modeled in the dynamic simulation tool IDA ICE to characterize the thermal system of a swimming pool facility in Trondheim. The results showed that the model worked quite well in the prediction of evaporation, but larger deviations were found in the heating needs. Much of the deviations were explained by a discrepancy between the model control strategies for heating and dehumidification and the real control strategies, and the omission of the heat pump found in the real unit.

In a study released back in 2014, the TRNSYS software was used to determine pool losses and pool hall energy demand. TRNSYS is a component-based software package used to investigate transient systems [39]. One part of the software, the engine (or kernel), reads, process and solve the problem under scope. The other part consists of components, which the users are able to combine in different ways in order to achieve the desirable performance of the system to be studied. By modeling the energy balance of the swimming pool, the aim of the study was to investigate the impact of different water- and air temperatures on the energy losses. As one could expect, the results from the simulation showed that, by reducing the hall air temperature and pool water temperature, the total swimming pool hall losses decreased.

In a Ph.D. thesis from January 2019 [40], the energy performance and water usage of an aquatic center in Australia was investigated by using the simulation tools DesignBuilder and EnergyPlus. The combination was used, since DesignBuilder does not have the possibility to add the swimming pools into the model. However, since the interface of DesignBuilder is more user-friendly, the model without the pools was created here before it was exported as an IDF-file to EnergyPlus. A comprehensive and detailed model of the swimming facility was made, to get the most representative results from the simulations. The results showed that the heat losses through the building envelop only contributed to a minor part of the total energy performance of the facility. Calibration against measured energy and water data was done before the evaporation from the pools was validated. In this process, the results from the simulations was compared to calculated values based on the ASHRAE equation [9]. A high correlation between the simulated results and manual calculations was obtained, indicating a high accuracy of the simulation model. Parametric studies were also performed, to come up with possible energy measures. For instance, a 1°C reduction in pool water and air temperature resulted in 6.1% decrease in energy use.

Due to the high indoor air setpoint temperature, the process of heating the fresh air entering the AHU is very energy consuming. The same yields for the dehumidification of the return air, where large amount of energy would have been lost if solutions for recovering this energy was not implemented. The aim of a study from 2008 published in *Applied Thermal Engineering* was to optimize the design of the heat pump system in the AHU, in order to minimize the energy costs [41]. In this case, the heat pump circuit consisted of two parallel condensers: for air heating and pool water heating. By using the conservation of mass and energy for both the ventilation system and water system, the state of the air and water at the heat pump evaporator and condensers was calculated. Further, the heat absorption in the evaporator and heat rejection in the condensers are calculated. Finally, the particle swarm algorithm [42] was used to find the optimum outdoor air mass flow rate, heat conduction of the heat exchangers and compressor and boiler types. The results showed that the optimum energy supply of the water heating boiler decreased with a rising enthalpy of the outdoor air. As this value reaches zero, the performance of the performance of the evaporator, condensers and compressor is optimized, and the heat pump is preferred to cover all the heating load.

In a study presented on the American IBPSA conference in 2012 [43], a combination of the simulation tools MATLAB/Simulink, BCVTB and EnergyPlus was used to simulate the swimming pool environment at the National University of Ireland. The AHU and its controls were modeled in Simulink, which at each time step received updated variables from MATLAB needed in the calculations. Simulink calculated the supply air temperature and other variables needed in the next iteration of the simulation process. The signal was sent

through MATLAB and the BCVTB into the building model in EnergyPlus. In addition, the BCVTB also calculates the latent heat of the evaporation from the pool. Based on these inputs, and the weather file available in EnergyPlus, a feedback signal is sent from the EnergyPlus model to the BCVTB and MATLAB/Simulink model, which recalculates the input variables. Different operational scenarios were implemented in the BCTVB in order to investigate the response of the system. Both a fixed and a dynamic setback operation was implemented, with almost no difference in energy consumption. Compared to no setback, the dynamic operation however resulted in 30% energy savings.

3 System description

Measurements are performed in a swimming pool facility at Dalgård Primary School and Resource Centre in Trondheim. This chapter gives a brief introduction to the facility in terms of swimming pool, water treatment system and AHU.

The swimming pool at Dalgård is part of larger building housing a primary school. It is located at Byåsen in Trondheim and is used both by classes during school hours and various associations in the evenings. During weekends and holidays, the pool is normally empty.

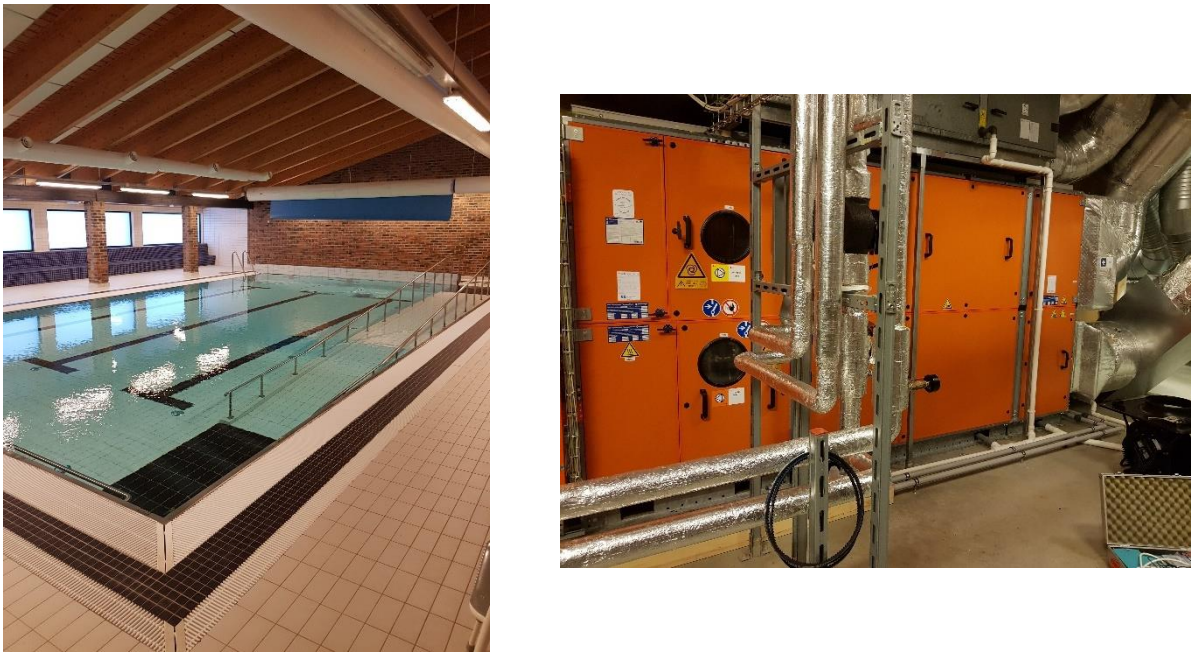

Figure 3-1: Swimming pool and AHU at Dalgård

The swimming pool has a water surface area of 89.375 m^2 (101.91 m^2 including the overflow channels), and the setpoint water temperature is 33°C. Supply air diffusers are located both beneath the windows and in a horizontal duct at the ceiling, as could be seen in Figure 3-1. A pool cover is used when the pool is not used (nights and weekends) to reduce the evaporation. There are two return air grills located at the opposite end of the room of the supply air diffusers: one close to the ceiling, and another at the floor level. The total area of the room, including the water surface, is 203.5 m^2, and the volume is close to 775 m^3.

3.1 Water treatment system

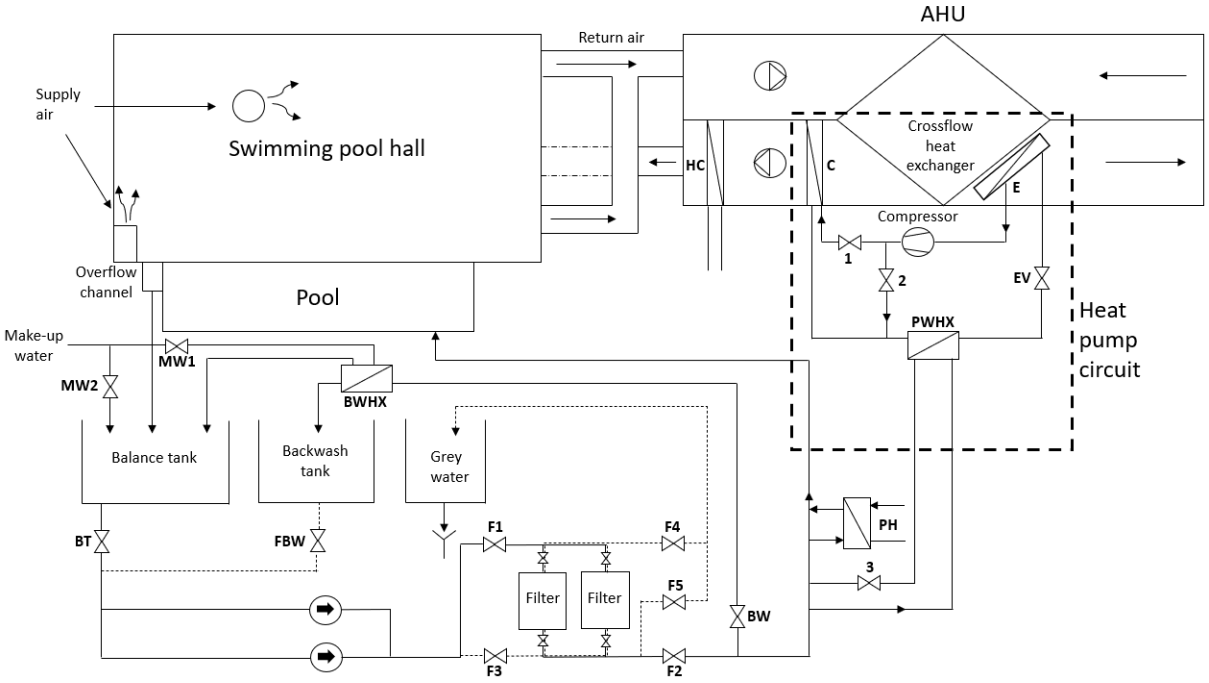

Figure 3-2: System sketch of Dalgård Swimming Pool. The sketch is based on an illustration of the water treatment system retrieved from the SD system of the facility, as well as own observations of the system. pH regulation and UV radiation are omitted in this illustration.

Figure 3-2 shows the layout of the swimming pool hall in connection with its AHU and water treatment system. Pool water flows continuously into the overflow channel, and further down into a balance tank with base area 10.88 m^2, which aims to maintain a stable water level in the pool. To compensate for the water loss through evaporation, wet bodies leaving the room and filter backwashing, there is a need for make-up water. The make-up water is either fed directly into the balance tank, or through the backwash water heat exchanger (BWHX). A small flow is steadily fed into the tank through the backwash water heat exchanger, while valve MW2 only opens to supply a larger flow when the water in the tank has dropped to a level of 0.55 m. During filter backwashing valve BT, F1 and F2 closes, and valve F4 opens. Thus, the water is directed the opposite way through the filers (for cleaning), and the water is fed into the greywater tank and further into the drain. During the week, a total of 7000 liters of water is used for filter backwashing.

After the balance tank, the water is pumped through the sand filters from top to bottom, where particulates are captured. Downstream of these filters, a small partial flow is led to the backwash tank, through the backwash water heat exchanger, to be stored for filter backwashing. The rest of the flow is returned to the pool through a 3 kW UV-lamp, either directly or through the heat exchangers if there is a heating need. There are two heat sources: heat exchanging with AHU heat pump refrigerant and primary heat (district heating). The pool water condenser, PWHX, is located in a partial flow loop upstream of

the primary heat exchanger partial flow loop, as illustrated in Figure 3-2. In this way, excess heat from the AHU heat pump circuit could be utilized when there is little or no need for ventilation heating.

3.2 AHU

The AHU is of the type MENERGA ThermoCond 370611, and serves only the swimming pool hall. The unit works to achieve a setpoint temperature of 31.5°C and a RH of 50% by altering the compressor power, position of the dampers (labeled 2, 9, 10, 12 and 13 in Figure 3-3), volume flow rate and heating coil valve position. Damper 10, which is a defrosting damper, is neglected in this analysis. It was observed that the defrosting damper was always closed during the measurements, and the omission will not affect the results. For heat recovery, there are both a crossflow heat exchanger (3) and a heat pump, whose compressor is on/off controlled, installed. The main purpose of the heat pump is to dehumidify the return air, where the latent heat of the humid air obtained by the refrigerant (R407C) in the evaporator/dehumidifier (11) is utilized to heat the supply air at the air condenser (4) or the pool water through the pool water condenser (PWHX) (see Figure 3-2). This is controlled by the two solenoid valves labeled 1 and 2 in Figure 3-1, which are either fully open or closed.

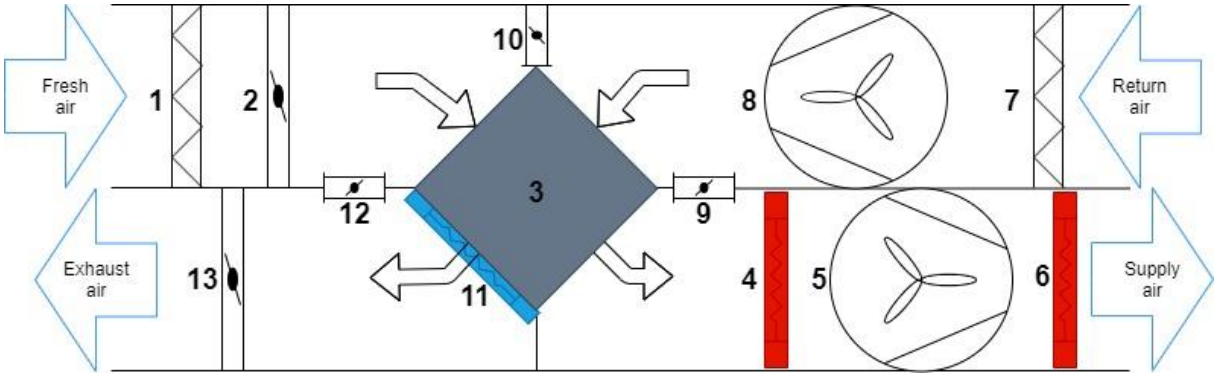

Figure 3-3: Illustration of the AHU

There are three filters in the AHU: a fresh air filter (1) a return air filter (7) and a supply air filter located after the heating coil (6). Their purpose is to prevent contaminants and harmful particles from being carried with the supply air and protect the components in the AHU against damage. The crossflow heat exchanger has an annual temperature efficiency of 70%, while the supply and return air fans (5 and 8) have a total efficiency of 74 and 76%, respectively. Other dimensions and rating conditions of the various components in the AHU can be found in the user manual and technical documentation of the unit, provided by Menerga [44][45]

In order to maintain the setpoint temperature and RH, the AHU runs according to a quite complex control strategy. This control strategy is generally divided into a temperature

control and a return air RH control. As the temperature and RH deviates from their setpoints, various actions are initiated in order to bring the state of the air back to the setpoint. The temperature control is illustrated in Figure 3-4, which shows the actions initiated at different deviations from the setpoint. In this AHU, $\dot{V}_{min}$is 69% of the maximum total volume flow rate, $\dot{V}_{max}$ of 6300 m^3/h. A similar layout of the RH control is illustrated in Figure 3-5.

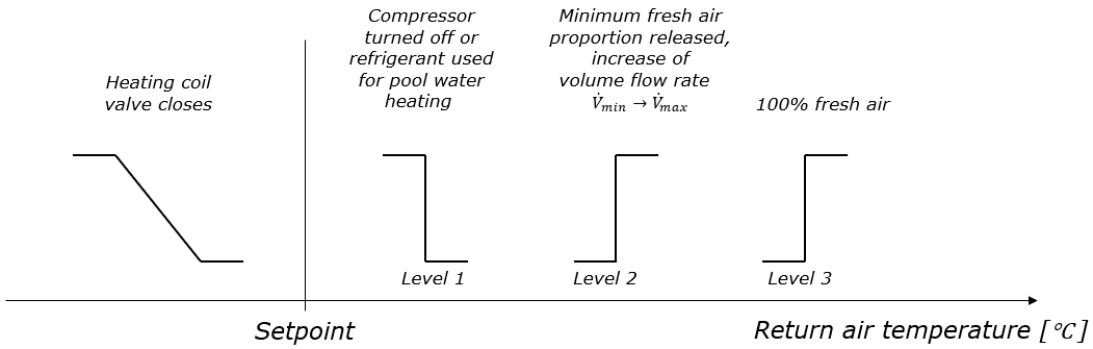

Figure 3-4: Temperature control. The sketch is based on an illustration of the control strategy in the technical documentation of the AHU provided by Menerga

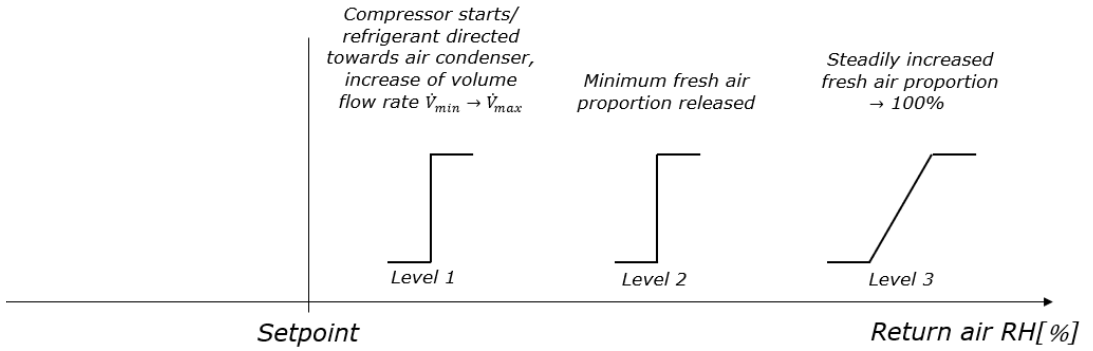

Figure 3-5: RH control. The sketch is based on an illustration of the control strategy in the technical documentation of the AHU provided by Menerga

In both the temperature and RH control strategies one or more controllers compares a measured value with a given setpoint. As illustrated in Figure 3-6, these controllers produce signals which through the control algorithms determines how the actuators in the AHU should react. A description of the temperature and RH control strategies are given in the following two sections.

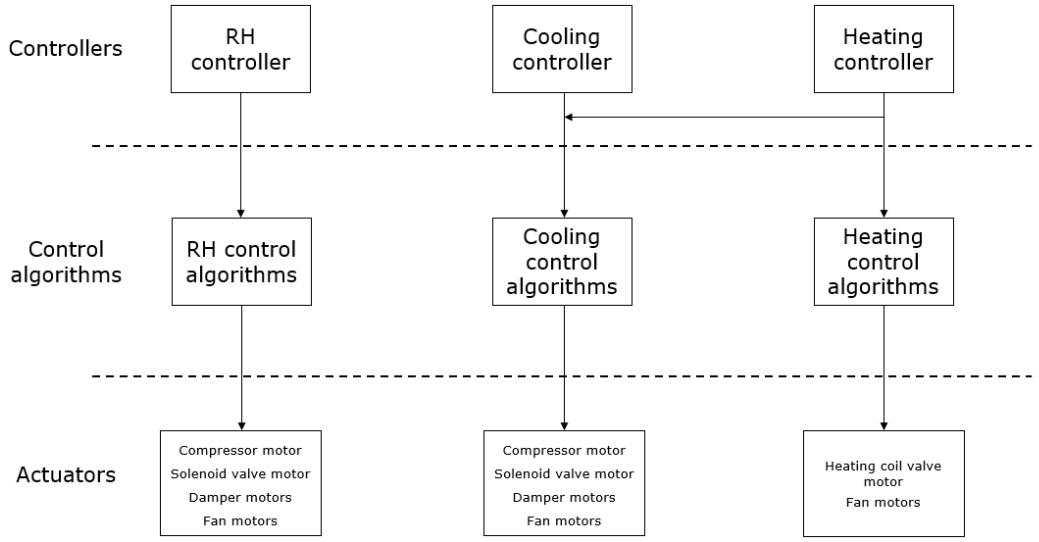

Figure 3-6: AHU control strategy

3.2.1.1 Temperature control

Three units in the AHU ensures that the supply air achieves the necessary temperature to keep the return air temperature setpoint before it enters the swimming pool hall. These are the crossflow heat exchanger, the air condenser in the heat pump cycle and the heating coil, where the heat exchanged in the two latter units are thoroughly controlled by the temperature control strategy. This strategy might be divided into a cooling control strategy and a heating control strategy.

A PI controller compares the measured return air temperature with the given setpoint. If the measured temperature exceeds the setpoint, the cooling control algorithms are initiated. These algorithms occur at different levels of the output signal, as depicted in Figure 3-4. At the first level, the compressor is turned off, or eventually the refrigerant of the heat pump cycle is directed towards the pool water condenser, to avoid any temperature rise in the air condenser. Should the return air temperature still be too high, the integrator term of the controller ensures that the output signal will continue to rise to the next level. At the second level, the fresh air damper is opened, such that a minimum fresh air proportion of 33% is achieved. In addition, the volume flow rate through the fans are increased from $\dot{V}_{min}$ to $\dot{V}_{max}$, resulting in a higher replacement of warm indoor air with colder air from outside. For an even higher output signal from the cooling controller, the AHU will run with 100% fresh air (third level), where the dehumidification damper and recirculating heating damper (labeled 12 and 9 in Figure 3-3) are closed.

If the supply air temperature drops too low, and a cooling sensation is felt inside the swimming pool hall, another controller ensures that a minimum supply air temperature is kept. This minimum setpoint is outdoor temperature dependent, and the controller has a limiting effect on the output signal from the cooling controller.

In the heating control strategy, shown in Figure 3-7, a cascade of two controllers is used to give a signal to the heating coil valve motor. The first controller is a return air temperature controller which compares the measured return air temperature with the given setpoint. This produces a signal that becomes the setpoint for the second controller, the supply air temperature controller. The higher the deviation measured in the return air temperature controller, the higher becomes the setpoint for the supply air, until it eventually reaches a maximum of 53°C. After a comparison between the measured supply air temperature, the second controller produces a signal that determines the load on a motor, which adjusts the position of the heating coil valve accordingly. In this way, one ensures that the supply air temperature is kept high enough to maintain the return air temperature setpoint. For supply air temperatures between 45 and 50°C, the volume flow is increased from $\dot{V}_{min}$ to $\dot{V}_{max}$.

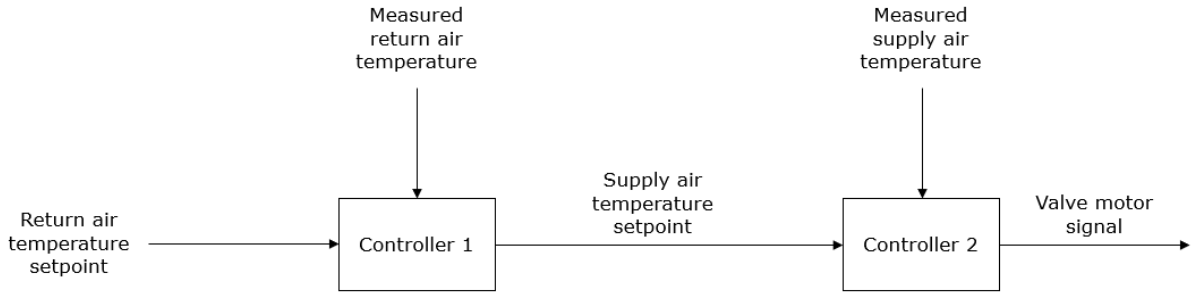

Figure 3-7: Cascade heating control

3.2.1.2 RH control

Dehumidification of the air inside the swimming pool hall is controlled by, as indicated in Figure 3-5, either adjusting the cooling rate at the heat pump evaporator, the fresh air proportion of the supply air, or the total volume flow rate through the fans. All these measures aim to reduce the RH of the ambient air of the swimming pool. A PI controller compares the measured return air RH with the given setpoint, resulting in a signal that increases with the deviation.

When the output signal reaches the first level, the compressor starts, causing the air at the evaporator to cool down and the water vapor to condense. In this way, the air recycled through the dehumidification damper (labeled 12 in Figure 3-3) achieves a lower absolute humidity, and the RH of the mixed supply air decreases. (If the suction pressure of the compressor drops too low, freezing may occur at the dehumidifier (evaporator), and the compressor is turned off). In addition, the total volume flow rate is increased from $\dot{V}_{min}$ to $\dot{V}_{max}$. At the second level, a minimum fresh air proportion of 66% is released. The effect can be observed in the Mollier chart in section 2.3.3, where a higher proportion of fresh air will move the state of the supply air towards left in the chart, an thus achieve a reduced

humidity. Similar to the temperature control, the AHU at the third level of the control strategy will run with 100% fresh air.

Regardless of the state of the air inside the swimming pool hall, the AHU in bathing mode will always operate with a minimum amount of fresh air to satisfy the indoor air quality. This amount appears as 10% fresh air, with an addition of 50 m^3/h per kg of evaporation. In night mode, a higher RH inside the swimming pool hall is tolerated if the outside temperature is high enough. This is indicated in Figure 3-8, where the return air RH setpoint increases linearly from 50 to 65% for outdoor temperatures between 10 and 25°C.

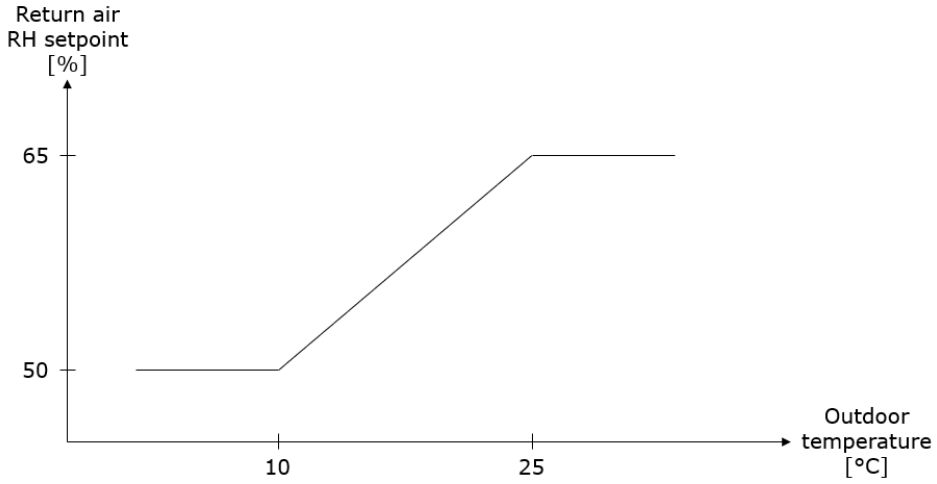

Figure 3-8: RH setpoint night mode. The figure is based on an illustration in the AHU technical documentation provided by Menerga

3.2.1.3 Priority of output signals

As a result of the fact that fresh air proportion increases for higher cooling and RH controller signals, the maximum output signal from the cooling and RH control should be used to control the fresh air damper position. The logical connection between the control output signals and the heating damper is shown in Figure 3-9:

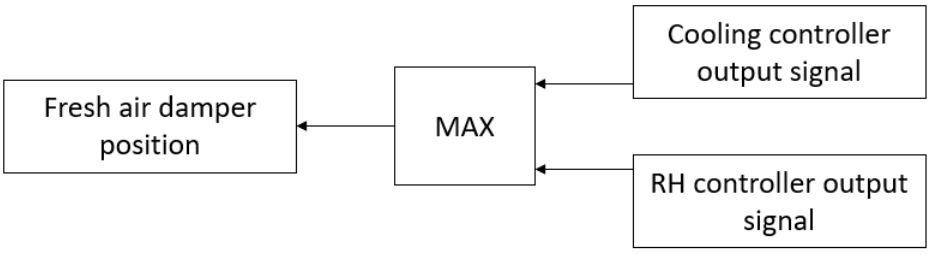

Figure 3-9: Fresh air damper control

The cooling control aims to stop the heat pump compressor, to reduce the supply air temperature. On the opposite, a high measured return air RH will require more dehumidification of the supply air, and therefore start the compressor. If there is a cooling

need and dehumidification need at the same time, the compressor should be turned off, and the dehumidification need is covered by an increased fresh air proportion of the supply air.

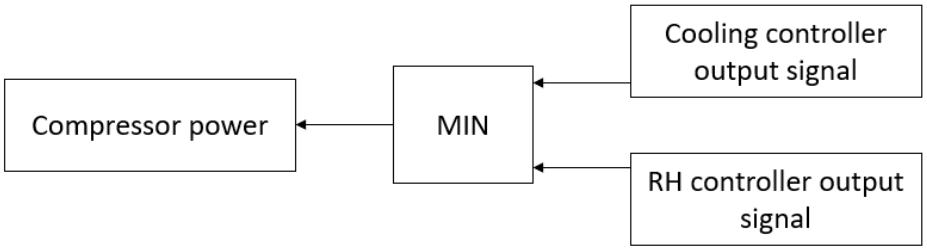

Figure 3-10: Compressor control

Both an increased dehumidification rate and cooling effect are achieved by an increased volume flow rate, and the signal sent to the fan motor will be the highest of the cooling controller output signal and RH controller output signal, as illustrated in Figure 3-11.

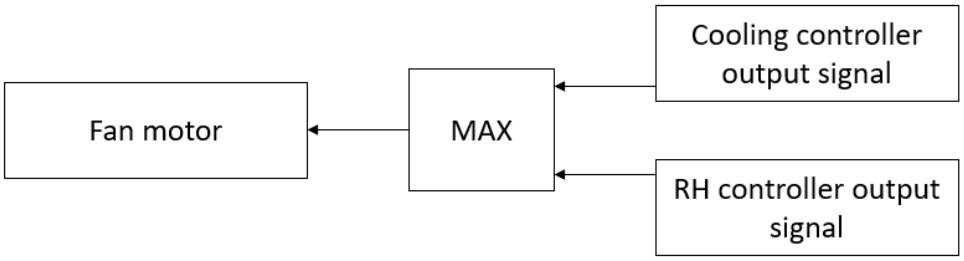

Figure 3-11: Fan control

4 Methodology

A detailed dynamic model of the swimming pool facility is built in IDA ICE, and measurements within the thermal systems of the facility are carried out on site. The intention was to collect data from a long period of time, to capture various operating situations that are characteristic of the swimming pool. A swimming pool that is not in use is of little interest and activity in the pool is necessary to be able to say something about the typical operating situation. For the swimming pool at Dalgård, data from normal operation were collected from February 25 to March 11, until the facility closed down due to the COVID 19 virus.

4.1 Measurements

In the facility at Dalgård, measurements were carried out to investigate two important aspects of the thermal system: evaporation from the water surface and heating needs in both the AHU and the water treatment system. Unfortunately, the compressor was damaged and the integrated heat pump idle during the entire period of analysis. All the necessary calculations regarding the analysed thermal characteristics of the facility are performed in excel, based on the measured data.

4.1.1 Location of sensors

Temperature and RH were measured at different positions in the facility using the following sensor devices:

- WS-DLTa-p100 (pt100) [46]
- WS-DLTc [47]
- WSE-DLCc [48]

Signals from the sensors were transmitted to a base station, which was connected to a computer where the measured variables were logged with a time step of one minute. The pt100 sensor measures temperature with an accuracy of $\pm 0.1\%$. WS-DLTc was used for both RH and temperature measurements, with an accuracy of $\pm 1.8\%$ and $\pm 0.3^{\circ}C$, respectively. Temperature and RH in two adjoining rooms, as well as inside the swimming pool hall close to the water surface, were measured using the WS-DLCc sensor, with the same accuracy as the WS-DLTc sensor.

The power delivered in the heating coil of the AHU and the primary heat exchanger of the pool water circuit is measured using a TA-SCOPE [49], which calculates the power based on measurements of the pressure drop over the balancing valve, mass flow rate, and

temperature of the water, with an accuracy of 1% for pressure and mass flow rate, and 0.2°C for temperature.

Volume flow rates (in m^3/h) of the supply and return air of the AHU are retrieved from the integrated sensors in the unit. From the pool water circuit, the mass flow rate of the make-up water, level of the balance tank, power consumption of the pumps and delivered power of the UV-lamp are retrieved from the monitoring system of the plant. Power delivered to the pool water from the pumps are calculated from $P = UI$, where the voltage is 230 V.

Figure 4-1 shows the location of the sensors used for temperature and RH measurements, TA-SCOPEs, and integrated AHU volume flow sensors. Temperature and RH were measured at two different locations inside the swimming pool hall; one sensor located near the floor level close to the water surface, and the other one at a height of 3 meters. The following symbols are used:

- WS-DLTa-p100 (pt100)
- WS-DLTc
- WSE-DLCc
- TA-SCOPE
- AHU volume flow sensor

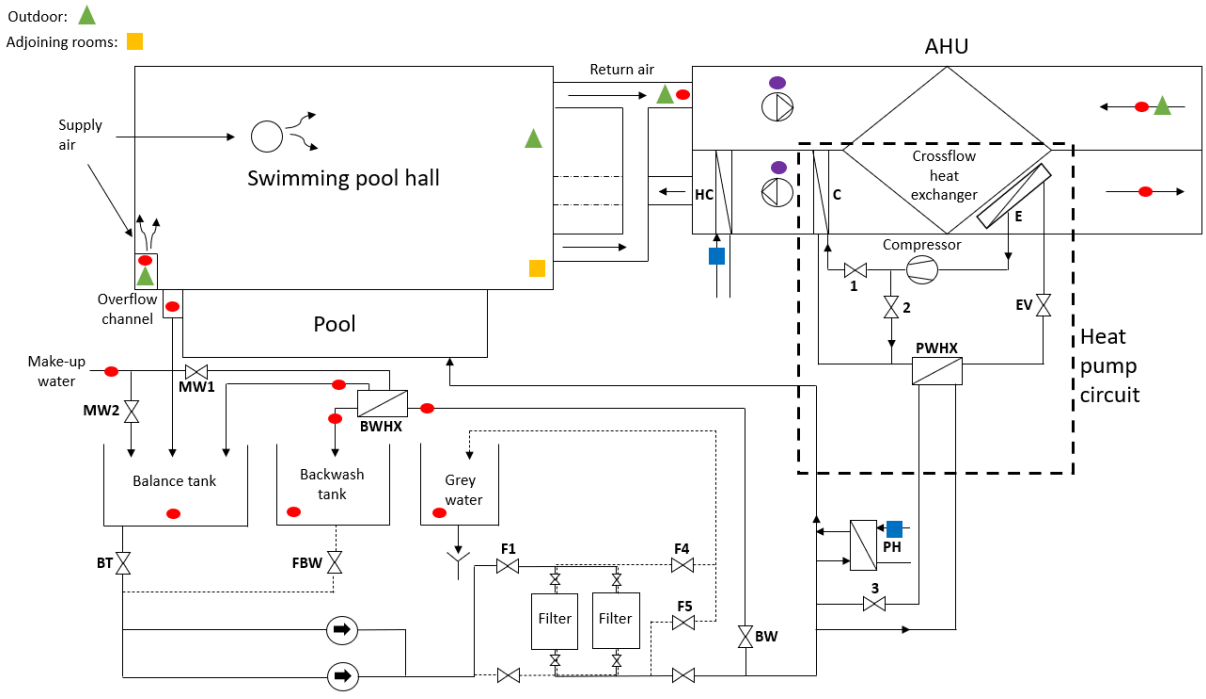

Figure 4-1: Sensor locations

4.1.2 Activity log

The activity in the pool is registered by observation of the number of swimmers, their activity level, and the time of the session. Activity level is a subjective perception, and in

this context, it is decided to construct a five-point scale for registration. The scale is shown in Figure 4-2, where low, medium, and high activity are given the values 1, 2, and 3, respectively. Intermediate values of 1.5 and 2.5 are used when the activity level is perceived as a middle of the other values.

Figure 4-2: Activity level scale

Activity was registered by person during most of the day from 8 am to 4 pm. For activities outside this schedule, a log, in which the users could register the number of swimmers, activity level, and time, was made. After the measurement period, the log was compared to the water in the balance tank, which clearly indicates when the pool is in use. This is illustrated in Figure 4-3, where activity appears as an elevated water level of the balance tank. The rise in the night is due to supply of make-up water. On a weekly basis, the activity in the pool follows a repetitive cycle with fairly fixed schedules. Thus, when estimating the number of swimmers and their activity level, it is assumed to be similar to what as observed the corresponding time in the previous or following week. The registered activity could be found in Appendix K.

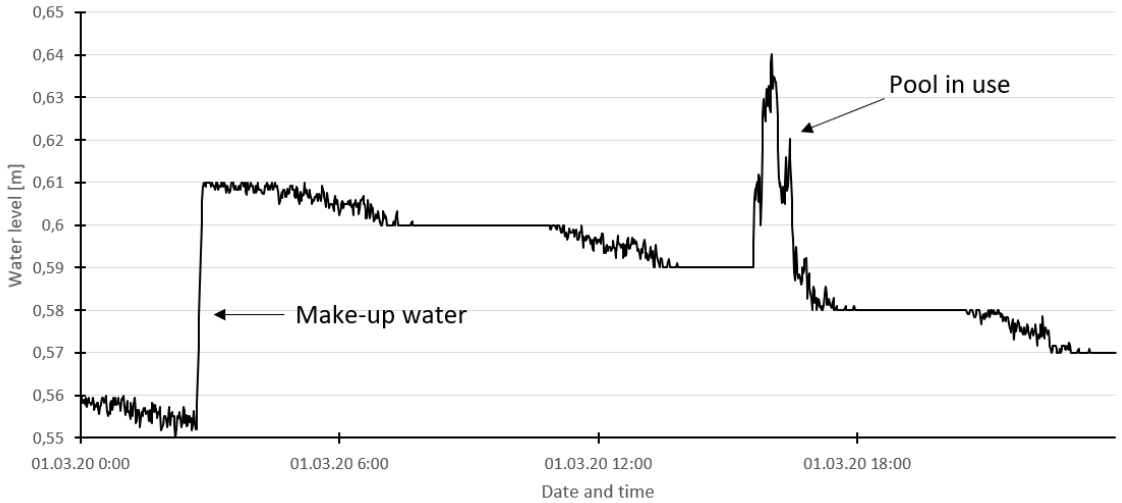

Figure 4-3: Water level of balance tank

4.1.3 AHU operation mode, pool cover and temperature setpoint

It is observed that the AHU runs according to the following schedule:

- Weekdays:
  - 06:00 – 22:00 – Bathing mode
  - Otherwise – Night mode

- Weekends:
    - 10:00 – 20:00 – Bathing mode
    - Otherwise – Night mode

In the beginning of the measurement period, the AHU was forced to run in bathing mode from February 25 to February 27. For the rest of the period, the operation mode was according to the presented schedule above. The entire operation mode for the measurement period is shown in Figure 4-4.

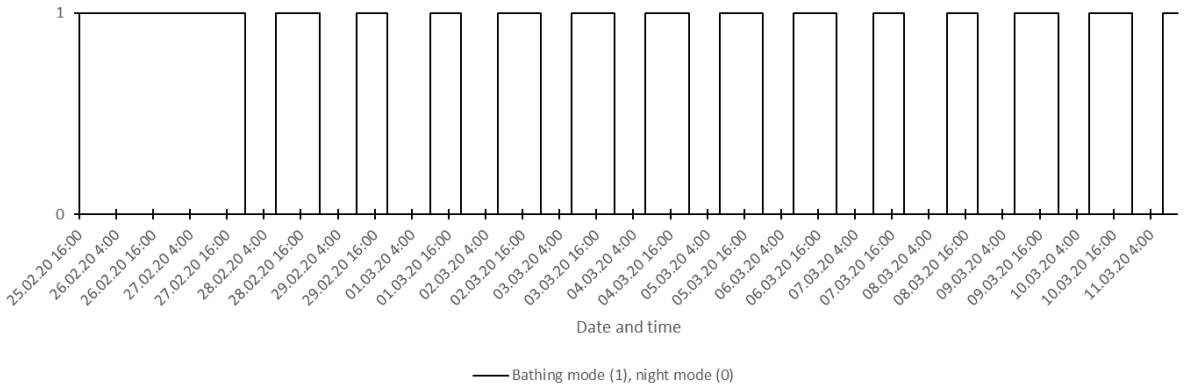

Figure 4-4: Operation mode AHU

The pool cover is used to reduce the evaporation in periods where the pool is unoccupied. To investigate the effect of the pool cover, the pool cover is never used in the second half of the measurement period. The schedule is shown in Figure 4-5.

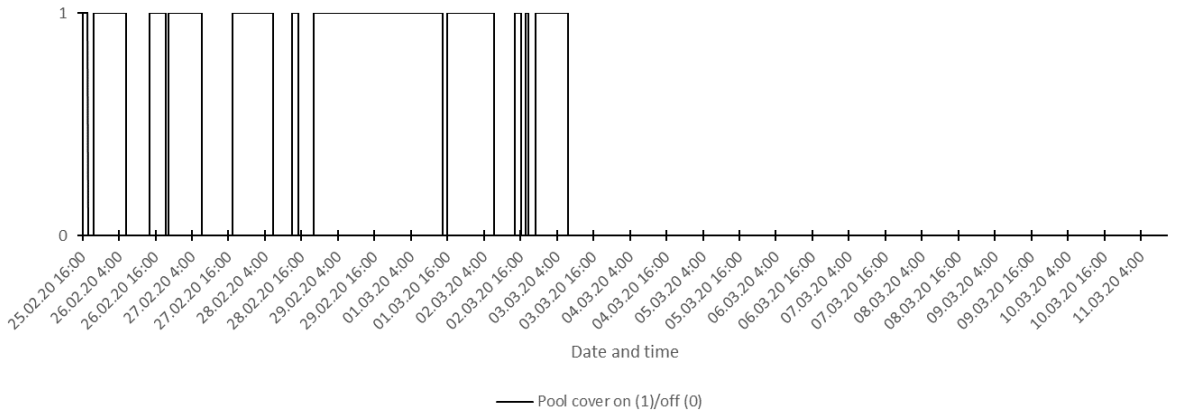

Figure 4-5: Pool cover

From theory, it is known that a reduced ambient air temperature of the pool will increase the evaporation rate, and that the opposite is observed for higher temperatures. During the period of measurements, the setpoint air temperature is altered to verify this phenomenon. The return air temperature setpoint is shown in Figure 4-6.

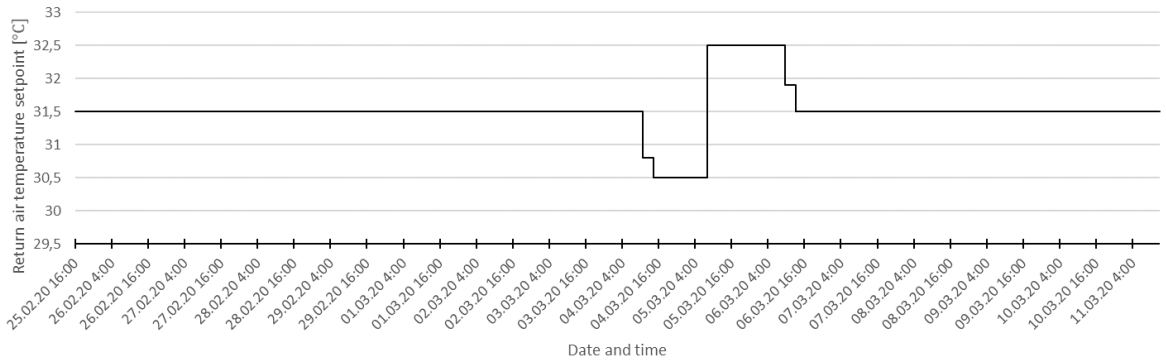

Figure 4-6: Return air temperature setpoint

4.1.4 Calculation of evaporation rates

The evaporation rate from the swimming pool is estimated by the mass balance in equation 5.1, presented in section 2.1.4. It requires the volume flow rate, density, and absolute humidity of the supply air, return air and infiltrated air, as well as the volume and change in vapor pressure and temperature of the swimming pool hall.

$$\dot{m}_{evap} = \dot{m}_{v,return} - \dot{m}_{v,supply} - \dot{m}_{v,inf} + \frac{dm_{v,room}}{dt} \tag{4.1}$$

Combining equation 2.9 - 2.11, the following expression is achieved:

$$\dot{m}_{evap} = \left(\frac{p_a}{\frac{R}{M}T}\dot{V}x\right)_{return} - \left(\frac{p_a}{\frac{R}{M}T}\dot{V}x\right)_{supply} - \left(\frac{p_a}{\frac{R}{M}T}\dot{V}x\right)_{inf} + \left(\frac{V}{\frac{R}{M}}\left(\frac{p_v}{T}\right)\frac{d}{dt}\right) \tag{4.2}$$

The measured variables are the temperature and RH of the return and supply air (pt100 and WS-DLTc), return and supply air volume flow rate (integrated AHU sensor), and temperature and RH inside the swimming pool hall (WS-DLTc). For the temperature and RH inside the room, the upper sensor at the height of 3 meter is used, as the air at this position is assumed to be more representative for the total air volume than what it is close to the floor.

Dry air partial pressure (p_a) is calculated from the measured temperature and RH, and by combining equation 2.1 and 2.2, it is given by equation 5.1.

$$p_a = p_{tot} - p_v = p_{tot} - RH \cdot 0.61121e^{\left(18.678 - \frac{T}{234.5}\right)\left(\frac{T}{257.14+T}\right)} \tag{4.3}$$

The total air pressure, p_{tot}, is assumed to be constant 1 atm, or 101.325 kPa. Absolute humidity (x) could be calculated from equation 2.4, but in this case the excel extension *HxLib* is utilized. This program is an excel add-on which provides a library of functions that may be used to calculate various properties of humid air based on a given set of input

parameters [50]. For absolute humidity calculations, the total air pressure, temperature, and RH are given as input variables.

Infiltration volume flow rate is assumed to be equal to the difference in return air and supply air volume flow rate ($\dot{V}_{return} - \dot{V}_{supply}$), where a negative difference is assumed to represent an exfiltration. It may occur both through the outer walls and inner constructions, but in this case, it is assumed that all vapor transmission occurs through the inner construction due to visible leaks around the doors. To illustrate, if one assumes an outdoor temperature an RH of 5°C and 50%, and a temperature and RH of 20°C and 25% for the adjoining rooms of the swimming pool, the corresponding vapor mass flow rate of 50 m^3/h outdoor air infiltration and 200 m^3/h infiltration from adjoining rooms is 0.17 kg/h and 0.89 kg/h, respectively.

For infiltration ($\dot{V}_{return} > \dot{V}_{supply}$), the temperature and RH of the adjoining rooms are used to calculate $\dot{m}_{v,inf}$. As a simplification, a constant temperature of 20°C and RH of 25% is used for the entire period, based on an average of the measured variables in two adjoining rooms (WSE-DLCc). In case of exfiltration ($\dot{V}_{return} < \dot{V}_{supply}$), the upper sensor (WS-DLTc) inside the swimming pool hall, shown in Figure 4-1, was used, as it is assumed that this sensor location is more representative for the air mix inside the room.

4.1.5 ASHRAE equation

In the results, the calculated evaporation based on the mass balance in equation 4.2 is compared with the evaporation calculated with the ASHRAE equation [9] (equation 2.7). To confirm that the air velocity above the pool was within the required range for the ASHRAE equation, samples were taken three times during the measurement period, using a Swema 3000 device [51]. All the samples lay between 0.03 and 0.13 m/s, which makes the ASHRAE equation applicable.

The saturation pressure at water temperature and air dew point temperature is calculated with the Buck equation [6] (equation 2.2), with the measurements from the lower sensor (WS-DLTc) inside the swimming pool hall and the pt100 sensor in the overflow channel. When the pool cover is used, the area of the overflow channels is inserted into the equation, while the total water surface area including the overflow channels is used when the pool cover is off. Estimated activity factor, F_a, is based on the number of people in their pool and their activity level, and the complete method for how this is estimated is given in section 5.1.

4.1.6 Thermal energy gains and losses

The thermal energy needs of the swimming pool facility consist of pool water heating and heating of the supply air in the AHU. As the integrated heat pump was out of order, the

latter is obtained entirely through the heating coil. The total heat gains in the pool water circuit are assumed to be the sum of the heat obtained through the pumps, from the UV-lamp and through the primary heat exchanger, calculated as

$$\dot{Q}_{pool\ water,gain} = \dot{Q}_{P1} + \dot{Q}_{P2} + \dot{Q}_{P3} + \dot{Q}_{UV} + \dot{Q}_{primary\ heat} \quad 4.4$$

where $P1$ and $P2$ are the pumps in the main circuit, and $P3$ is the pump in the partial stream through the primary heat exchanger. The losses are calculated as

$$\dot{Q}_{pool\ water,loss} = \dot{Q}_{MW} + \dot{Q}_{BW} + \dot{Q}_{evap} \quad 4.5$$

In equation 4.5, losses through the pipes and pool walls are assumed to be negligible. The heat loss from supply of make-up water, or fresh water, ($\dot{Q}_{MW}$) is calculated from measurements of temperature and mass flow rate of the incoming water, and temperature inside the balance tank. The temperatures are measured with pt100 sensors (WS-DLTa-p100), while the mass flow rate is extracted from logged data in the monitoring system of the plant. $\dot{Q}_{MW}$ is then expressed as

$$\dot{Q}_{MW} = \dot{m}_{MW} c_{p,water} (T_{balance\ tank} - T_{MW}) \quad 4.6$$

where $c_{p,water}$ is assumed to be constant 4187 J/kgK.

In the simulations, the ventilation loss, or the net energy lost through the AHU exhaust, will be calculated from equation 4.7:

$$\dot{Q}_{vent,loss} = \left(\dot{m} c_p T\right)_{ea} - \left(\dot{m} c_p T\right)_{fa} \quad 4.7$$

4.2 IDA ICE models

A detailed model of the swimming pool facility at Dalgård is built in the building performance simulation package IDA ICE. This section describes the process of developing the model, and simplifications made are highlighted.

4.2.1 Building models

When creating a project in IDA ICE, it is possible to work in various folders depicted in Figure 4-7. In the *general* tab, it is possible to change the global data of the building. These includes, among others, the ambient climate, ground properties, orientation of the building, and the details of the constructions. It is also possible to access the HVAC systems, in this case the AHU and pool water circuit. The sizes of the building constructions are adjusted in the *floor plan* tab. In the *schematic* tab, the connections between the building constructions, HVAC systems and ambient outdoor variables are shown. The general tab and schematic view are shown in Figure 4-7 and Figure 4-8.

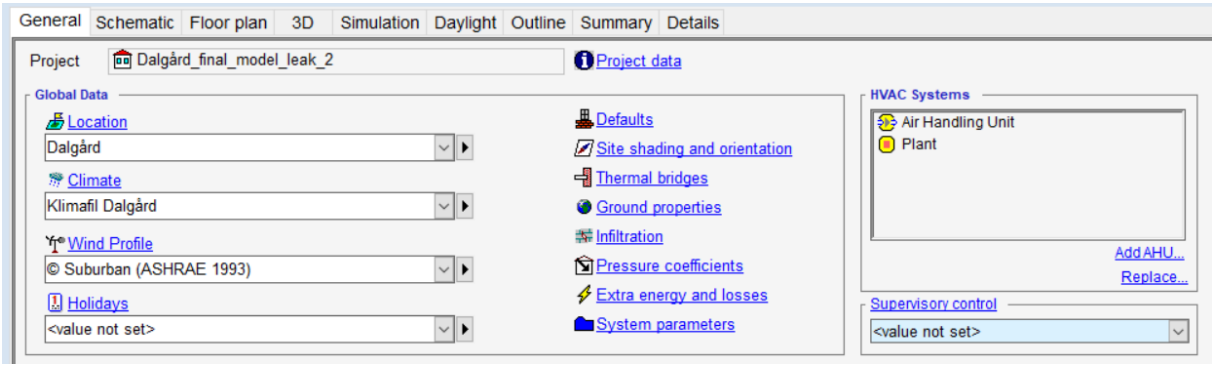

Figure 4-7: General folder of an IDA ICE model

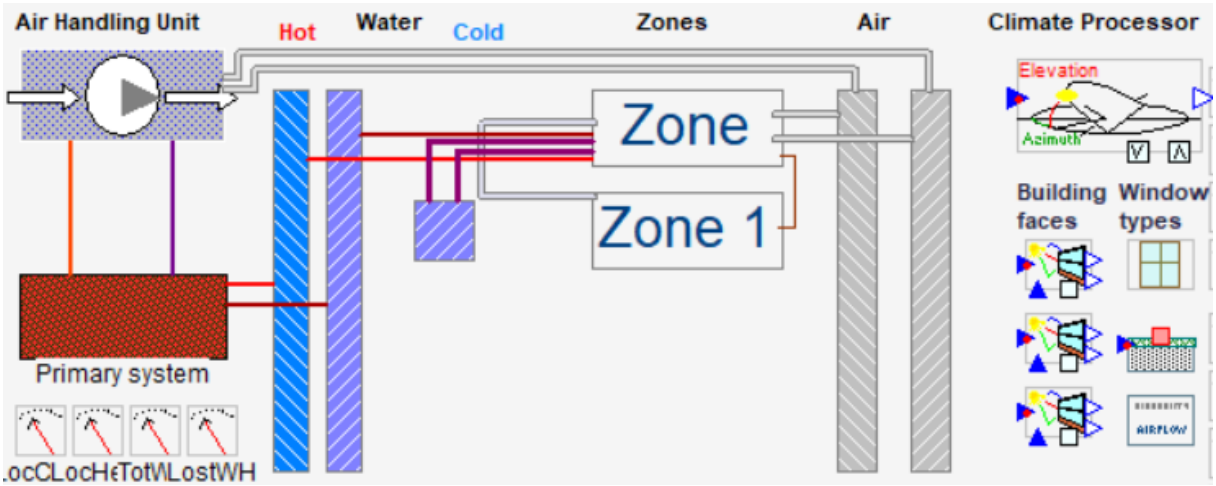

Figure 4-8: Schematic view of an IDA ICE model

For the building constructions in the model, the following is assumed. The swimming pool at Dalgård was built in 1978, and was refurbished and expanded in 2014. At the same time, the old windows were replaced with new ones with three-layer energy saving glass. For this new part, U-values according to TEK 10 are chosen, except the windows. The glazing consists of three-layer energy saving glass, with an approximated U-value of 0.8 W/m^{2}K, according to the passive house standard.

The thermal properties of the facades which was not refurbished in 2014 is assumed to fulfill the TEK 87 level of U-values. The U-values are given in Table 2-3, and the materials of the different layers in the constructions (both external and internal) are chosen based on observations. For the internal constructions, the opposite sides are given a constant temperature, based on temperature measurements in the adjoining rooms. Due to old constructions, the building model of Dalgård is given a normalized thermal bridge value of 0.1 W/m^{2}K. Figure 4-9 shows the 3D view of the IDA ICE model.

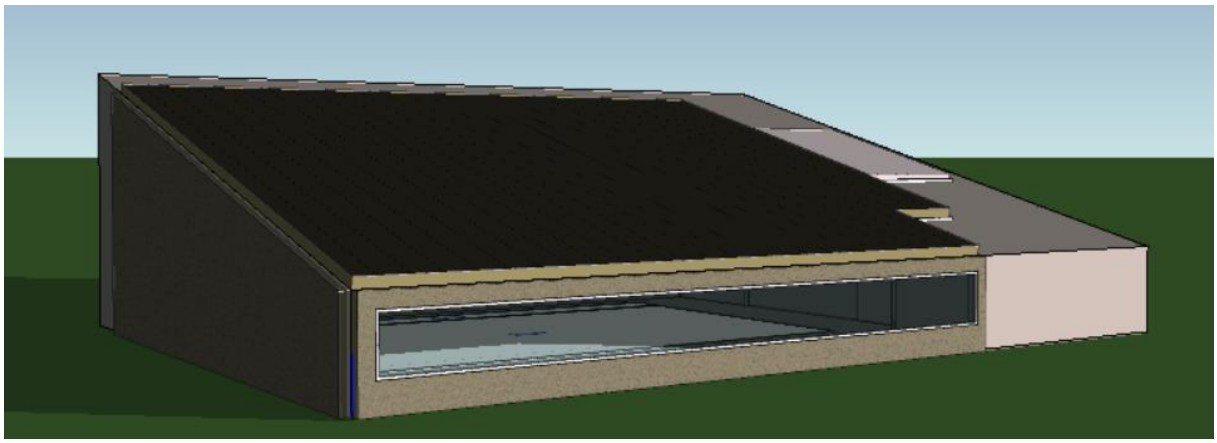

Figure 4-9: 3D view of IDA ICE model of Dalgård swimming pool

4.2.2 Climate data

All IDA ICE models need a climate file (hourly based) that sets the state of the air at the intake of the AHU and in connections with the external constructions. These files require the temperature, RH, direct and diffuse radiation, wind speed components and cloudiness, as shown in Figure 4-10. The outdoor temperature and RH are measured, while the rest of the variables are retrieved data from the nearest meteorological stations. None of these stations measure the direct and diffuse radiation, but instead, global radiation data are found. Thus, it is assumed a constant cloudiness of 100%, resulting in no direct normal radiation. Since the global radiation is the sum of direct normal radiation and diffuse radiation, the resulting diffuse radiation equals the global radiation.

Date	Variables						
	Dry-bulb temperature, Deg-C	Rel humidity of air, %	Direct normal rad, W/m2	Diffuse rad on hor surf, W/m2	Wind speed, x-component, m/s	Wind speed, y-component, m/s	Cloudness, %
2020-02-26	-6.5	71.0	0.0	57.9	-0.2	0.3	100.0
2020-02-27	-4.7	54.9	0.0	59.8	-0.1	2.1	100.0
2020-02-28	-3.4	66.8	0.0	55.2	-0.2	0.7	100.0
2020-02-29	-2.5	81.2	0.0	89.9	-0.3	0.5	100.0
2020-03-01	-3.7	68.0	0.0	33.3	-3.1	-2.4	100.0
2020-03-02	-1.6	70.7	0.0	67.5	-3.1	-3.0	100.0
2020-03-03	-0.7	61.6	0.0	75.0	-1.2	-0.9	100.0
2020-03-04	-0.0	68.6	0.0	24.9	-1.4	-0.3	100.0
2020-03-05	0.6	82.8	0.0	57.7	0.9	1.3	100.0
2020-03-06	2.3	62.9	0.0	54.1	1.3	1.7	100.0
2020-03-07	0.8	57.4	0.0	89.6	0.8	2.6	100.0
2020-03-08	5.6	63.4	0.0	24.2	0.5	5.3	100.0
2020-03-09	4.5	75.9	0.0	49.2	1.0	1.6	100.0
2020-03-10	3.4	70.1	0.0	78.7	-0.2	2.6	100.0
2020-03-11	4.6	67.1	0.0	44.3	0.9	2.2	100.0
mean	-0.4	68.3	0.0	57.8	-0.3	0.9	100.0
mean*357.0 h	-131.6	24368.0	0.0	20648.1	-117.0	326.5	35700.0
min	-6.5	54.9	0.0	24.2	-3.1	-3.0	100.0
max	5.6	82.8	0.0	89.9	1.3	5.3	100.0

Figure 4-10: Climate file

The x (west → east) and y (south → north) component of the wind is calculated from the hourly averages of the wind speed and wind direction in degrees (360°: from north, 90°: from east). The wind measurements used in the weather file is taken from the weather station at Voll (distance 5.5 km), while global radiation data are retrieved from a station

located at Gløshaugen (distance 4 km). Maps of the location of the swimming pool and the distance to the meteorological stations are shown in Figure 4-11.

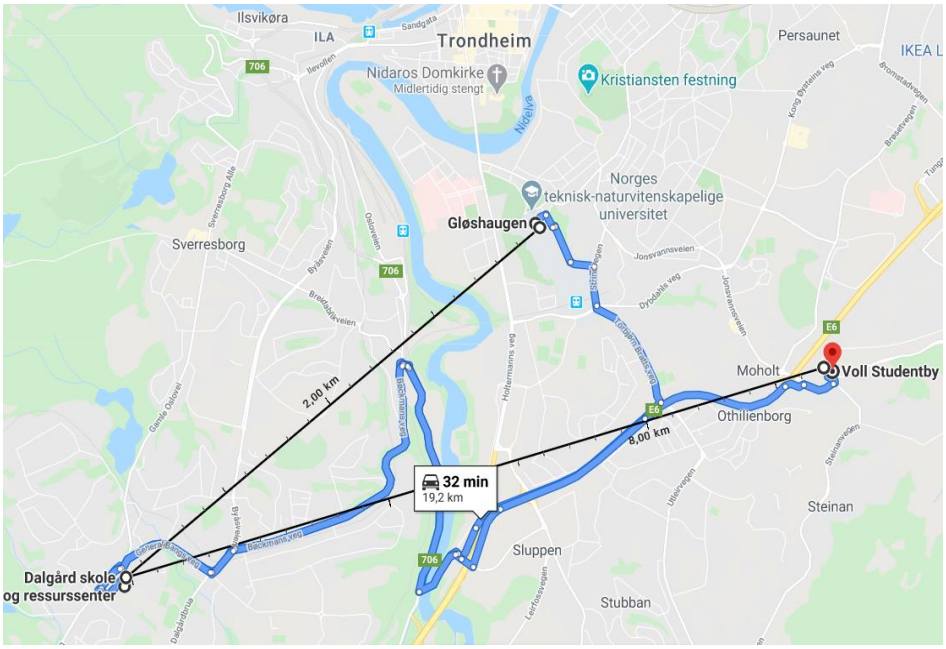

Figure 4-11: Distance between swimming pools and weather stations (Google Maps)

4.2.3 Pool model

Figure 4-12 shows the schematic view of the pool model component in IDA ICE. The pool component is connected to the pool water circuit (which is found in the model *plant*), swimming pool hall (through surface equations), and adjoining technical room (heat loss equation). In this case, the surface temperature in the adjoining room is set to constant 21°C, based on an average of measurements. The input parameters are the physical size of the pool basin, temperature setpoint and the activity factor. The evaporation rate from the water surface is calculated with the ASHRAE equation [9].

Due to the pool cover used at Dalgård, two pool model objects are included in the model: (1) the swimming area, (2) the surface area of the overflow channel. Thus, when the pool cover is used, the activity factor for the largest pool is set to 0, while the second pool has a constant activity factor of 0.8. For occupied pool, the activity factor of the largest pool is set according to the description in section 4.1.4. The pool model and water surface equations are given in Appendix J.

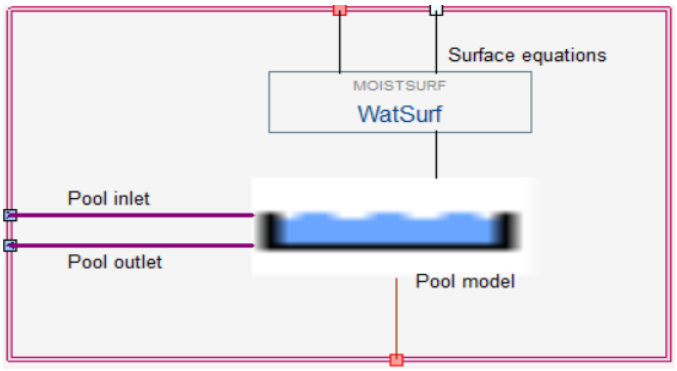

Figure 4-12: Pool models

4.2.4 Air handling unit

The BPS model of the AHU is built in accordance to the description given in section 3.2. The AHU model, including the control system, is made as a detailed copy of the installed device, with the same properties and the same components and control algorithms. Some simplifications are nonetheless inevitable due to limitations in the IDA ICE component library. Figure 4-13 shows the model of the AHU at Dalgård in a schematic view, with its physical components, and the control strategies hidden in their own *macro objects*. The macro object is a utility model from the component library, which can be used to hide control algorithms or other parts of the model to make the structure tidier.

The AHU object is connected to the zone model (swimming pool hall) through air terminals located outside the object. These terminals, and the fans, receives the signal from the control strategies, determining whether the AHU should run with minimum or maximum volume flow rate. In addition, the model is connected to the climate file, and the heating coil is connected to a primary heating boiler located in the plant, given a heat capacity in accordance with the description found in the user manual of the AHU. The heat pump is omitted since it did not run during the period of measurements. All components are further described in section 4.2.5.

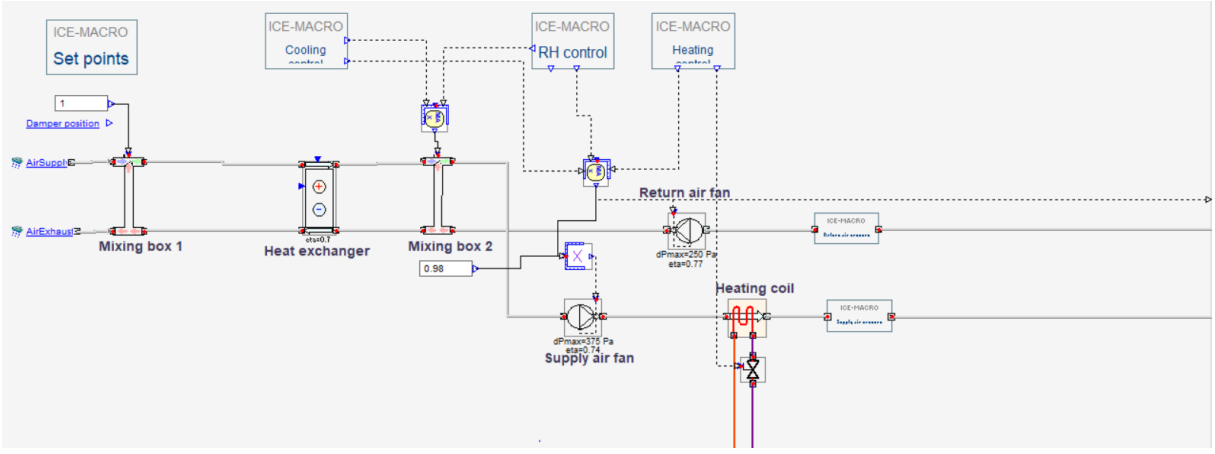

Figure 4-13: Schematic view of the AHU model for Dalgård

4.2.5 AHU components

Two *mixing boxes* components are used to achieve an approximately equal property as the dampers in the real unit shown in Figure 3-3. A signal between 0 and 1 controls how much of the return air is recirculated before (mixing box 2) and after (mixing box 1) the crossflow heat exchanger. Figure 4-14 shows the interfaces of the component and its input parameters and input/output variables. If either the cooling control or RH control request the minimum fresh air proportion, the damper of mixing box 2 in Figure 4-13 opens to the position where $\frac{\dot{m}_{supply,in}}{\dot{m}_{supply,out}} = control\ signal = \dot{m}_{fresh\ air,min}$, see Figure 4-14.

In bathing mode, the dehumidification damper (labelled 12 in Figure 3-3) is always closed, and thus the damper of mixing box 1 in position 1 (no recirculation after the dehumidifier). In this way, the fresh air proportion of the supply air will always be equal to the control signal sent to mixing box 2. In night mode, the fresh air proportion of the supply will often be smaller than the control signal of mixing box 2, as the dehumidification damper is not always closed. The component code is given in Appendix C.

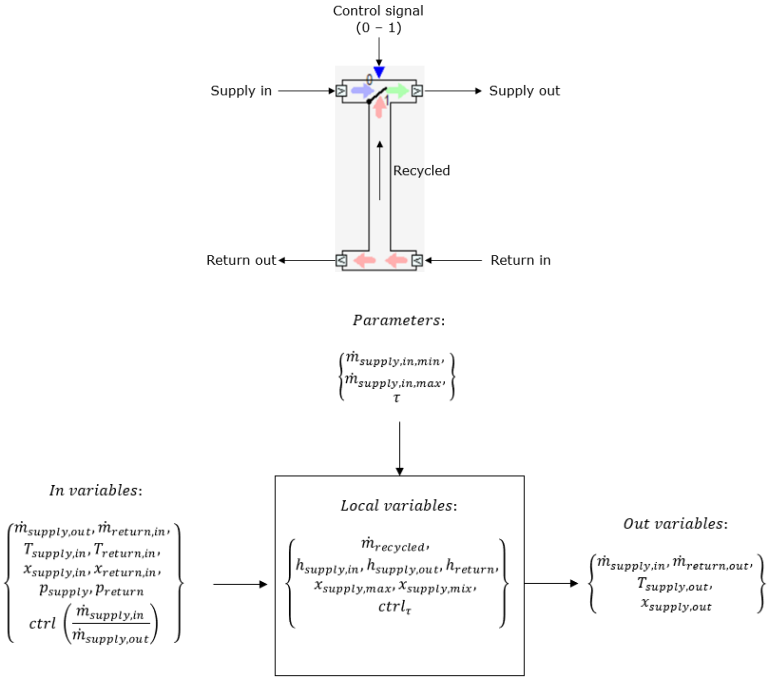

Figure 4-14: Illustration of the IDA ICE mixing box

To represent the real crossflow heat exchanger, the air-to-air latent heat exchanger shown in Figure 4-15 is utilized. The input parameters of this model are a supply side effectiveness, η, and its corresponding rated volume flow rate, $\dot{V}_{\eta}$, and a minimum allowed leaving temperature. A modified effectiveness, η', for volume flows other than the rated is calculated based on the two former parameters. It is also possible to give a setpoint for the leaving supply air temperature and control the device with a control signal. In this case the control signal should always be 1 (heat exchange does always occur) and the

temperature setpoint is set to 40°C to not limit the heat exchange. In the real heat exchanger, there is an air pressure drop through the unit. The model component has no pressure drop.

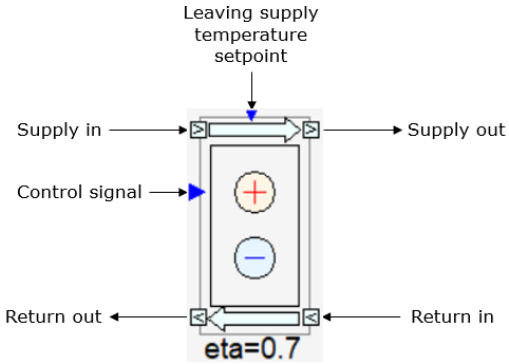

Figure 4-15: IDA ICE air-to-air heat exchanger

Based on the input parameters and the variable states of the entering supply and return air, the actual heat transfer and states of the leaving airflows are calculated. The method is similar to the Number of Transfer Units (NTU) Method [52], which is used in cases where only the inlet temperatures of the heat exchanger are known. Possible condensation on the heat transfer surface is taken into account in the model. It proceeds by calculating the available heat transfer, $\dot{Q}_{available}$, by using η'. $\dot{Q}_{available}$ is used to find an attainable leaving supply air temperature, which is finally used to calculate the actual heat transfer $\dot{Q}_{actual}$. A compressed code is given in Appendix D.

The fans take the pressure rise at maximum volume flow rate (dp_{max}), the total efficiency (η_{tot}), the motor efficiency (η_{motor}) and the rated volume flow rate ($\dot{V}_{rated}$) as input parameters, and calculates the power supply ($\dot{Q}_{fan}$) of the fans and the outlet temperatures (T_{out}) based on the mass flow rates ($\dot{m}_a$) and states of the inlet airflows ($\rho(T_{in}, x_{in})$).

Figure 4-16 shows the interfaces of the component, and the equations are given in Appendix E. The maximum pressure rise is adjusted to compensate for the lack of pressure drop trough the crossflow heat exchanger, and through the filters found in the real unit.

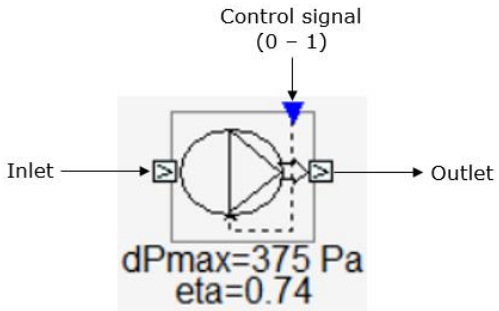

Figure 4-16: IDA ICE fan

Figure 4-17 shows the heating coil used in the model. The component has many parameters and variables, where the known parameters are adjusted so that the unit provides the same heat transfer under rating conditions as the real unit. A counterflow configuration is chosen, as this is believed to be in line with reality. The model uses the NTU method to calculate the actual heat transfer rate ($\dot{Q}$) and the outlet temperatures ($T_{air,out}, T_{water,out}$). A simplified code is given in Appendix F.

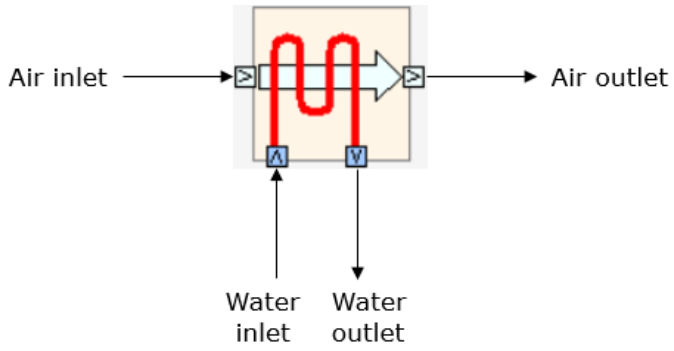

Figure 4-17: IDA ICE heating coil

The heating coil valve component, shown in Figure 4-18, is a much simpler model, with maximum mass flow rate ($\dot{m}_{max}, control\ signal = 1$) and minimum mass flow rate ($\dot{m}_{min} \approx 0, control\ signal = 0$) as input parameters. For $\dot{m}_{min} = 0$, the variable mass flow rate through the valve is given by $\dot{m} = \dot{m}_{max} \cdot (control\ signal)$.

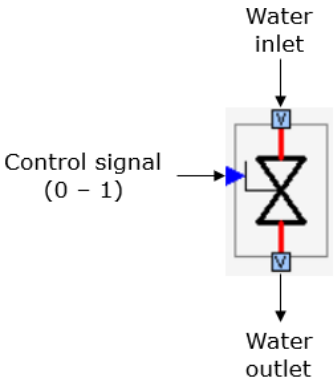

Figure 4-18: IDA ICE valve

A standard boiler is used both for heating of water to the heating coil and for heating of pool water. The standard boiler in the IDA ICE library has six interfaces, where the four depicted in Figure 4-19 are used in this model. Among the input parameters are the boiler efficiency (η_{boiler}), maximum heating capacity ($\dot{Q}_{max}$), pump efficiency (η_{pump}), outlet temperature setpoint ($T_{out,set}$) and outlet pressure at full pump speed ($p_{set,max}$). The model equations are found in Appendix G.

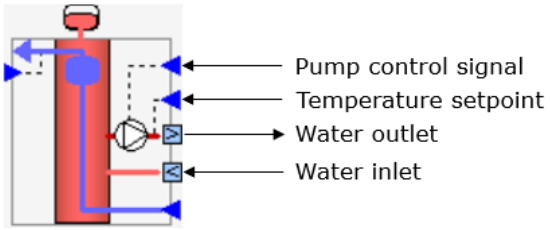

Figure 4-19: IDA ICE standard boiler

4.2.6 AHU control strategies

In this section, the construction of the RH control strategy, presented in section 3.2, is described. The other control strategies are made in a similar manner.

Figure 4-20 shows the inside of the RH control macro hidden in the schematic view of the AHU model in Figure 4-13. Yet another three macros are found within the RH control macro. The output signal from the RH controller (upper macro) is sent through measure links to the other macros; one for the night mode control strategy, another for the bathing mode control strategy. Based on a reference from the operation schedule, logical *switch* components decide which of these strategies that are used to control the actuators inside the AHU model.

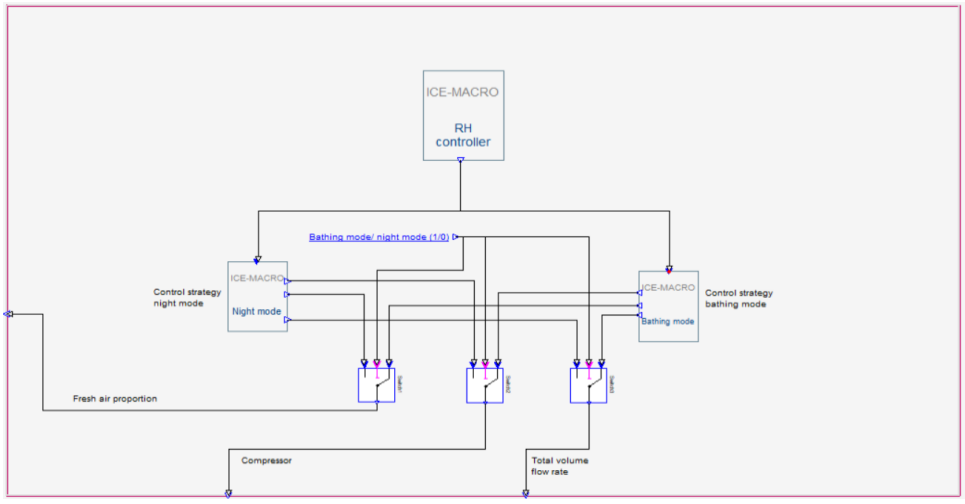

Figure 4-20: IDA ICE RH control macro

The RH controller macro is shown Figure 4-21. It contains the controller macro, neutralizer, and links to the measured RH, setpoint and controller output signal.

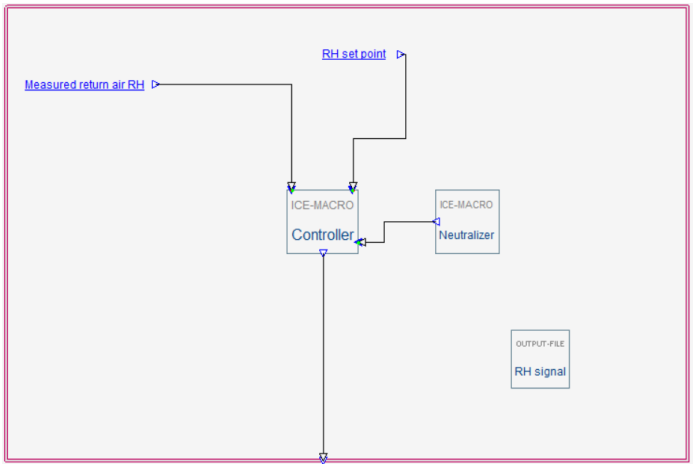

Figure 4-21: RH controller macro

The PI controller depicted in Figure 4-22 is constructed by Ole Smedegård. It contains a proportional term and an integrator term, which are tuned to achieve a satisfactory performance of the controller. The *Limiter* component limits the controller output signal, whose signal range is set according to observation of the monitoring signal in the real unit.

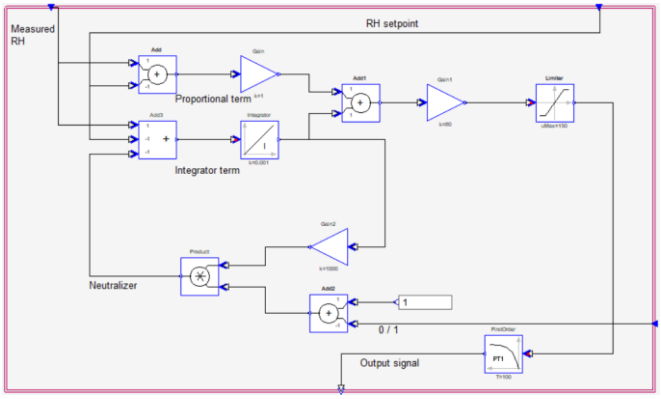

Figure 4-22: RH PI controller. Credit: Ole Smedegård

Due to lack of knowledge about the PI controllers in the MENERGA ThermoCond 37 AHU, the controllers are constructed according to the description of the controllers in another commonly used AHU in swimming pools, MENERGA ThermoCond 39 [53]. They operate as P controllers up to a certain deviation, where the integrator term is activated. The integrator term remains active until the deviation becomes equally large at the opposite side of the setpoint. For instance, the integrator term of the RH controller is activated when the measured return air RH is 2% higher than the setpoint, and remains active until the measured RH becomes 2% below the setpoint. At this point, the controller is neutralized. The controller is illustrated in Figure 4-23.

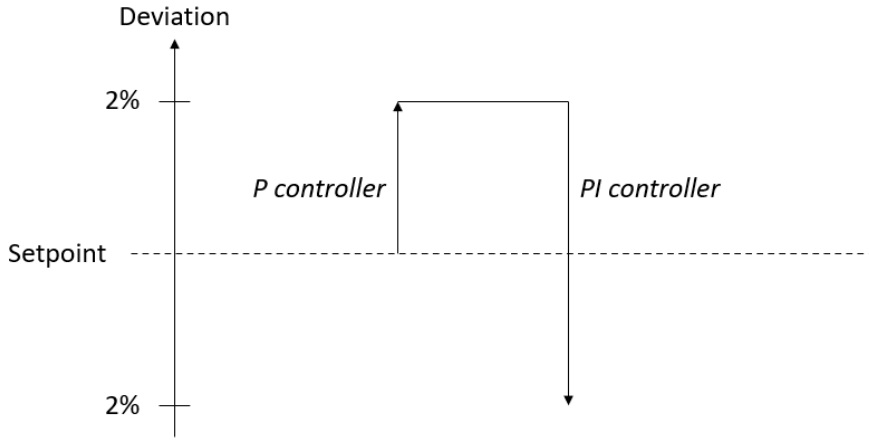

Figure 4-23: RH controller hysteresis. Idea: Ole Smedegård

It is assumed that the controllers operate with this PI hysteresis characteristic in both bathing mode and night mode. The model of the neutralizer algorithm is shown in Figure 4-24. In addition to the PI hysteresis, a logical statement which says that the integrator term should only be included if the controller output signal is within the range set in the limiter in Figure 4-22. This is ensured by the lower input of the logical *AND* component, whose output is true only of both inputs are true. The integrator term of the controller is neutralized if the output signal from the *switch* component becomes 0.

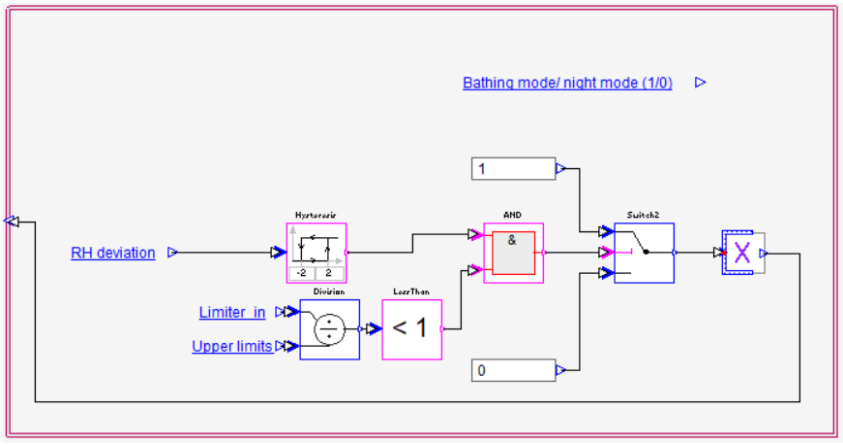

Figure 4-24: Controller neutralizer

The algorithms of the different levels of the RH control strategy in bathing mode for the AHU at Dalgård are shown in Figure 4-25. Various logical components are utilized in order to achieve similarity with the description given in section 3.2.1.2. Figure 4-26 shows how piecewise proportional controllers are used to convert the controller output signal to a value between 0 and 1, which in this case is used to release the minimum fresh air proportion. The piecewise proportional controller can also be used to make stepless controls, by adding more x-coordinates, which is used in the third level of the control strategy, according to the description in section 3.2.1.2.

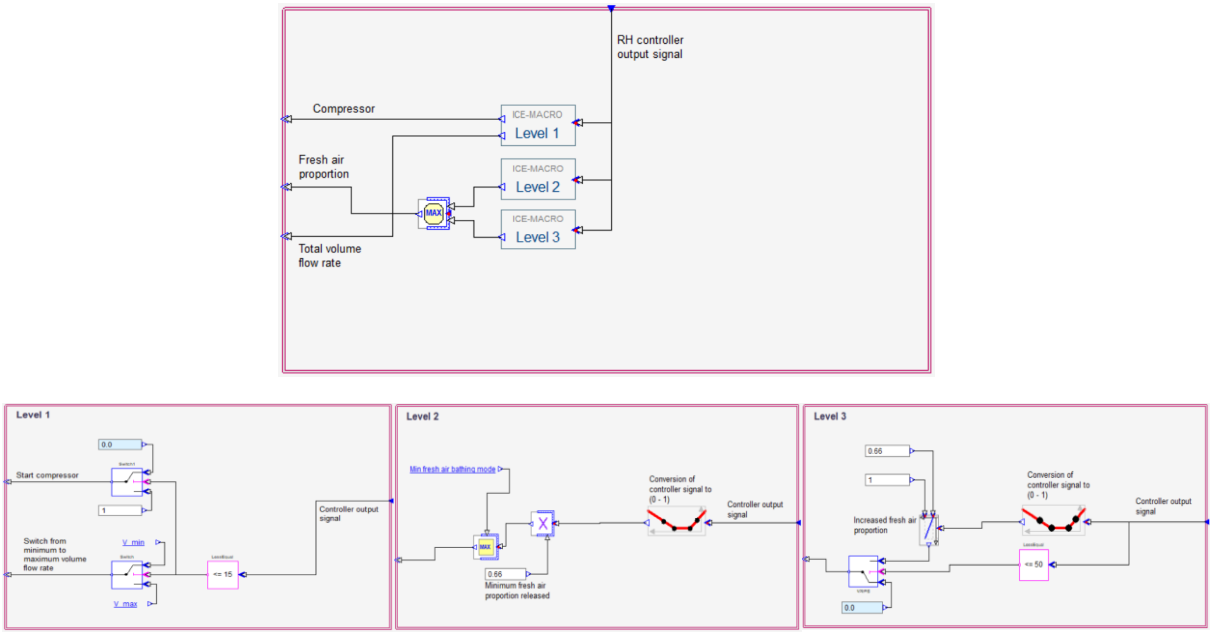

Figure 4-25: Levels of RH control, bathing mode

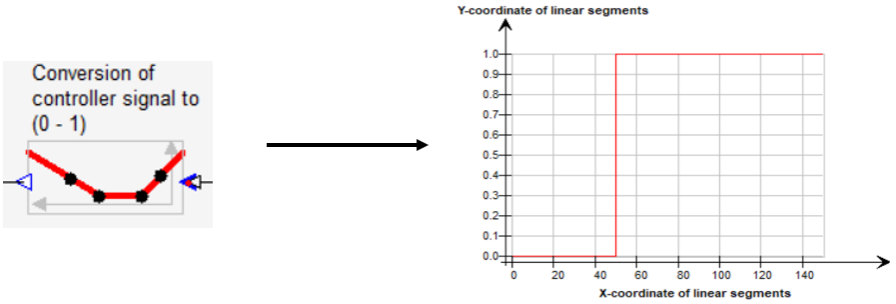

Figure 4-26: IDA ICE piecewise proportional controller

4.2.7 AHU model with heat pump

A second model of the AHU at Dalgård is made to investigate how the heat pump will affect the results if it was running. As there are no heat pump models in the IDA ICE library including both an air condenser and water condenser, an air to water heat pump is utilized. The water circuit at the condenser side of the heat pump is connected to the air condenser and pool water condenser through a self-constructed solenoid valve (Figure 4-28) hidden in the macro shown in Figure 4-27. The control macro works in such a way that the water is fed to the air condenser when there is a need for heating of air, while it is fed directly to the pool water condenser when the air temperature inside the swimming pool hall is too high.

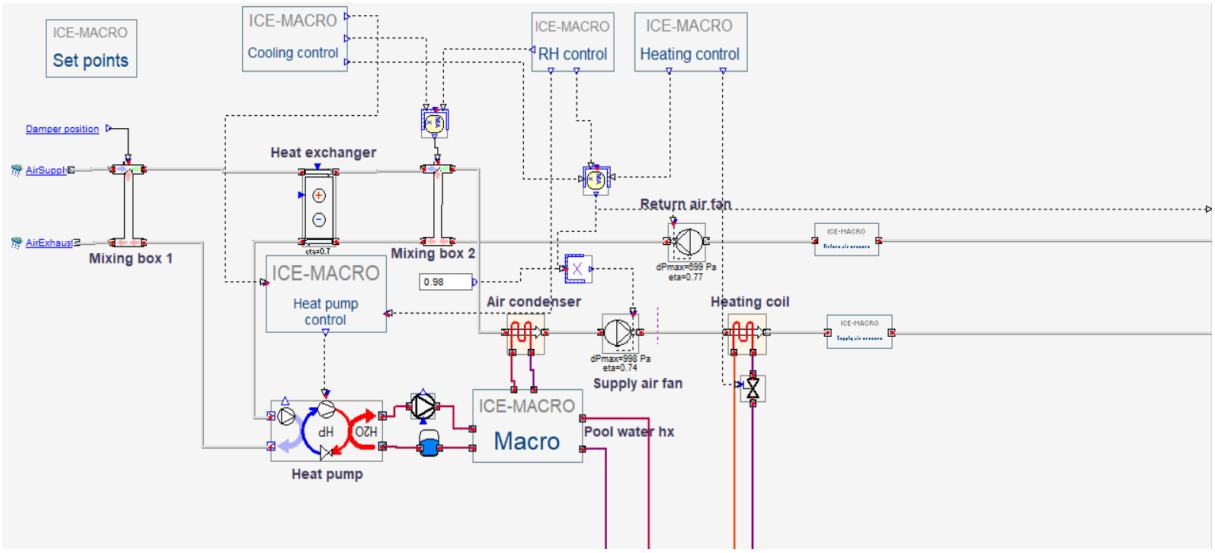

Figure 4-27: Schematic view of the AHU model for Dalgård, including the integrated heat pump

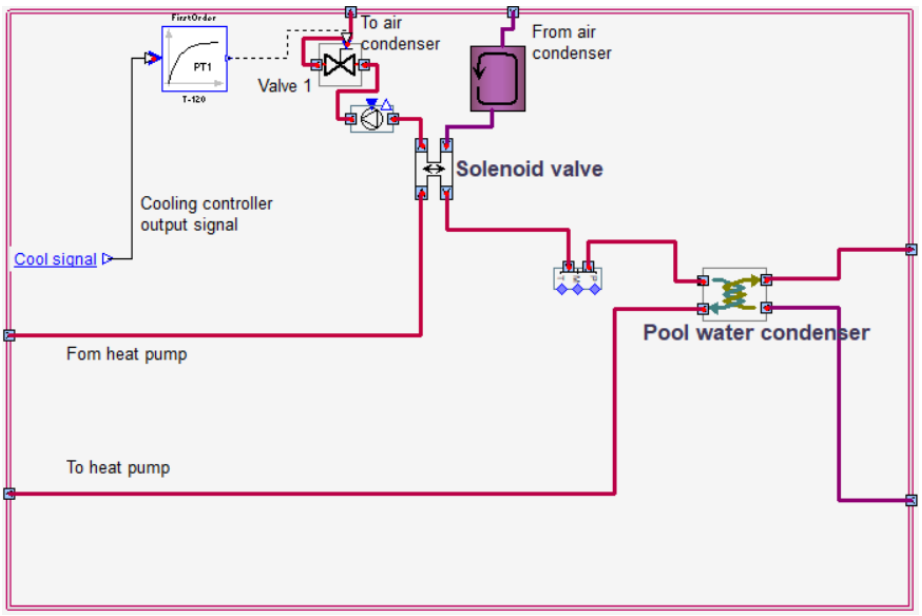

Figure 4-28: Condenser side of heat pump circuit

Figure 4-29 shows the air to water heat pump used in the model. The control signal received from the RH and cooling control strategies determines the operation of the compressor, according to the description given in section 3.2. Among the input parameters, the total heating capacity and COP are adjusted according to the description of the real units.

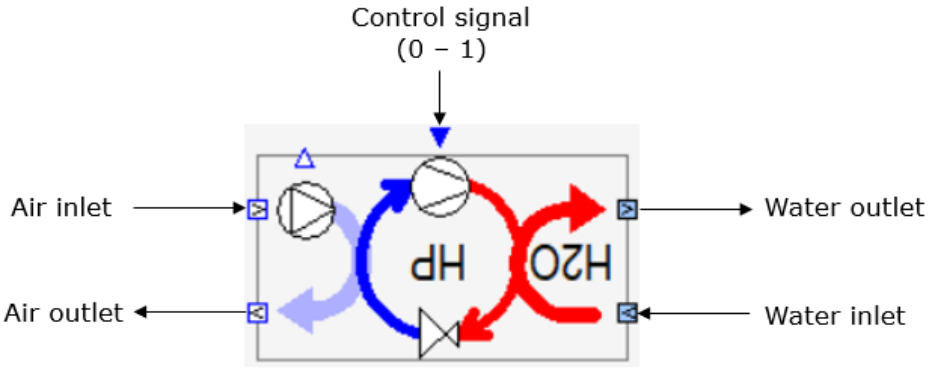

Figure 4-29: IDA ICE air to water heat pump

4.2.8 Pool water circuit

The model of the pool water circuit at Dalgård is shown in Figure 4-30, and the balance tank interconnections hidden in the macro is shown in Figure 4-32. It is a simplified version of the real system, but contains the most important components in terms of energy balance. Also included in the model plant is the heat source for the AHU heating coil.

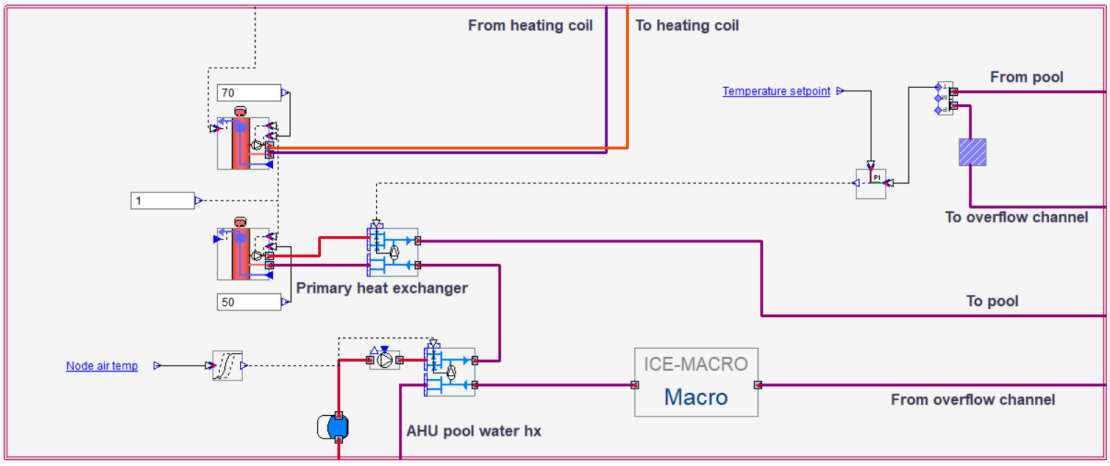

Figure 4-30: Schematic view of the pool water circuit model for Dalgård

To represent the partial flow to the primary heat exchanger, PH, illustrated in the system sketch in Figure 3-2, the model component *PMTMultiT*, shown in Figure 4-31, is used. It is an idealized liquid temperature controller with multiple possible heating/cooling source links. In this case, the input parameters are the amount of circulation in the pool water circuit ($\dot{m}_{circ}$) and the maximum mass flow rate from the boiler ($\dot{m}_{heat,max}$). A PI controller, which compares the measured pool water temperature and setpoint, gives a signal ($ctrl$) that controls the mass flow rate from the boiler ($\dot{m}_{heat}$), and thus the heat transfer. The model equations are found in Appendix H.

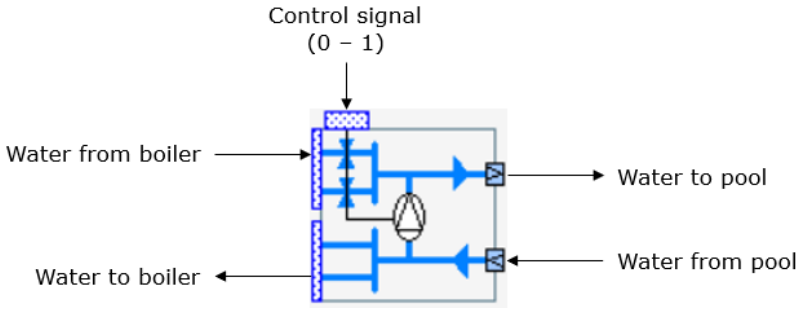

Figure 4-31: IDA ICE *PMTMultiT* component

4.2.9 Balance tank

The balance tank is assumed to have no stratification, due to the high stirring of water observed in reality. As shown in Figure 4-32, the inlet flows are the return water from the overflow channel, make-up water directly into the tank, and make-up water through the backwash heat exchanger. The backwash amount of 7000 liters per week is evenly distributed to a value of 0.011574 kg/s, with the same temperature as the balance tank outlet. The model equations for the tank is found in appendix I.

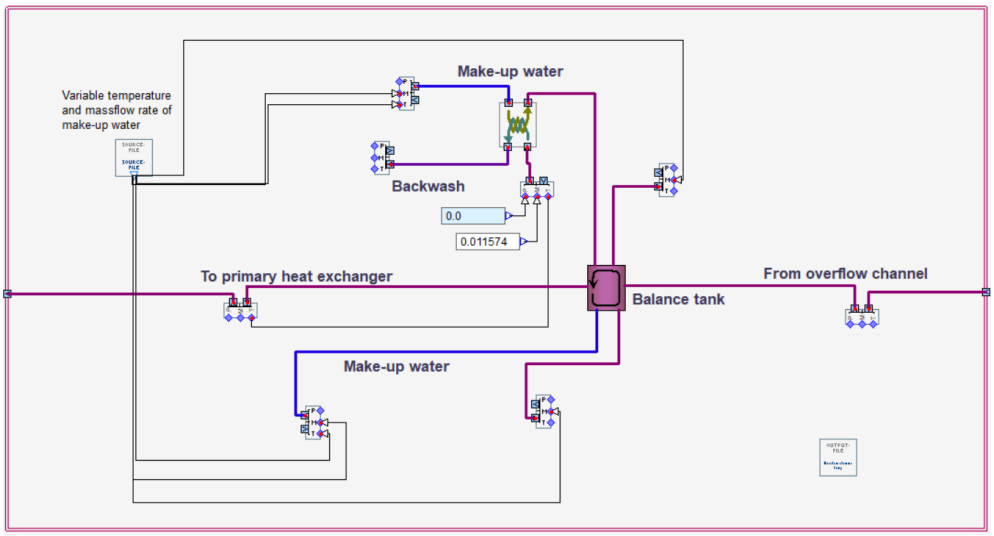

Figure 4-32: Balance tank model

A variable mass flow rate and temperature of the entering make-up water is achieved by utilizing a *source file*, which is an object that makes it possible to feed the model with a set of variable data in the columns of a text file. In this case, the source file contains the real measured mass flow rates and temperatures of the two different make-up water inlets shown in Figure 4-32.

4.2.10 Summary of simplifications and assumptions

The IDA ICE model consists of components treated as nodes described by stationary equations. Thermal inertia is absent, and the setpoints of different variables are easier to keep than in the real facility. In addition, the following simplifications and assumptions are made:

- Surface temperatures in adjoining rooms are assumed constant. These temperatures are based on an average of measurements.
- In the climate files, wind and radiation data are not measured on site, but retrieved from the nearest possible weather stations. The sky is assumed to be overcast, with no direct radiation. Temperature and RH are taken from onsite measurements, and thus in line with reality. Air pressure is assumed to be 1 atm.
- Filters are not included in the AHU models (not possible in IDA ICE), and the pressure rise through the fans is adjusted to achieve reasonable pressures at the air terminals in accordance with reality.
- Dampers are excluded from the model and instead replaced with two mixing boxes: one for return air recirculation before the crossflow heat exchanger and fresh air proportion control, and another for exhaust air recirculation after the dehumidifier.
- The integrated heat pump with refrigerant R407C is replaced by an air-to-water heat pump model, thus using water as heat carrier in the air condenser and pool water condenser. However, the heat transfer rates at rating conditions are set according to the description of the real unit.
- Pumps, filters, and UV-lamp in the pool water circuit are omitted, and the model pipes have no heat loss.

5 Results

In the present chapter, results from measurements and calculations will first be compared with those coming out of simulations in IDA ICE. Both the evaporation rate and the characteristics of the various thermal systems in the plant are considered. Furthermore, it is considered what effect it could have had on the results if the integrated heat pump in the air treatment unit had worked. Finally, a sensitivity analysis of the model was carried out to see if the results it gives in different operating situations are in accordance with what one would expect from theory.

5.1 Estimated activity factors

The activity factor, F_a, is estimated as:

- $F_a = 0.8$ for the overflow channels (constant)
- $F_a = 0.6$ for the pool water surface (without pool cover)
- $F_a = 0.65$ for the pool water surface in periods of pool cleaning
- For occupied pools, the activity factor is given as:

$$F_a = 0.3753(0.0163N + 0.6222) + \frac{AL + 1}{4}(0.0163N + 0.6222) \quad 5.1$$

where N is the number of people in the pool, and AL is the activity level determined from the scale presented in Figure 4-2. This is an empirical equation that is constructed to give satisfying results for a number of people in the pool between 5 and 25.

The activity factor of 0.6 for unoccupied pool (without pool cover) is higher than the typical activity factor found in the ASHRAE Handbook [9] given in Appendix B. This is done to calibrate the correlation to the base case of no activity. It is reasonable that the activity factor should be higher for this pool, as the water temperature of 33°C is higher than the typical water temperature for public pools given in Table 2-1. From the theory, it is known that a higher water temperature will result in a higher evaporation rate. F_a = 0.65 is used for the periods where a pool cleaning robot was used inside the pool. This is due to observations of small movements in the water surface, as shown in Figure 5-1.

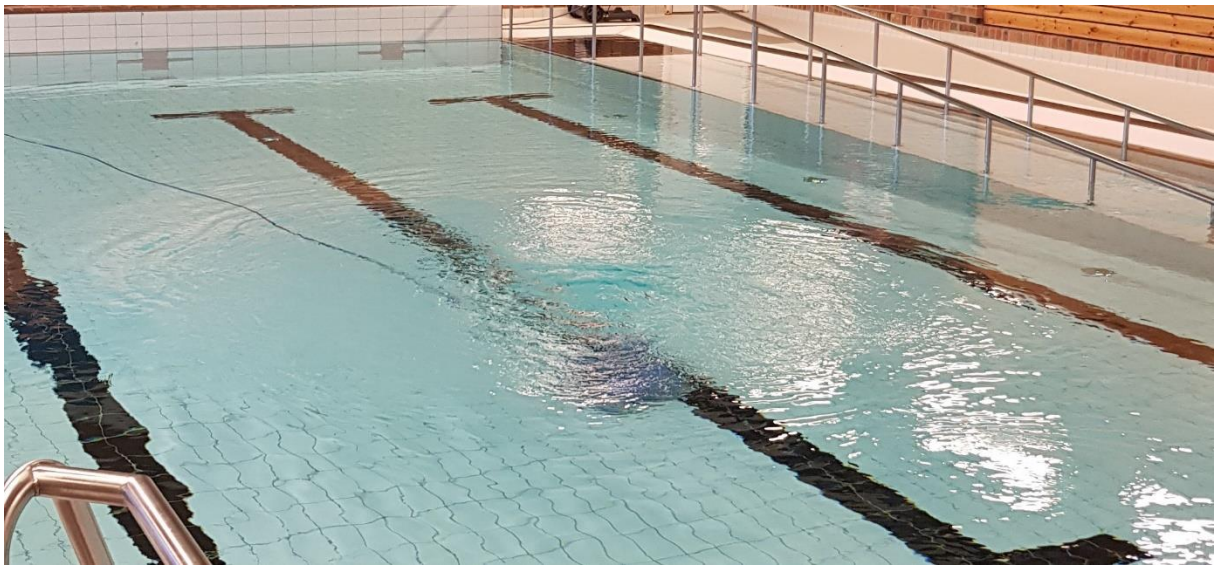

Figure 5-1: Illustration of water movements due to pool cleaning robot

When the pool cover is used, there will still be evaporation from the overflow channels. Water drops from the pool water surface into the channels, resulting in waves and higher water agitation than for unoccupied pool without pool cover. The value of 0.8 is empirical, and is chosen to fit the evaporation rate to the corresponding value obtained using the water vapor mass balance given in equation 4.2.

The utilized activity factor for occupied pools are obtained from the following procedure:

- $\dot{m}'_{evap}$ is calculated from the mass balance in equation 4.2 (minute values)
- The calculated $\dot{m}'_{evap}$ is inserted into the ASHRAE equation [9] (equation 2.7) to find F'_a
- F'_a is plotted against the corresponding registered numbers of people in the pool, to obtain to following correlation:

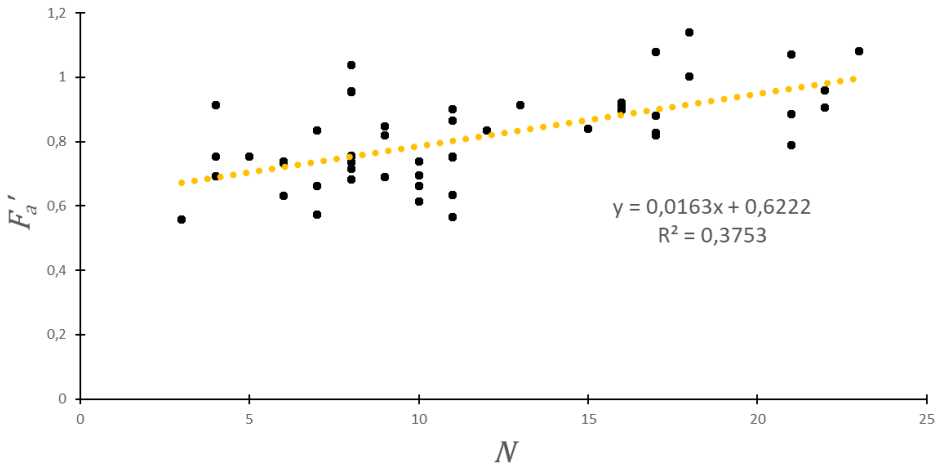

Figure 5-2: Correlation for estimating F_a

A linear trendline for the plotted values is given by the equation $y = 0.0163x + 0.6222$ with an R^2 value of 0.3753. This means that 37.53% of the correlation between F_a' and N can be explained by linearity, while the rest is due to other influencing factors [54]. In this case, the *rest* of the influencing factors on equation 5.1 is assumed to be attributed the activity level of the swimmers. The activity level (AL) is included in the second term of equation 5.1, which is tuned to obtain satisfying results.

5.2 Model validation

A good compliance between measurements and results from simulations is important for the model to be valid. In this section, the model will be validated both in terms of evaporation, air conditions, and the energy requirements for room heating and pool water heating.

5.2.1 Evaporation rates

Figure 5-3 shows the evaporation rate from the pool surface obtained from mass balance calculations (equation 4.2), ASHRAE and Shah correlations, and simulation, presented as an hourly moving average throughout the measurement period (February 25 to March 11). Included in the figure are also the setpoint temperature of the air, and during which periods the pool cover was used. It is clear that the pool cover is an effective tool, with a significantly lower evaporation rate during the periods in which it is used. The calculated (mass balance) average evaporation rate in periods of empty pool increases from 4 kg/h to 25 kg/h when the pool cover is removed. The latter is significantly higher than the typical value for unoccupied pools of 10 kg/h stated in Byggforsk [25] (Table 2.3).

The setpoint temperature in the swimming pool at Dalgård is 33.5°C, while the reference temperature for unoccupied pools given in Byggforsk is 28°C. A higher evaporation rate than 10 kg/h outside occupancy is therefore as expected. From the Buck equation [6], it can be calculated that the vapor saturation pressure at water temperature increases from 3.78 to 5.18 kPa, if the water temperature is raised from 28 to 33.5°C. A higher vapor saturation pressure at water temperature ($p_{sat,w}$) inserted into the ASHRAE equation [9], shows that the evaporation will be higher at a water temperature of 33.5°C compared to 28°C.

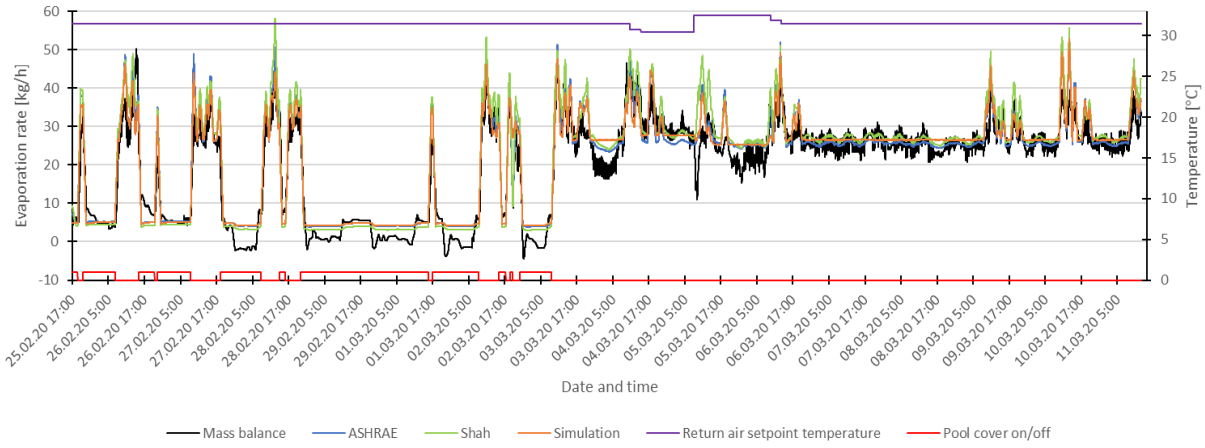

Figure 5-3: Observed evaporation rate by mass balance, different correlations and simulation

Within activity, Byggforsk [25] states a typical evaporation rate of 0.35 – 0.5 kg/m^{2}h for therapeutic pools with water temperatures between 32 and 36°C. As the size of the water surface at Dalgård is just below 100 m^2, the results shown in Figure 5-3 are in good agreement with Byggforsk within activity.

5.2.2 Correlations

Figure 5-4 shows the correlation between the evaporation rate calculated from water vapor mass balance and estimated by the ASHRAE equation [9]. On average, the estimated evaporation rate from the AHRAE equation is 9.2% higher than mass balance calculations throughout the measurement period. The coefficient of determination [54], or R^2, is 0.89, which means that there is a high linear relationship between the two methods.

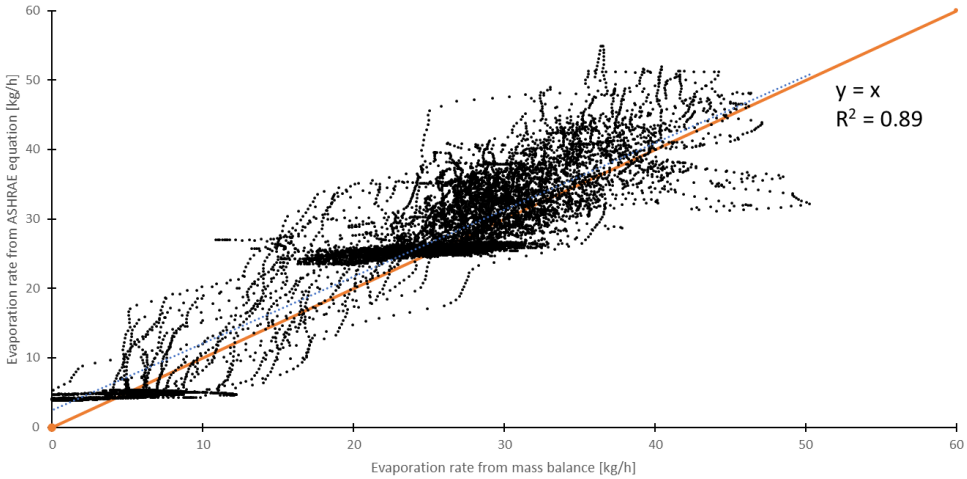

Figure 5-4: Correlation between evaporation rate calculated from mass balance and with ASHRAE equation

The relationship between calculated evaporation from mass balance and using the Shah equation [18] (given in Appendix A) is shown in Figure 5-5. It shows that the Shah equation to a larger extent overpredicts the evaporation rate, especially at higher activity levels.

This can also be observed in Figure 5-5, where the Shah equation (green line) has higher peaks than the mass balance (black line). For the entire period, the Shah equation gives, on average, a 13.7% higher evaporation rate than the mass balance calculations do. The resulting R^2 is slightly reduced, and 87% of the correlation could be explained by linearity between the two methods.

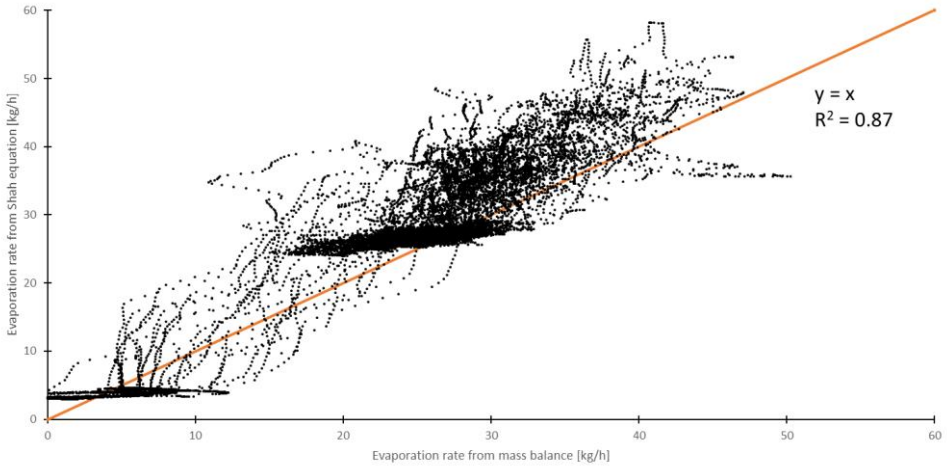

Figure 5-5: Correlation between calculated evaporation rate from mass balance and with Shah equation

A comparison between the calculated evaporation rates from mass balance and the results from simulations, shown in Figure 5-6, looks very similar to the correlation found in Figure 5-4. The similarity is as expected since the IDA ICE model calculates the evaporation rate with the ASHRAE equation. Compared to the mass balance calculations, the average evaporation rate, for the entire period, is 8.5% higher for the simulations. As for the ASHRAE equation, the R^2 value is 0.89.

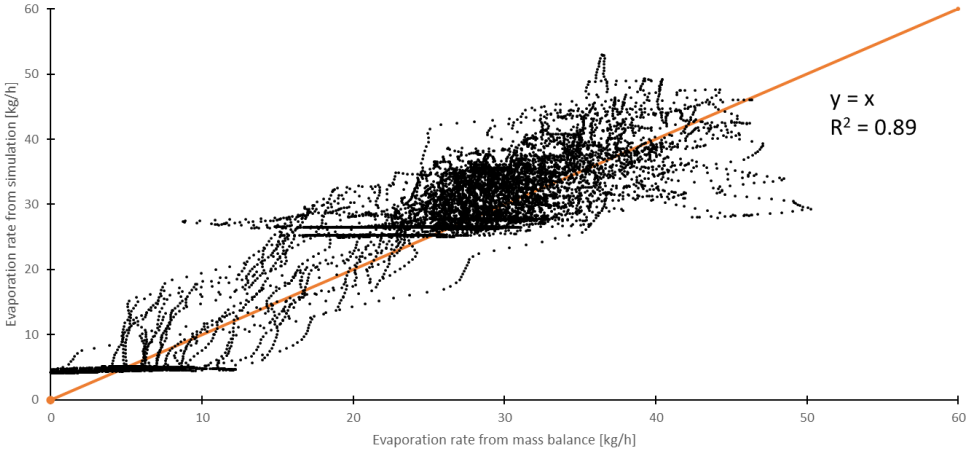

Figure 5-6: Correlation between calculated evaporation rate from mass balance and simulation

5.2.3 Effect of variable air temperature on evaporation

From the theory, it is known that the air temperature above a pool will affect the evaporation rate from the water surface. During the measurement period, the set point temperature of the air was lowered and raised from the default value of 31.5°C to study this effect. It is here chosen to look at the periods when there is no activity in the pool and the pool cover is not in use.

Comparison between mass balance and simulations

Figure 5-7 shows how the calculated and simulated evaporation rate decreases, as the temperature of the surrounding air increases due to a raised setpoint.

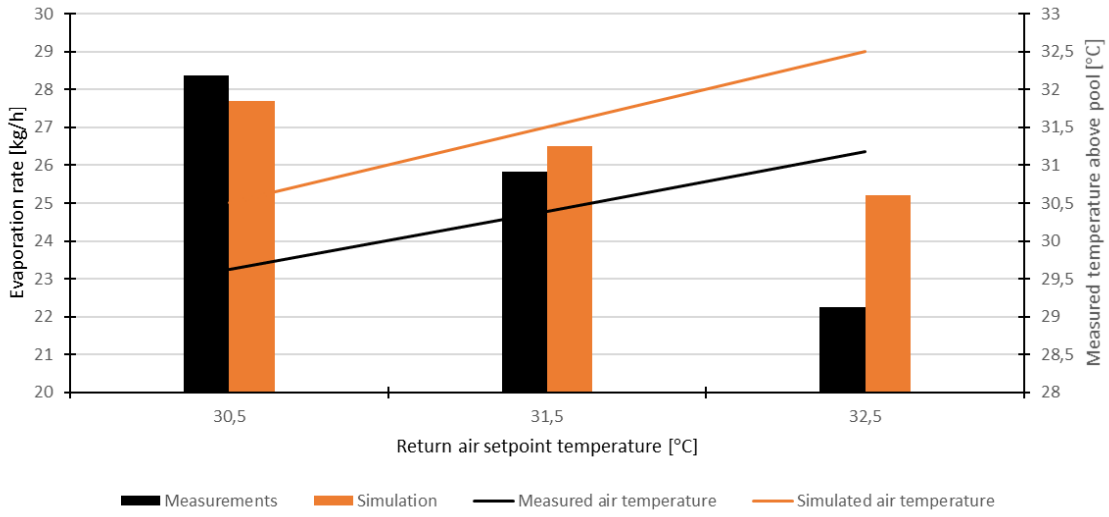

Figure 5-7: Comparison of average evaporation rate versus return air setpoint temperature for unoccupied pool (mass balance and simulation)

In Figure 5-7, it can be observed that the difference between simulated and the calculated average evaporation rate is higher at a return air setpoint temperature of 32.5°C. With a setpoint temperature of 30.5°C, the difference is 0.6 kg/h, while at a setpoint temperature of 32.5 C, it is 3 kg/h. In the model, the return air temperature is always very close to the setpoint since it does not contain any thermal inertia. This is a result of all components in IDA ICE being treated as single nodes, described by stationary equations. In the real swimming pool, on the other hand, there are large inertia, due to a large room volume and long ventilation ducts, as well as inertia in water heating for both the pool and the heating of supply air. This makes the system difficult to regulate, and differences between setpoints and measured values are inevitable. Overshoots and undershoots may occur when setpoints are changed.

Comparison between ASHRAE equation and simulations

Figure 5-8 shows the same comparison for the evaporation rates obtained in the simulations and by using the ASHRAE equation with an activity factor of 0.6 as described in section 5.1.

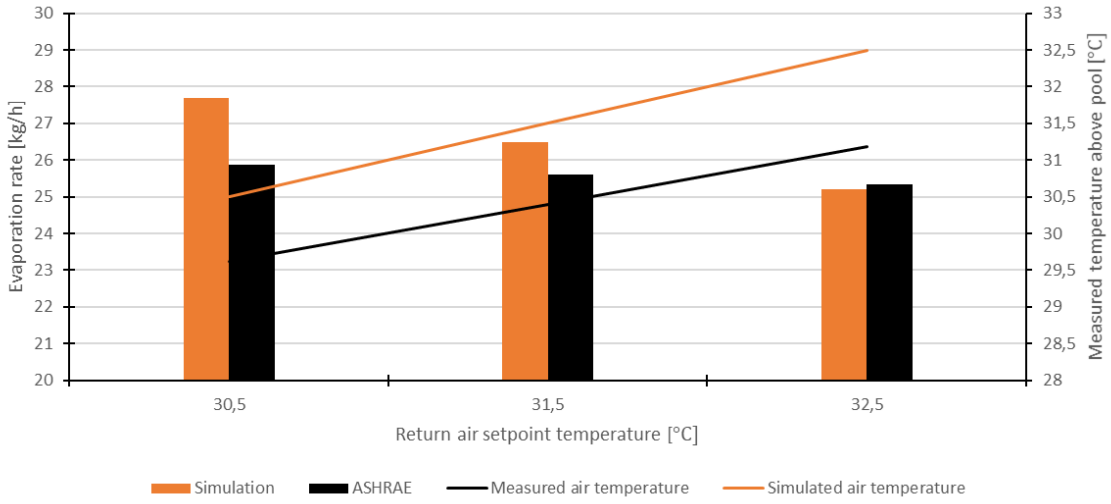

Figure 5-8: Comparison of average evaporation rate versus return air setpoint temperature for unoccupied pool (ASHRAE and simulation)

The reduced evaporation rates are explained by the ASHRAE equation [9], which, for unoccupied pools, says that the evaporation rate is only a function of the vapor saturation pressure at water temperature and air dew point temperature (the activity factor is constant). For higher dew point temperatures, and thus higher $p_{sat,dp}$, the difference $(p_{sat,w} - p_{sat,dp})$ is reduced, which results in lower evaporation rates. The same result is obtained if the water temperature, and therefore $p_{sat,w}$, is reduced.

From a Mollier chart, it can be found that a reduction in RH will result in a lower dew point temperature if the air temperature is kept constant. Figure 5-9 and Figure 5-10 shows the measured and simulated RH and water temperature for the same periods shown in Figure 5-8. A small reduction in measured RH, and a slightly higher measured water temperature can be observed at a higher return air temperature setpoint. However, the increased air temperature above the pool is in this case found to have a greater impact on the evaporation rates.

In the period with a return air setpoint temperature of 30.5°C, the measurements showed that the difference in vapor saturation pressures, $(p_{sat,w} - p_{sat,dp})$, was 2.94 kPa with the corresponding measured air temperature, RH and water temperature. At the setpoint of 32.5°C, the resulting $(p_{sat,w} - p_{sat,dp})$ was 2.87 kPa. Consequently, the estimated evaporation rate with the ASHRAE equation is lower at the setpoint of 32.5°C than at the

setpoint of 30.5°C, although there is a slightly increase in measured water temperature and reduction in RH.

For the simulations, the water temperature and RH above the pool are unchanged at the different return air temperature setpoints. Thus, the difference in vapor saturation pressures, ($p_{sat,w} - p_{sat,dp}$), is only a result of the air temperature. Consequently, Figure 5-8 shows a slightly higher variation in the evaporation rates at the different return air temperature setpoints for the simulations than for estimations with the ASHRAE equation.

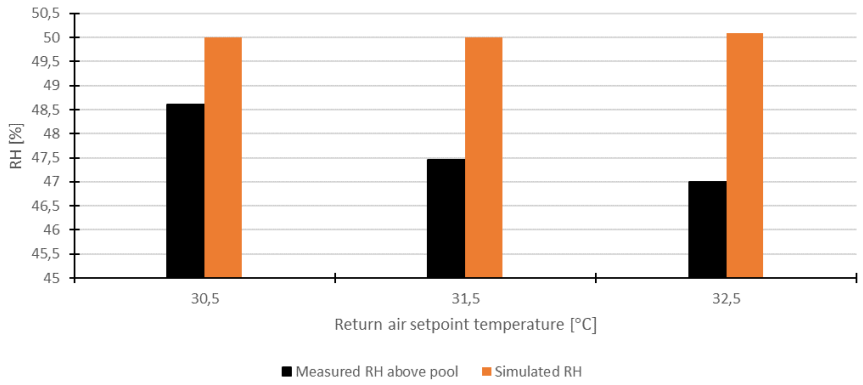

Figure 5-9: Comparison of measured and simulated RH in periods of no activity in the pool, at different return air temperature setpoints

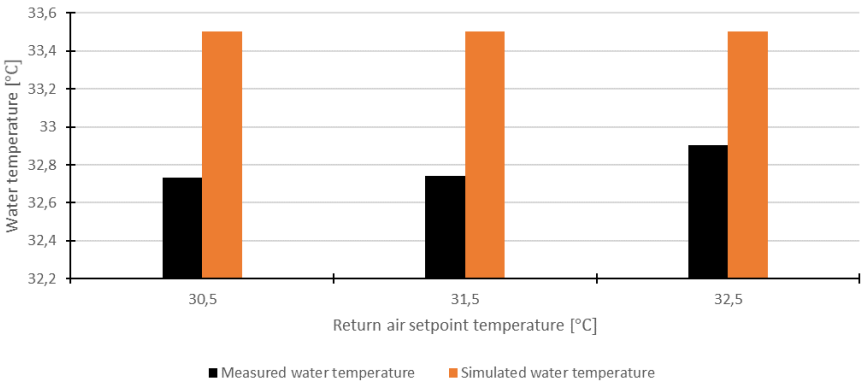

Figure 5-10: Comparison of measured and simulated water temperature in periods of no activity in the pool, at different return air temperature setpoints

5.2.4 Room air and water temperature

The results given in section 5.2.3 indicated that both the measured temperature above the pool and water temperature were lower than what was obtained in the simulations. In Figure 5-11, the measured return air temperature and measured temperature above the pool is compared with the simulated air temperature for the entire measurement period. The simulated air temperature is at the setpoint throughout the entire period, while the measured return air temperature is slightly higher. Above the pool surface, the

temperature is, on the other hand, about 0.5°C lower than the setpoint. This indicates thermal gradients that is not observable in the model, as the entire air volume is treated as a single node. However, the shapes of the curves are very similar, and the control strategies in the model AHU seems to be in compliance with the real unit.

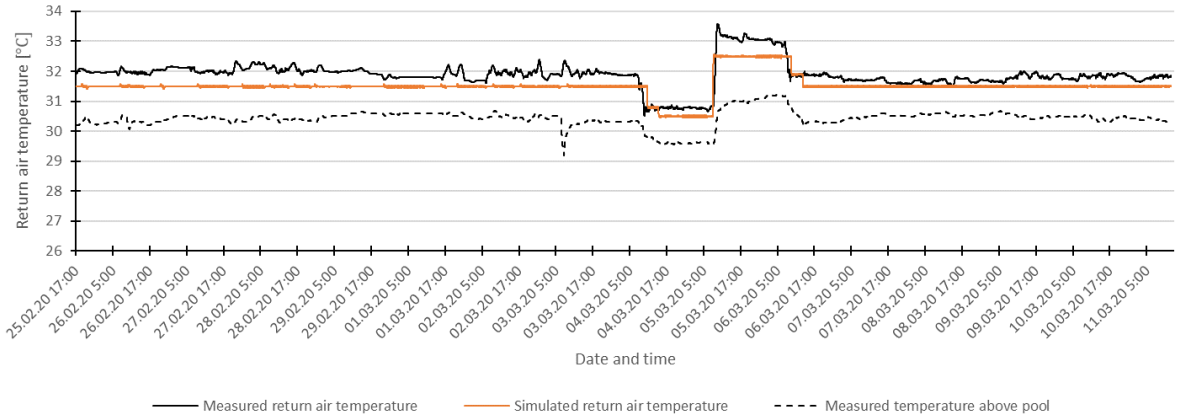

Figure 5-11: Comparison of measured and simulated air temperatures (hourly moving average)

In Figure 5-12, the measured water temperature is found to be, on average 0.7°C below the setpoint temperature of 33.5°C. It can be observed that the simulated water temperature is quite stable, close to the setpoint, while the measured temperature follows a more fluctuating manner. A reasonable explanation is the thermal inertia of the real pool water, that is not found in the model, or a small calibration error in the thermostat of the real plant.

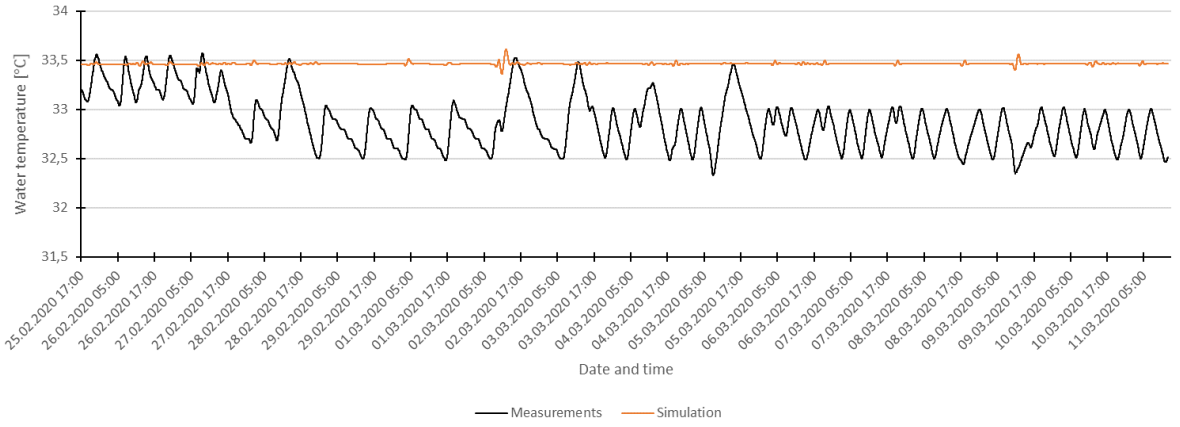

Figure 5-12: Comparison of temperature in overflow channel (hourly moving average)

As both the measured water temperature and air temperature above the pool is lower than the simulated values, the impact on the evaporation rates will be minimal. For instance, air at 31.5°C and 50% RH, and a water temperature at 33.5°C, gives a difference in saturation pressures ($p_{sat,w} - p_{sat,dp}$), of 2.87 kPa. Air at 32.5°C and 48% RH, and a water

temperature at 32.8°C gives $p_{sat,w} - p_{sat,dp}$ = 2.89 kPa. Thus, the evaporation rates presented in section 5.2.1 are not affected to any significant extent.

5.2.5 Return air characteristics

Figure 5-13 shows the measured and simulated return air volume flow throughout the measurement period. In the first half of the period, when pool cover was used overnight, the simulated volume flow rate fluctuates more between $\dot{V}_{min}$ and $\dot{V}_{max}$, than what the measured volume flow rate does. This may be due to a quicker response in the controllers within the model, than for the real controllers. In the second half of the measurement period, both the real unit and the model run with maximum airflow, which makes sense as evaporation is higher without the use of pool cover. Since the graphs show the hourly moving average of the measurements, it may appear that the volume flow rates for some periods are at a value between $\dot{V}_{min}$ and $\dot{V}_{max}$, which is not the case for this unit, which has no stepless regulation between these levels.

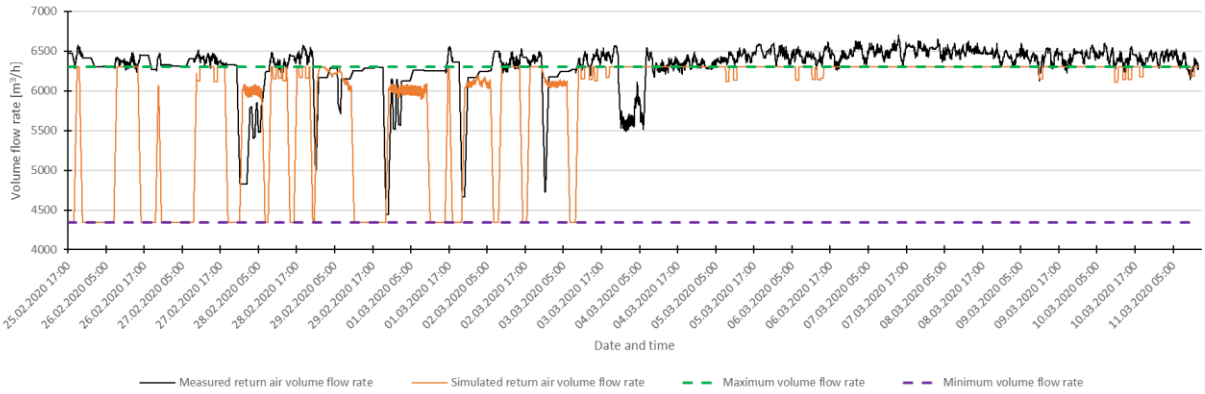

Figure 5-13: Measured and simulated return air volume flow rate (hourly moving average)

In Figure 5-14, it can be observed that the shape of the curve for the simulated return air RH is in high accordance with the simulated volume flow rate. This indicates that the model works as intended, where the AHU operates with higher volume flow rates when the RH inside the swimming pool hall is elevated. The figure shows that the measured RH with the WS-DLTc sensor is about 5% lower than the setpoint of 50% throughout the entire measurement period. At the same time, the integrated sensor in AHU shows a measured RH close to the setpoint. As this sensor is not calibrated, a higher RH than what is actually the case is perceived. There is, however, a great compliance between the curves for the measured and simulated return air RH, as a result of a model control strategy for RH regulation similar to the one found in the real unit.

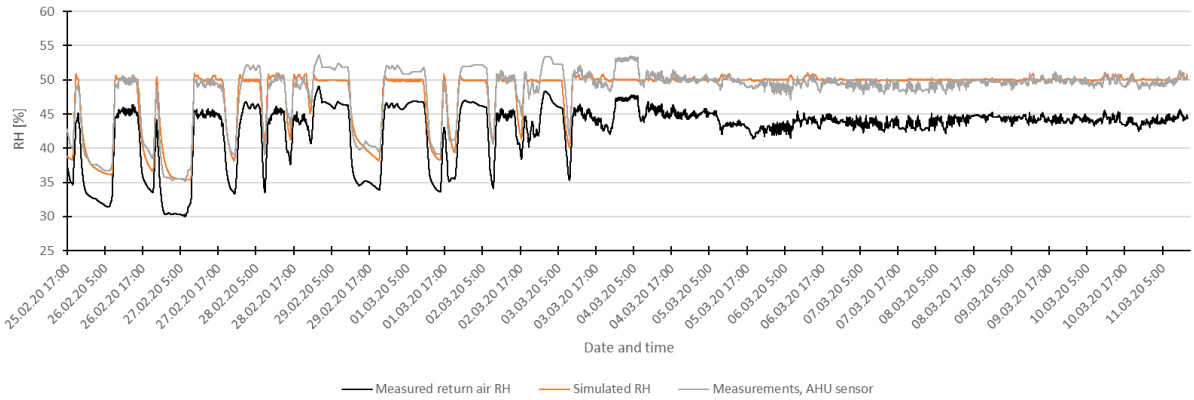

Figure 5-14: Measured and simulated RH (hourly moving average)

5.2.6 Exhaust air temperature

The exhaust air temperature is an indicator for how efficient the heat recovery system in the air handling unit is. In Figure 5-15, some variations are observed between the measured and simulated exhaust air temperature, but the average is 19.9°C in both cases. The high temperature is a result of the idle heat pump, thus lacking an important energy-saving measure within the AHU. Both the measured and simulated exhaust air temperature follow the same shape, with five significant peaks. These peaks correspond to the periods when the AHU ran with the minimum volume flow rate, shown in Figure 5-13. In these periods, smaller volume flow rates through the cross-flow heat exchanger results in a reduced heat transfer, and thus a higher exhaust air temperature.

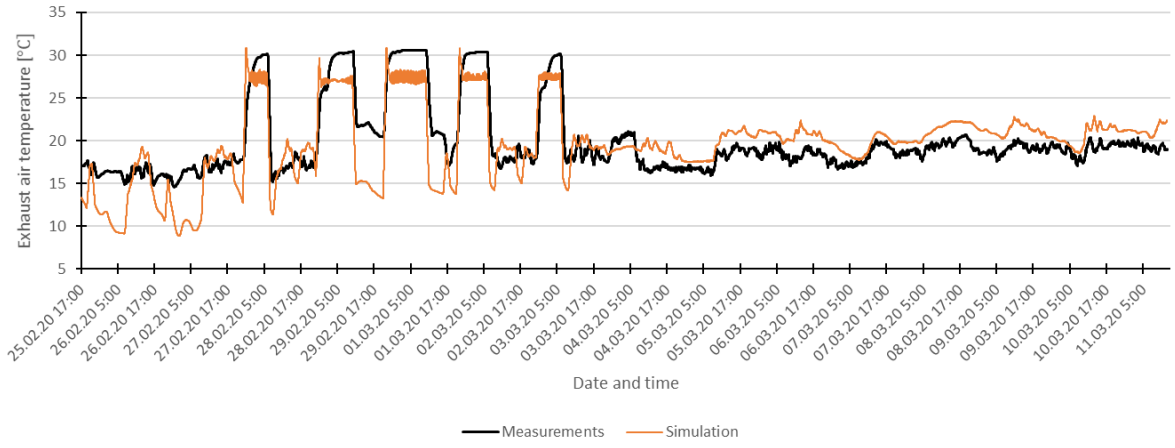

Figure 5-15: Exhaust air temperature (hourly moving average)

5.2.7 Thermal energy needs

In the real pool water circuit, the water will be heated both through the pumps, by UV radiation, and through the primary heat exchanger, as illustrated in Figure 2-4. In the model, however, all the heat transfer takes place in the primary heat exchanger since

pumps and UV are not included. Figure 5-16 shows the average heat transfer in the various components of the real circuit, as well as the total heat transfer for both the real circuit and the model, for the entire measurement period from February 25 to March 11. The results indicate a slightly higher average power for pool heating than the real circuit does, with an average of 19 kW and 17 kW, respectively.

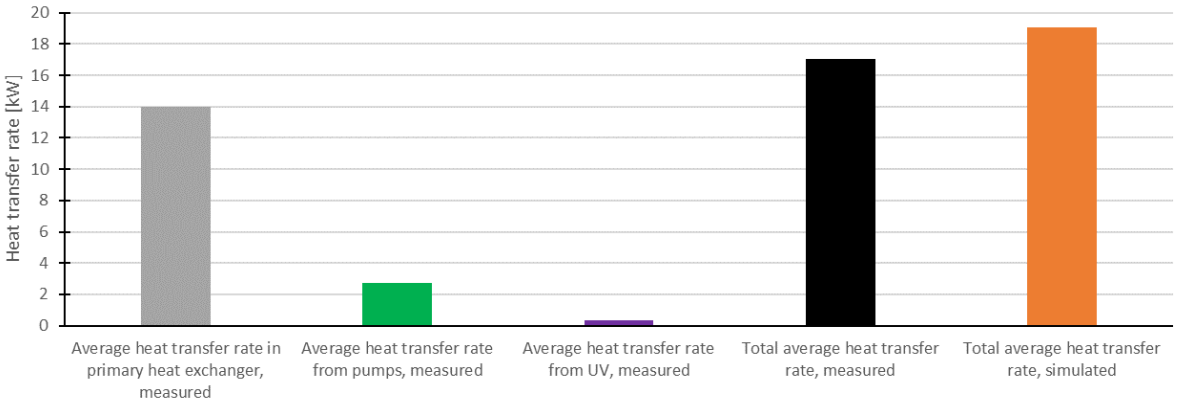

Figure 5-16: Average pool water heat gains [kW], measured and simulated

The mass flow rate and temperature of the make-up water is similar in both reality and the model, and does not explain this difference. In section 5.2.2, an 8.5% higher average evaporation rate was obtained in the simulations compared to the calculated evaporation rate from a water vapor mass balance. Thus, in the model, there will be a higher heat loss through evaporation from the water surface. The results obtained here may indicate that the estimated activity factors described in section 5.1 are a little too high.

Figure 5-17 shows the comparison of measured and simulated supply air temperature. Both graphs follow the same trend, and the results of the changed return air setpoint temperature are clearly evident. The simulated temperature is slightly lower than the measured one, with an average of 34.8°C compared to a measured average of 35.8°C. This may indicate that the real swimming pool facility has a larger thermal heat loss than the model. This is due to the multifunctionality of the AHU, described in section 3.2, which also include covering of the pool hall space heating demand.

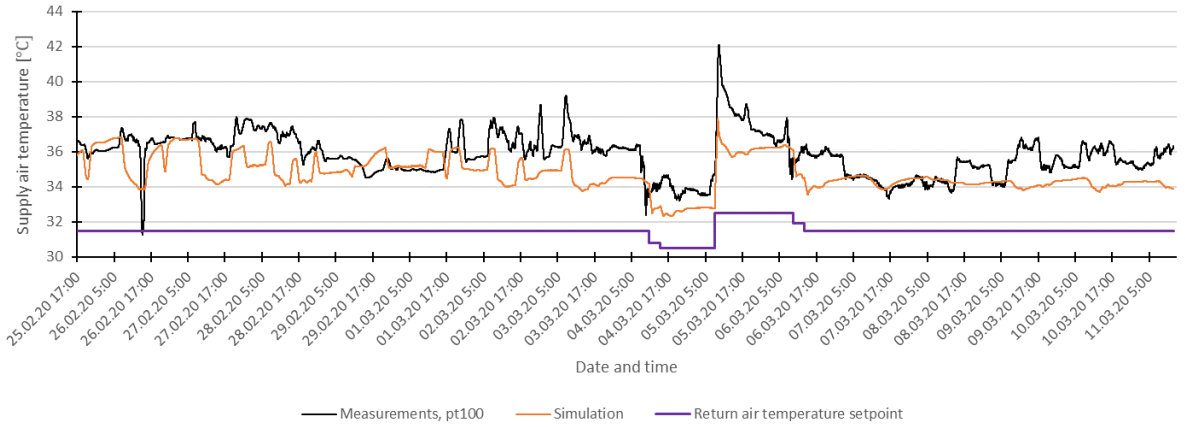

Figure 5-17: Comparison of supply air temperatures (hourly moving average)

The heat transfer in the heating coil obtained from both the measurements and the model is shown in Figure 5-18. It shows good compliance, where the average heat transfer for the real measurements is 8.6 kW, compared to 8.2 kW in the simulations. This corresponds to a 4.7% lower heat transfer in the simulations than the measured one. Again, this is a result of possibly a slightly higher heat loss in the real swimming pool than in the model, and is in line with the simulated supply air temperature being somewhat lower than the measured.

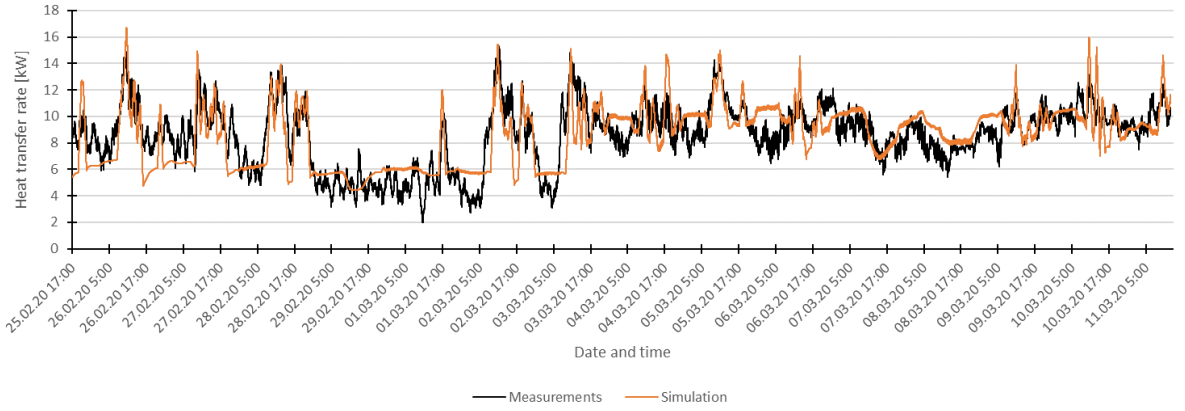

Figure 5-18: Comparison of heat transfer in the AHU heating coil (hourly moving average)

5.3 Results with heat pump

The results so far have been for the facility without the integrated heat pump in the AHU in operation. In modern well-functioning plants, the integrated heat pump is an important part of the thermal system. This section deals with simulations were the heat pump is included in the model, according to the schematic shown in Figure 4-27, achieving a higher heat recovery at the exhaust and dehumidification at nights. Since the heat pump is intended to be an energy-saving measure in the thermal system of the swimming pool

facility, the results will be compared to those obtained from the model without the heat pump.

The first thing to note is that the exhaust air temperature out of the AHU drops significantly, as shown in Figure 5-19. This shows that the heat pump has an important function in recovering much of the energy in the exhaust air, which would otherwise be lost. Compared to the model without heat pump, the net heat loss through the ventilation air drops from 12.27 to 8.95 kW, a reduction of 27%.

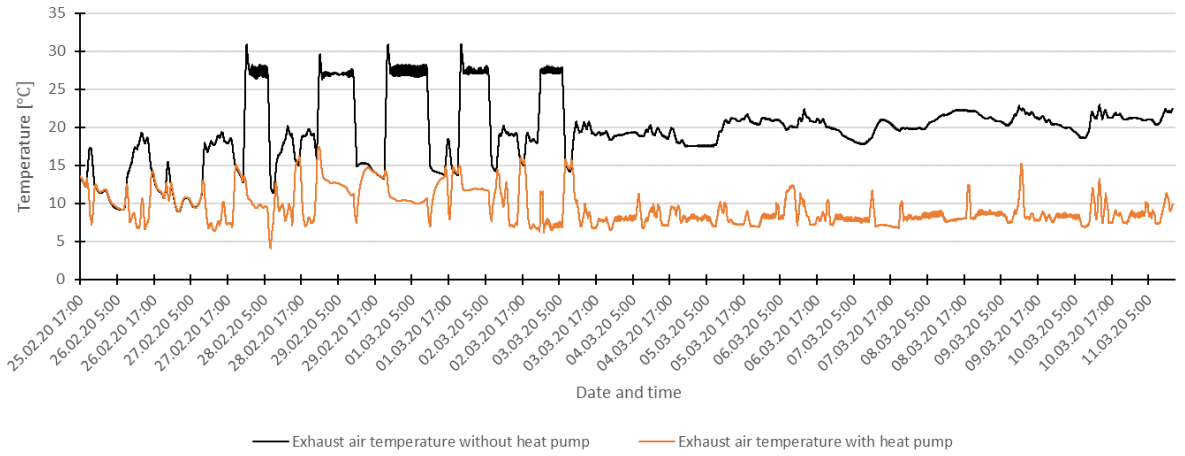

Figure 5-19: Comparison of AHU exhaust air temperature, with and without heat pump (hourly moving average)

The heat absorbed in the evaporator of the heat pump will, as described in section 3.2, either be used to heat the supply air in the air condenser or eventually heat the pool water. Figure 5-20 shows that the average heat demand for heating of supply air in the heating coil decreases considerably with the introduction of the integrated heat pump. The reduction is as much as 50.6%, from 8.26 to 4.08 kW.

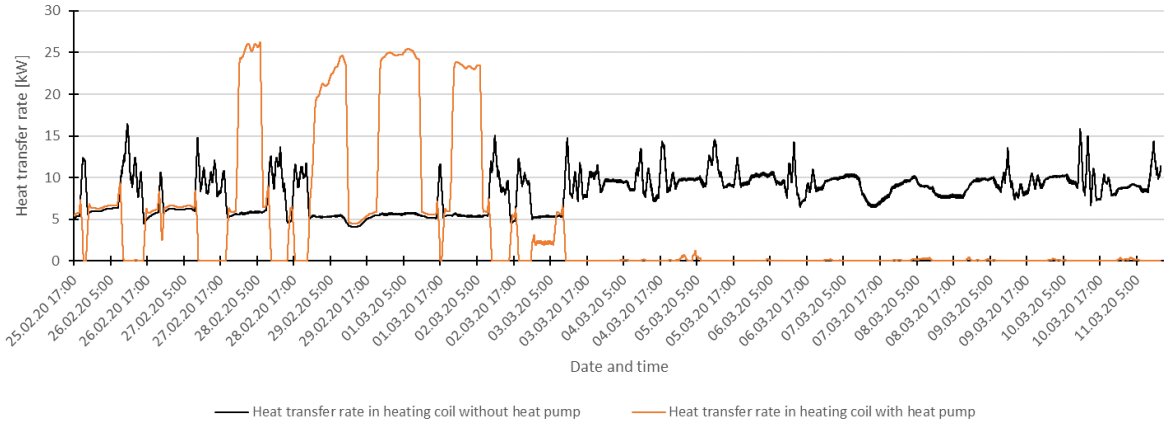

Figure 5-20: Comparison of heat transfer rate in AHU heating coil, with and without heat pump (hourly moving average)

When comparing the heat transfer in the air condenser and the heating coil, Figure 5-21 shows that the air condenser largely takes over the task of heating supply air. The air condenser will be used to heat supply air as long as there is both a heating demand and a dehumidification need. The figure shows that the heating coil and the air condenser complement each other well, according to the system description given in section 3.2, where the heating coil is utilized when the air condenser is not sufficient or the compressor is switched off due to low dehumidification needs.

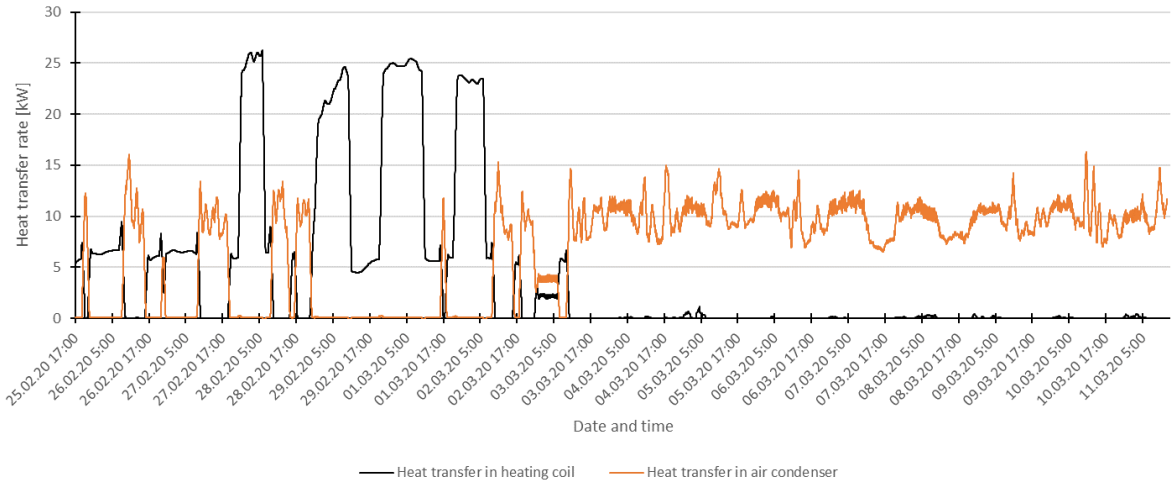

Figure 5-21: Heat transfer rate in air condenser and heating coil (hourly moving average)

With an average heat transfer of 7.0 kW in the air condenser and 4.08 kW in the heating coil, the total thermal power for heating supply air becomes 11.08 kW, which is 1.19 kW lower than the heating coil gave without the integrated heat pump. This can be explained by the fact that the dehumidification damper after the dehumidifier, illustrated in Figure 3-3, is now in use. More air with a higher temperature than the outdoor air is recovered, and the heating demand decreases.

The high peaks in the heating coil heat transfer rate observed in Figure 5-20 and Figure 5-21 are due to periods of very low humidity inside the swimming pool, as could be observed in Figure 5-23. The AHU will run with minimum volume flow rate, shown in Figure 5-22, and since the compressor is switched off, all the heating needs must be covered by the heating coil. Some discrepancy between control strategy and the one implemented in the model, may be the reason for the drops in RH.

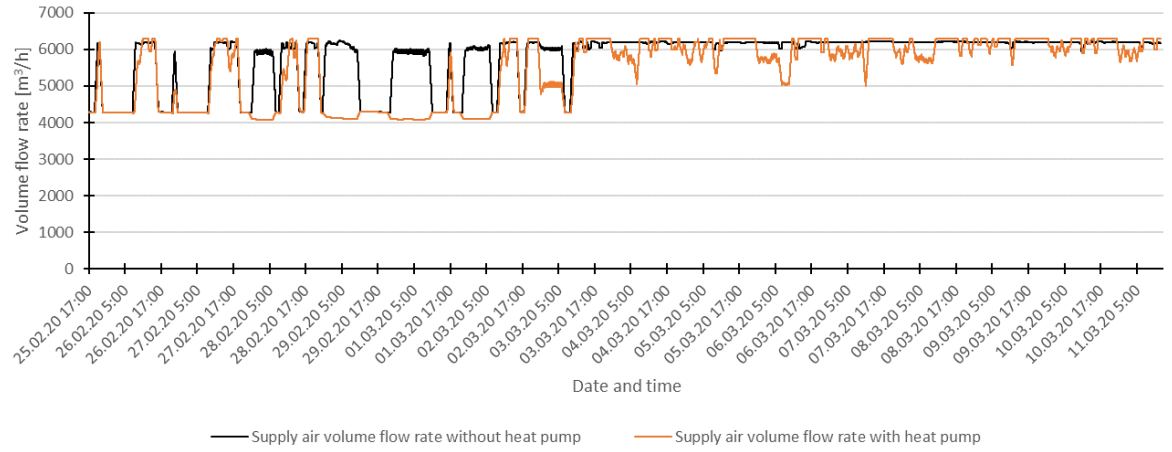

Figure 5-22: Comparison of supply air volume flow rates (hourly moving average)

According to the control strategy described in section 3.2, the compressor is turned on when the return air RH exceeds the set point of 50% and turns off when the RH has fallen 2% below the set point. This may be somewhat unclear in Figure 5-23, due to values presented as hourly moving averages. The compressor has no part load operation, which it may look like, but presenting minute values would give a messy figure.

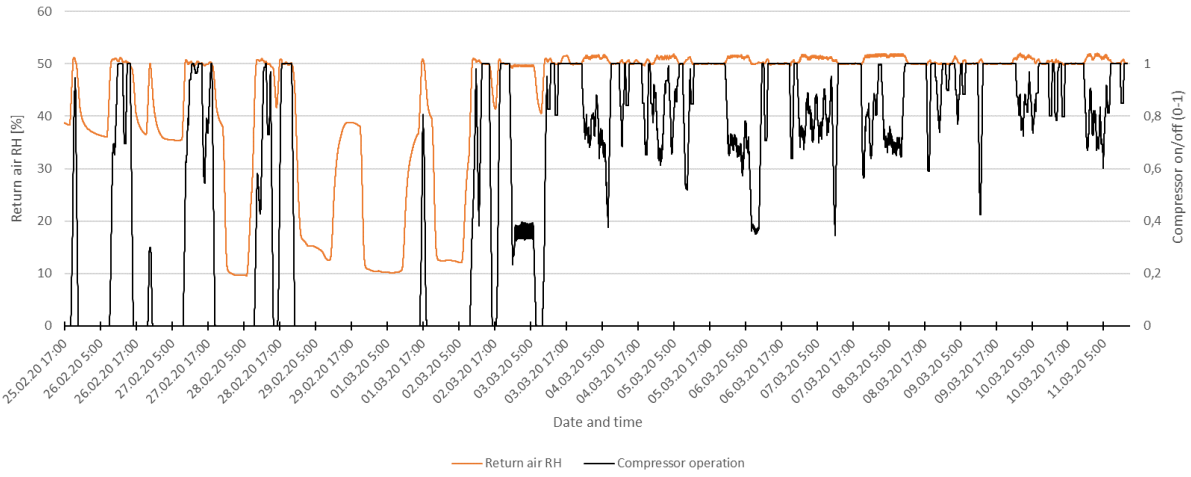

Figure 5-23: Comparison between heat pump operation and return air RH (hourly moving average)

Figure 5-24 shows the heat transfer rate in the pool water condenser and the primary heat exchanger in the pool water circuit. The AHU integrated heat pump makes a significant contribution to pool water heating, with an average of 5.62 kW. Overall, this means that the heat demand in the primary heat exchanger is reduced by 30.4%, from 19 kW without the pool water condenser, to 13.62 kW when the heat pump is in operation. In total, the model shows that if the heat pump were running, the total delivered energy to the swimming pool facility would have dropped from 10 379 kWh to 6 610 kWh for the period February 25 to March 11.

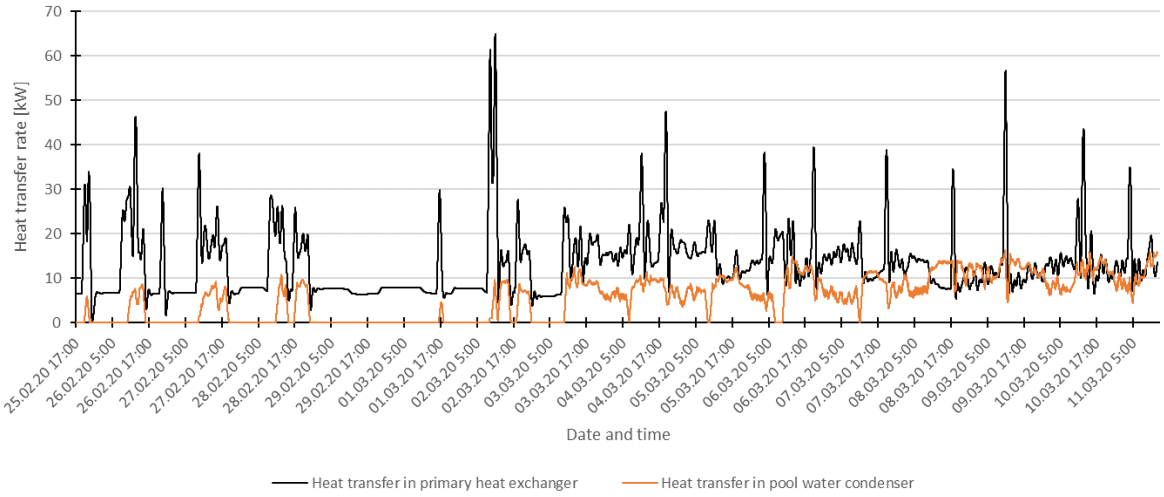

Figure 5-24: Heat transfer rate in pool water condenser and primary heat exchanger (hourly moving average)

5.4 Annual energy consumption

In this section, the results from a one-year simulation of the model both with and without the integrated heat pump will be presented. Swimming pools typically have a large energy consumption compared to other building categories, and a comparison of the facility at Dalgård with key numbers found in the literature will be interesting.

In these simulations, the occupancy schedules are simplified compared to the detailed schedules from the analyzed measurement period. The following schedule for activity in the pool is used

- Weekdays: 08:30 – 15:00 and 17:30 – 21:30
- Weekends: No activity
- June 20 to August 16 (summer holiday): No activity

The operation schedule for the AHU is the same as the one described section 4.1.3, except the summer holiday, where it is assumed to run in night mode operation. An average activity factor of 0.9 is used for all periods with activity in the pool, and the pool cover is assumed to be applied outside activity.

Figure 5-25 shows the total annual energy consumption of the swimming pool facility with and without the integrated heat pump in the air handling unit. In these numbers, both the thermal energy consumption and electricity consumption are included. The purple bar shows the average energy consumption found in the study at Statistics Norway in 2008 [1].

The results show that the total energy consumption is reduced by 26%, from 914 to 676 kWh/m^2 usable floor area, using a heat pump in AHU. This is a significantly higher value

than the 14% reduction predicted in the Swedish study from 2001 [28], presented in section 2.3.2. Compared to the average energy consumption of 300 kWh/m^2 found in the study from Statistics Norway, the energy consumption both with and without heat pump is very high.

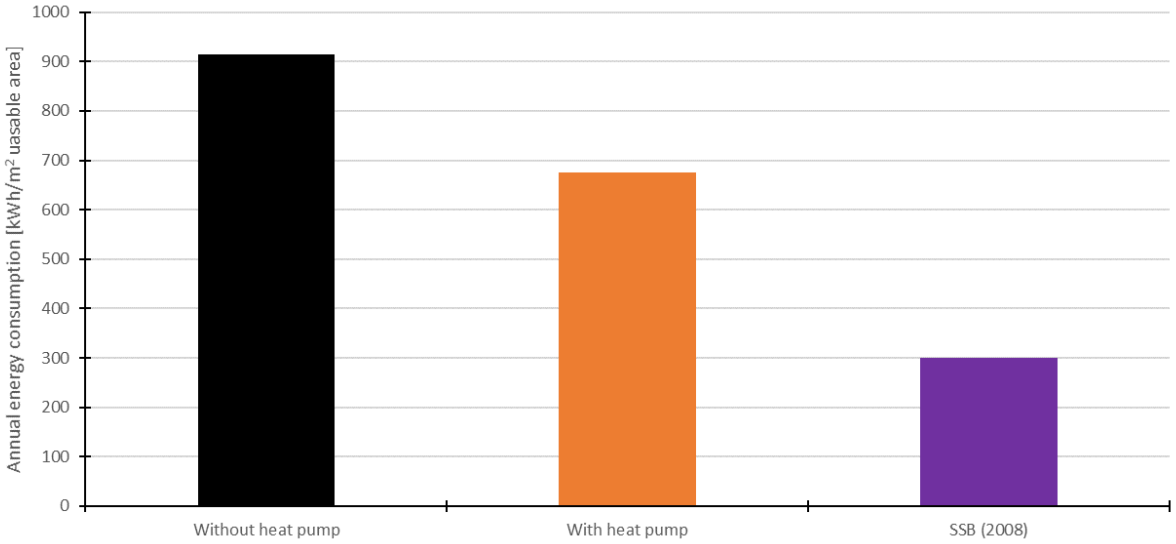

Figure 5-25: Comparison of annual energy consumption per usable floor area

On the other hand, if one looks at the total energy consumption per square meter of water surface, the picture looks quite different. In Figure 5-26, the total energy consumption for the model without heat pump is 2,080 kWh/m^2 water surface, while it has been reduced to 1,540 kWh/m^2 water surface when the heat pump is included. Both these values are within the lower range of energy consumptions found by Kampel et al. for 41 Norwegian swimming facilities [2].

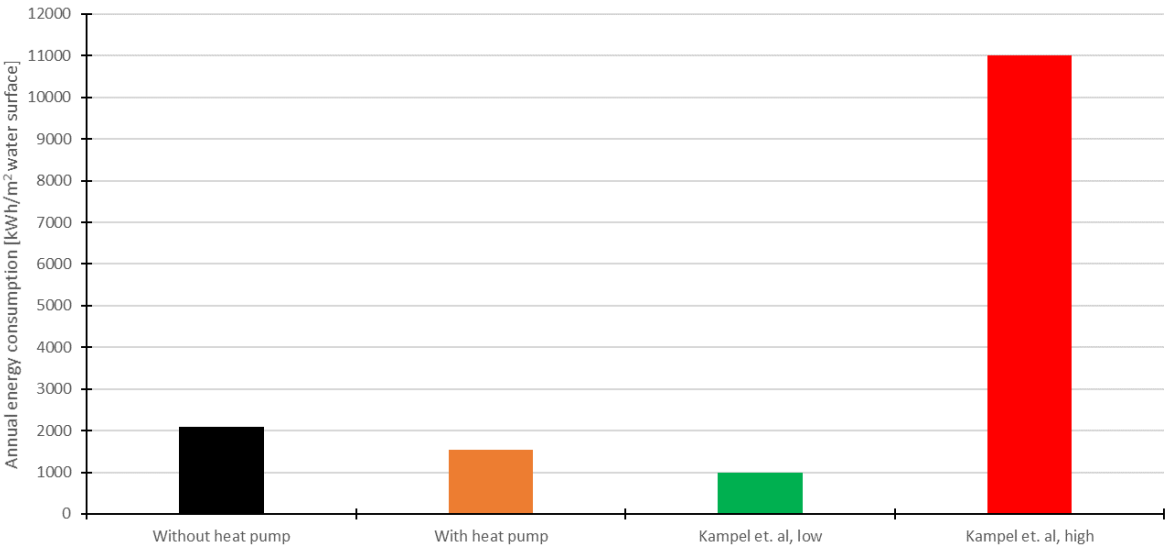

Figure 5-26: Comparison of energy consumption per water surface area

5.5 Model sensitivity analysis

In order to investigate whether the model behaves as desired with different input parameters, a sensitivity analysis has been performed here. The results from the simulations in such an analysis will be interesting, as they can give an idea of what measures that could have been implemented in the real swimming pool facility to improve the performance of various thermal posts. The analysis is based on the measurement period from February 25 to March 11, where the heat pump was not in operation.

5.5.1 Reduced water temperature setpoint

If the water temperature is lowered and the setpoint air temperature is kept constant at 31.5°C, the evaporation rate from the water surface will, according to the theory, decrease. This is shown in Figure 5-27, where the average evaporation rate in the entire analyzed period (including the periods of occupied pool) decreases from 21.5 to 11.2 kg/h when the water temperature setpoint is reduced from 33.5 to 28°C. Similarly, the heat demand for pool water decreases from 19.1 to 6.4 kW, which would give a significant saving of 66.5 %. In contrast, the simulations show that the heating demand in heating coil increases by 33.4%, from 8.26 to 11.0 kW. This is a natural consequence of the fact that a colder water temperature will cause less heat loss to the surrounding air.

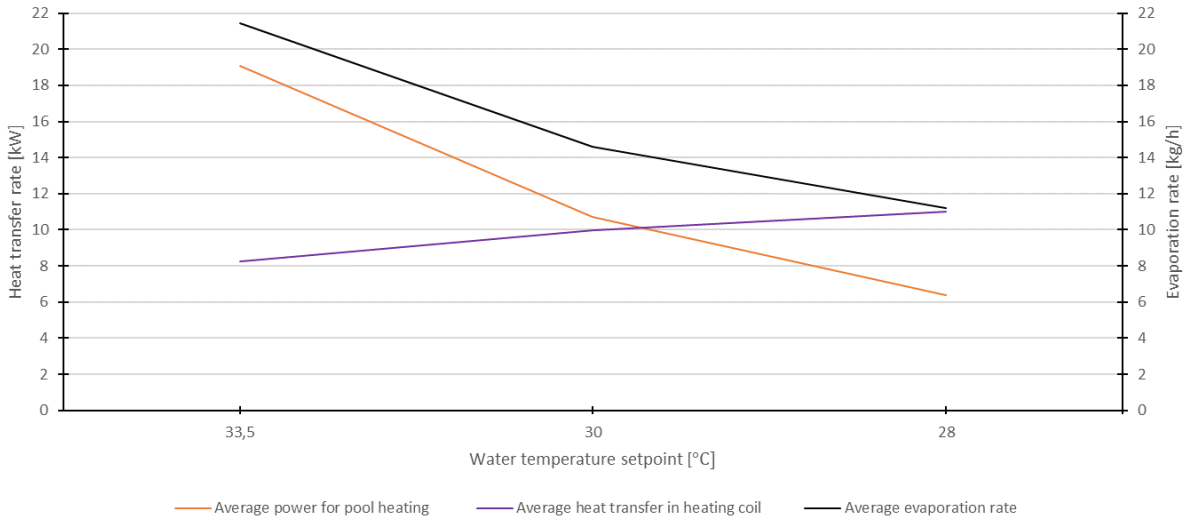

Figure 5-27: Sensitivity analysis of reduced water temperature setpoint

5.5.2 Impact of pool cover

During the second half of the measurement period, from March 3 to March 11, the pool cover was removed so that it was not used when the pool was empty. Table 5-1 shows the impact on the average evaporation rate and the heating demand for pool water during this part of the measurement period, compared to a scenario where the pool cover was used during the nights. It is assumed that the pool cover is applied right after the last activity

in the pool. With pool cover, the results show that the average evaporation rate would drop from 28.54 to 13.64 kg/h, a reduction of 52.2%. The heating demand for pool water is shown to be reduced by 44.9%, from 24.08 to 13.27 kW.

Table 5-1: Impact of pool cover

	Model without pool cover at night	Model with pool cover at night
Average evaporation rate [kg/h]	28.54	13.64
Average power for pool heating [kW]	24.08	13.27

5.5.3 Increased insulating ability of the building constructions

The swimming pool at Dalgård is an old building, and although accurate U-values for the various building structures are not known, much indicates that large parts of the outer structures have a relatively poor insulating ability. This is shown in Appendix L, where various parts of the outer structures are photographed with a thermography camera. The pictures show that the interior surface of some parts of the external constructions keep a temperature of 15 to 16°C. The problem is particularly great in the transition between walls and ceilings, and at the positions of the studs. From a Mollier chart, one can find that the dew point temperature of air at 31.5°C and 50% RH is about 20°C, which means that there will be significant condensation problems at these locations.

Figure 5-28 shows what impact an increasing insulation thickness in the older parts of the outer structures would have on the total delivered power to the swimming pool, the average heat transfer in the heating coil, and the supply air temperature, during the period the measurements were carried out. In addition, the figure includes the results obtained if all external construction were in accordance with the passive house standard.

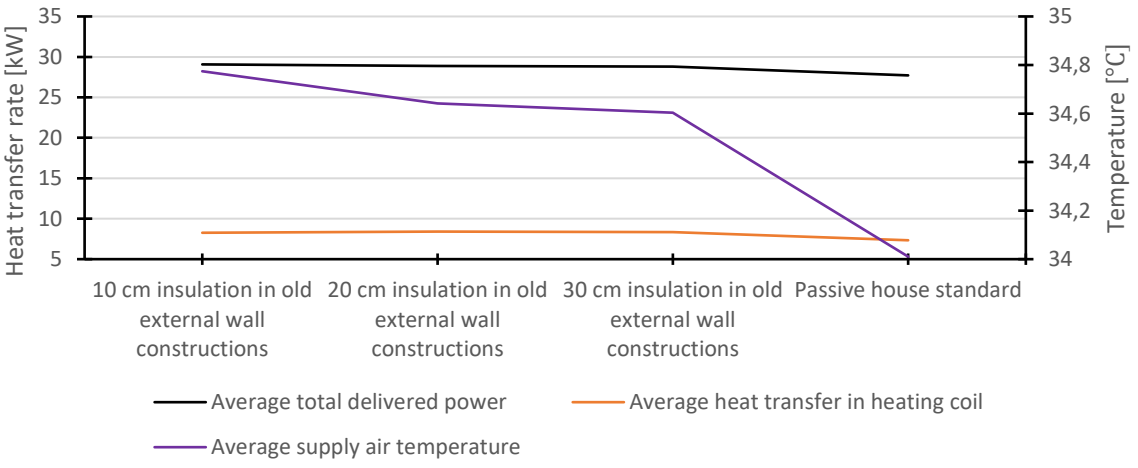

Figure 5-28: Impact of increased insulating ability of the external constructions

The results show that the average heat transfer in the heating coil and total delivered energy is little affected by the insulation in the old wall being increased from 10 to 30 cm, with only a reduction from 29.1 to 28.8 kW for the latter. In these simulations, the original normalized thermal bridge value of 0.1 W/m^{2}K is not changed. If, however, all the external constructions are upgraded to meet the requirements for U-values and normalized thermal bridge value given in the passive house standard, the average heat transfer in the heating coil and total delivered power drops to 7.3 and 27.7 kW respectively. This is a reduction of 11.6 and 4.7%, respectively. As a result of lower heat losses through the constructions, the average supply air temperature drops from 34.8 to 34.0°C.

6 Discussion

The comparison of real measurements and results from simulations with the IDA ICE model has been found to give a good match in the prediction of the energy needs and other characteristics of the thermal systems in the swimming pool analyzed. This chapter is devoted a discussion on the model's validity, the significance of the results, and what utility the model may have in future projects.

6.1 Model validity

The main purpose of this master thesis was to further validate dynamic models for swimming pools. A valid model should be a good representation of the real building, to be able to give a fairly correct description of the thermal characteristics. A great deal of effort has therefore been put into recreating the real control strategies for heating, cooling, and dehumidification of air, as well as heating of pool water. The use of the swimming pool is carefully logged through on-site observations, and at those times of the day when these observations have been deficient, estimates have been made based on the water level in the balance tank and repetitive schedules. In order to make the external influences on the model as real as possible, a weather file was created, where own on-site temperature and humidity measurements were entered together with other necessary weather data from the nearest available weather station. All of these actions were performed to give the model the most accurate input parameters.

However, small errors in the model's input parameters have been inevitable, and there will be deviations in both activity schedule, weather file, model's building construction and control strategies. Due to privacy rules, it was difficult to monitor the swimming pool through a camera. New solutions for this are emerging in the market, but in this context, it was considered that on-site observations were a good enough approach. The perception of the activity level in the pool will always be subjective, whether you see it through a camera or through your own eyes. A camera or sensor, on the other hand, would have been useful in those times when it was not possible to be present in person. Discrepancies in activity level are believed to mainly affect the results showing evaporation from the pool, and to some extent heating of pool water as a result of an either too high or too low estimated activity factor. Since the results showed a difference of 8.5% between calculated evaporation based on measurements and the model's estimate, it can be concluded that the estimated activity factor has been relatively good. The assumption of 1 atm air pressure

in the water vapor mass balance calculations proved to be good due to the high correlation obtained with the empirical formulas.

A higher correlation with the ASHRAE equation strengthens its position in relation to, for example, the Shah method, which was found to give a somewhat too high evaporation rate compared to the calculations. It is an easier equation to use in calculations, as Shah's method involves four different calculation steps, as shown in Appendix A. More calculation steps may increase the error, due to small uncertainties in the input variables. The ASHRAE equation is also more widely used, and thus suitable for comparison.

The air exchange inside the swimming pool mainly takes place through the ventilation unit, and with large supply air and return air volume flow rates, infiltration or exfiltration through the external constructions is assumed to be negligible in proportion. Wind variables in the weather file taken from a weather station a few kilometers away is therefore assumed to have minor impacts on the results. Assuming all radiation to be diffuse radiation is also considered to be fair since the measurements were carried out in the period February to March. For the one-year simulation, this assumption might have affected the results, in terms of a too low irradiation through the windows. In the warmest months, this would probably lead to a higher cooling demand, and thus a higher energy consumption in terms of larger volume flow rates within the AHU. In other periods, when the outdoor air temperature is lower, irradiation might reduce the energy consumption.

A more careful measurement of the U-values of the different building constructions and an overview of the different layers of the constructions could be advantageous in order to achieve a correct match between the heat losses in the model and the actual building. At the same time, the results of measured and simulated supply air temperature and heat demand for heating of supply air are in good agreement. A deviation of 4.7% in delivered power in the heating coil during one of the coldest periods of the year will not have a great impact on the total energy demand for heating of air throughout a year.

In the model, the temperature and dehumidification control strategies were carefully structured according to the description in the technical documentation of the real unit. Therefore, the main features of the model's control strategies should be fairly correct. The lack of some components in the IDA ICE library, on the other hand, means that the model air handling unit will differ somewhat from the real unit. For example, the real dampers had to be replaced with two mixing boxes, which controlled the ratio of fresh air, recycled air, and supply air in the most possible similar way as the real dampers do. The results showed that there was some deviation between when the actual unit and the model switched between the minimum and maximum volume flow rate, where the real unit ran to a greater extent with maximum volume flow rates than the model did. Uncertainty

regarding the uncalibrated integrated sensors in the real unit may explain some of these differences. The comparison of the return air RH supports the explanation of uncalibrated integrated sensors in the AHU, as the trend of the measured curve and simulated curve were very similar, and the main difference was the constant deviation of 5%.

The model lacks thermal inertia in the air and the water volumes of the swimming pool facility, as the model components are treated as nodes described by stationary equations. This means that the amplitudes of the different variables around their setpoints are reduced, and the regulation becomes faster. However, if the results are compared as averages over a longer period of time, this will be of less importance.

6.2 Significans of results

The results show that energy-saving measures are important to keep the energy consumption as low as possible. Just by using a pool cover at nights, the facility at Dalgård proved to be able to reduce the energy demand for pool water heating by 44.9% due to a greatly reduced evaporation rate. Based on these findings, it is clear that all swimming pools facilities should use pool covers during the periods when the pool is not in use.

If the energy consumption was evaluated at kWh per square meter of total area, it appeared that the swimming pool at Dalgård had a high energy consumption compared to typical values for Norwegian swimming pools. On the other hand, if the energy consumption was evaluated at kWh per square meter of water area, the model showed that the energy consumption was among the lower ones found for typical Norwegian swimming pools [2]. In the various ways of presenting the energy consumption, the relationship between water area and total area will have a big impact. At Dalgård, the pool covers 50% of the total area, and it is therefore natural to observe a "better" result when energy consumption is evaluated at kWh per square meter of water area. In facilities with a lower pool/deck ratio, and evaluation of kWh per square meter water surface will not yield as good results.

The fact that the heat pump was not functioning during the measurement period was shown to have a great influence on several of the thermal characteristics of the swimming pool facility. This was as expected, as much of the energy in the exhaust air will be lost without any further cooling at the heat pump dehumidifier. The humid return air contains large amounts of latent heat bound up in the water vapor, which can be recovered when the air cools and condenses. A 50% reduction in the heating demand in the heating coil, and 30% in the pool's primary heat exchanger for the analyzed measurement period is significant. It still makes sense, as the heat pump operates under favorable conditions relative to, for example, air-to-air heat pumps used in ordinary residences, in the form of a relatively stable temperature lift.

Normally, the integrated heat pump is an energy-saving solution that has already been implemented. Therefore, a sensitivity analysis was done to look at other measures that could improve energy performance. With a setpoint of 33.5°C, the pool temperature is quite high compared to what is usually found in public pools, and it requires large amounts of energy to maintain this temperature. Lowering the pool temperature can be controversial, as it is set to meet the needs of different user categories. But a reduction in the energy demand for pool water heating of 66.5% by lowering the water temperature from 33.5 to 28 C makes it interesting to challenge the current setpoint. Frequent changes in water temperature will be unfavorable, as the inertia of the systems is large. Instead, periods of maybe one week can be planned, where the setpoint is changed according to the needs of the user categories scheduled within those periods.

Upgrading the insulating capacity of the external constructions was found to have a much smaller impact on energy consumption than a reduced water temperature, or operation with and without a heat pump in the AHU. This is probably a result of the heat loss through the structures being small in relation to the heating needs of the large volumes of air and water. In contrast, low surface temperature observations suggest that upgrading the outer structures will be advantageous anyway. If moisture damage in the structure is allowed to develop over a longer period of time, it can potentially be much more expensive to rectify than to take preventative measures, such as better sealing in the transitions between walls and ceilings and other places in the structures where thermal bridges are a significant problem.

7 Conclusion

The aim of this thesis was to analyze different aspects of the thermal systems in a swimming pool facility, through modeling in the BPS package IDA ICE. It was chosen to investigate the evaporation from the pool water surface, and the thermal energy needs in the air handling unit and pool water circuit.

Evaporation was evaluated through a water vapor mass balance across the boundary of the swimming pool hall. These calculations were compared with estimated evaporation rates obtained from two different empirical correlations, as well as results from simulations. For the analyzed measurement period, the following observations were made:

- Estimated evaporation rate using the ASHRAE correlation was on average 9.2% higher than estimated evaporation rate from the water vapor mass balance.
- The estimated evaporation rate from the Shah correlation was on average 13.7% higher than the water vapor mass balance calculations gave.
- The results from simulations in IDA ICE yielded, on average, an 8.5% higher evaporation rate than the calculated evaporation rate from the water vapor mass balance.

Average evaporation rate was also found to be strongly influenced by the use of pool cover. For the last seven days of the measurement period, when pool cover was not used, simulations showed that the average evaporation rate could have been reduced by 50% if pool cover had been used at nights. During the same period, the energy needs for pool water heating could be reduced by 45%, due to less heat loss from the water surface.

For the thermal energy needs of the swimming pool facility, the results gave the following observations:

- The simulations showed an average 10% higher power demand for pool water heating than what was measured, with 19 kW versus 17 kW.
- An average heat transfer in the AHU heating coil of 8.2 kW was observed in the simulations, compared to 8.6 kW in the measurements; a deviation of 4.7%.

Through simulations, it turned out to have a major impact on the thermal performance of the swimming pool that the heat pump was out of operation. Significant reductions in heat demand through the AHU heating coil and the primary heat exchanger in the pool water circuit would have been achieved if the heat pump were running. A comparison of the model with and without heat pump gave the following results:

- 50.6% reduction in heat transfer in AHU heating coil for the analyzed period.
- 30.4% reduction in heat transfer in the primary heat exchanger in the pool water circuit for the analyzed period.
- An one-year simulation showed that the integrated heat pump may reduce the total energy consumption of the swimming pool facility by 26%, from 2 080 kWh/m^2 water surface area without use of the heat pump, to 1540 kWh/m^2 water surface are with heat pump operation.

Both a reduced water temperature and an upgrade of the external constructions were investigated as possible energy saving measures. Of these, a decrease in the water temperature had the greatest impact on the results, with a reduction in the energy demand for pool water heating of 66.5% for the analyzed period when the heat pump was not operating. At the same time, the need for heating of air increased by 33.4%. An upgrade of the external constructions to the passive house level gave only a 4.7% reduction in the total energy consumption for the swimming pool facility. However, improvements in these constructions are recommended, as observations of cold surfaces indicate that condensation and moisture can be a problem.

8 Further work

Ideally, measurements should have been performed in a facility where the integrated heat pump in AHU was operating, in order to be able to compare the heat pump model with real measurements. In that case, it would be possible to investigate if the heat pump model in IDA ICE is suitable for use in a swimming pool model. Currently, there are no heat pump models in IDA ICE with multiple condensers, and as this is common in integrated heat pumps in modern swimming pool facilities, it would be interesting to see if the solution used in this thesis provides a good approach.

Even more sensors inside the swimming pool could have been used to get a better picture of how temperature and relative humidity vary within the large volume of air. This would provide an even better basis for calculating the evaporation rate, both in a water vapor mass balance equation and using empirical correlations. If it is desirable to study the evaporation in even more detail, better solutions for observing activity in the pool will also be advantageous. These solutions must be in accordance to privacy rules.

In a future measurement setup, an own weather station, that also measures wind speeds, pressure, and radiation, should be installed outside the swimming pool hall. A pressure sensor will also be useful inside the building, for a more accurate calculation of infiltration through the constructions. Own sensors for the air flows at the inlets and outlets of the ventilation ducts will also make calculations of ventilation losses easier.

It would also be interesting to compare an estimated and simulated annual total energy consumption, to be able to determine with even greater certainty whether the model provides a good prediction of the energy performance of planned and existing swimming pool facilities. In addition to the thermal energy consumption, measurements must also be made of the electricity consumption at the various posts in the facility. Determination of heat loss through the various building constructions is also necessary in such a calculation. In new projects, the insulating ability, and thermal characteristics of the different parts of the constructions are often well known, and it will be possible to insert fairly accurate values in the model.

References

[1] A. S. Abrahamsen and M. Bergh, *Energibruk i bygninger for tjenesteytende virksomhet. 2008 Statistisk sentralbyrå • Statistics Norway Oslo-Kongsvinger*. 2011.

[2] W. Kampel, B. Aas, and A. Bruland, "Energy-use in Norwegian swimming halls," *Energy Build.*, vol. 59, pp. 181–186, Apr. 2013.

[3] Lovdata, "Lov om klimamål (klimaloven)," 2017.

[4] Direktoratet for byggkvalitet, "TEK 17, Kapittel 14."

[5] H. Alvestad, "Characterization of thermal energy needs of swimming pools using building performance simulation," NTNU, 2019.

[6] H. Voemel, "Water Vapor Pressure Formulations," 2016. [Online]. Available: http://cires1.colorado.edu/~voemel/vp.html.

[7] M. J. Moran and H. N. Shapiro, *Fundamentals of Engineering Thermodynamics*, 6th ed. John Wiley & Sons, 2010.

[8] J. V. Thue, *Bygningsfysikk, grunnlag*. Fagbokforlaget, 2016.

[9] ASHRAE, "2007 ASHRAE Handbook HVAC Applications," 2007.

[10] Norges byggforskningsinstitutt, *Bade- og svømmeanlegg*. Oslo, 2004.

[11] G. Rojas and J. Grove-Smith, "Improving ventilation efficiency for a highly energy efficient indoor swimming pool using CFD simulations," *Fluids*, vol. 3, no. 4, 2018.

[12] T. B. Nitter, W. Kampel, K. V. H. Svendsen, and B. Aas, "Comparison of trihalomethanes in the air of two indoor swimming pool facilities using different type of chlorination and different types of water," 2018.

[13] A. V Arundel, E. M. Sterling, J. H. Biggin, and T. D. Sterling, "Indirect Health Effects of Relative Humidity in Indoor Environments," 1986.

[14] Ø. Marstein, "Strategidokument," 2006.

[15] Norwegian Swimming Federation, "Spesifikasjon for svømmeanlegg," 2010.

[16] P. Blom, "Dimensjonerignskriterier for klimaanlegg," in *Bade- og svømmeanlegg*, Norges byggforskningsinstitutt, 2004, p. 183.

[17] Seresco, "Natatorium Design Guide," 2013.

[18] M. M. Shah, "New correlation for prediction of evaporation from occupied swimming pools," in *ASHRAE Transactions*, 2013, vol. 119, no. PART 2, pp. 450–455.

[19] W. H. Carrier, "The Temperature of Evaporation," *ASHVE Trans.*, vol. 24, pp. 25–50, 1918.

[20] M. M. Shah, "Calculation of Evaporation from Indoor Swimming Pools: Further Development of Formulas," *ASHRAE Trans.*, vol. 118, pp. 460–466, 2012.

[21] M. M. Shah, "Analytical Formulas for Calculating Water Evaporation from Pools," *ASHRAE Trans.*, vol. 114, pp. 610–618, 2008.

[22] M. M. Shah, "Prediction of evaporation from occupied indoor swimming pools," *Energy Build.*, vol. 35, no. 7, pp. 707–713, Aug. 2003.

[23] C. C.; Smith, G. O. G. Lof, R. W.; Jones, R.; Kittler, and R. Jones, "Rates of evaporation from swimming pools in active use," *ASHRAE Trans.*, 1998.

[24] B. Aas, S. Olsen, and O. Smedegaard, "Fresh look at the air flow," *sb - International magazine for sports, leisure and recreational facilities*, pp. 58–60, 2019.

[25] P. Blom and (BYGGFORSK), "Ventilasjon og avfuktning i svømmehaller og rom med svømmebasseng," 2003. .

[26] H. M. Mathisen, "Heat recovery," *TEP20, NTNU*.

[27] MENERGA, "Creating a good climate," 2016.

[28] L. Johansson and L. Westerlund, "Energy savings in indoor swimming-pools: Comparisons betweendifferent heat-recovery systems," *Appl. Energy*, vol. 70, no. 4, pp. 281–303, Dec. 2001.

[29] United States Environmental Protection Agency, "International Treaties and Cooperation about the Protection of the Stratospheric Ozone Layer."

[30] J. Stene, "Working Fluids (Refrigerants) for The Heat Pump Cycle," *Lect. TEP20, NTNU*, 2019.

[31] J. G. Balchen, T. Andresen, and B. A. Foss, *Reguleringsteknikk*, 6th ed. Institutt for teknisk kybernetikk, NTNU, 2016.

[32] Direktoratet for byggkvalitet, "TEK 17, Kapittel 13," 2017.

[33] Norsk Bassengbad Teknisk Forening, "Retningslinjer for vannbehandling i offentlige bassengbad." 2000.

[34] Direktoratet for Byggkvalitet, "Byggeforskrift 1987," 1987.

[35] Direktoratet for byggkvalitet, "TEK 10, Kapittel 14 Energi," 2017.

[36] Norsk Standard NS 3701, *Kriterier for passivhus og lavenergibygninger.* 2012.

[37] S. Carlucci, "BUILDING PERFORMANCE SIMULATION SPRING SEMESTER," *Lect. TBA4166, NTNU*, 2019.

[38] EQUA, "IDA Indoor Climate and Energy." [Online]. Available: https://www.equa.se/en/ida-ice.

[39] Transient Simulation Tool, "Welcome | TRNSYS : Transient System Simulation Tool." [Online]. Available: http://www.trnsys.com/.

[40] J. Jonathan Duverge BEng and Me. Mgt Charles, "Energy performance and water usage of aquatic centres," 2019.

[41] W. S. Lee and C. K. Kung, "Optimization of heat pump system in indoor swimming pool using particle swarm algorithm," *Appl. Therm. Eng.*, vol. 28, no. 13, pp. 1647–1653, Sep. 2008.

[42] S. Sun and H. Liu, "Particle Swarm Algorithm: Convergence and Applications," in *Swarm Intelligence and Bio-Inspired Computation*, Elsevier Inc., 2013, pp. 137–168.

[43] R. S. Garay, A. Costa, T. Messervey, C. Mastrodonato, and M. M. Keane, "SWIMMING POOL HALL HVAC MODELLING, SIMULATION AND END OF SETBACK NEURAL NETWORK PREDICTION: A DETAILED CASE STUDY."

[44] Menerga, "Technische Dokumentation MENERGA ThermoCond 370611."

[45] MENERGA, "User manual for MENERGA ThermoCond 370611." .

[46] WiSensys, "Product sheet for Wireless Sensor WS-DLTa-pt100." .

[47] Wisensys, "Product sheet for Wireless Sensor WS-DLTc." .

[48] Wisensys, "Product sheet for Wireless CO2 Sensor (WSE-DLC and WSE-DLC-abc)." .

[49] T. Hydronics, "Product sheet for TA-SCOPE innreguleringsinstrument." .

[50] T. Eikevik, "Funksjonskall i excel," 2014.

[51] SWEMA ABA, "Manual for Swema 3000." .

[52] F. P. Incropera, D. P. Dewitt, T. L. Bergmann, and A. S. Lavine, *Principles of Heat and Mass Transfer*, 7th editio. 2013.

[53] MENERGA, "Technische Dokumentation MENERGA ThermoCond 39." .

[54] M. S. Lewis-Beck, "Bivariate Regression: Fitting A Straight Line In: Applied Regression," 1980.

[55] "Models for Building Indoor Climate and Energy Simulation A Report of Task 22 Building Energy Analysis Tools," 1999.

Appendices

Appendix A – Shah correlation for evaporation [18]

Evaporation from an unoccupied pool where both natural and forced convection are taken into consideration:

$$E_0 = 35 \cdot A \cdot \rho_{sat,w}\left(\rho_{sat,dp} - \rho_{sat,w}\right)^{\frac{1}{3}}\left(x_w - x_{dp}\right) \quad \text{A.1}$$

$$E_0 = A \cdot 0.00005\left(p_{sat,w} - p_{sat,dp}\right) \quad \text{A.2}$$

Where equation A.1 and 5.1 gives the evaporation due to natural convection and forced convection, respectively. The larger of these should be used. A is the water surface area, while x_w and x_a are the absolute humidity of the air at water temperature and dew point temperature, respectively.

For occupied pools, evaporation is given by equation 5.1. It is an empirical correlation, developed from comparison with test data from four sources, and includes the effect of changes in density differences.

$$\frac{E}{E_0} = 1.9 - 21\left(\rho_{sat,dp} - \rho_{sat,w}\right) + 5.3\frac{N}{A} \quad \text{A.3}$$

where N is the number of people in the pool.

For $\frac{N}{A} < 0.05$, use linear interpolation between $\frac{E}{E_0}$ at $\frac{N}{A} = 0.05$ and $\frac{E}{E_0} = 1$ at $\frac{N}{A} = 0$.

For $(\rho_{sat,dp} - \rho_{sat,w}) < 0$, use $(\rho_{sat,dp} - \rho_{sat,w}) = 0$.

Appendix B – ASHRAE activity factors

Typical activity factors for various types of pools given in the ASHRAE Handbook [9]:

Type of Pool	Typical Activity Factor (F_a)
Baseline (pool unoccupied)	0.5
Residential pool	0.5
Condominium	0.65
Therapy	0.65
Hotel	0.8
Public, schools	1.0
Whirlpools, spas	1.0
Wavepools, water slides	1.5 (minimum)

Appendix C – IDA ICE mixing box

Model equations:

($\dot{m}$ [kg/s], T [°C], x [kg/kg], h [J/kg], p [Pa])

Control signal:

$$ctrl_\tau = ctrl\ with\ time\ constant\ \tau$$

Recirculated air:

$$\dot{m}_{recycled} = \max\big(0, min\big(\dot{m}_{return,in}, \dot{m}_{supply,out} - max\big(\dot{m}_{supply,in,min}, min\big(ctrl_\tau \cdot \dot{m}_{supply,out}, \dot{m}_{supply,in,max}\big)\big)\big)\big)$$

If the parameters $\dot{m}_{supply,in,\min}$ and $\dot{m}_{supply,in,max}$ are set to 0 and a very large number, and by using the fact that $\dot{m}_{return,in}$ and $\dot{m}_{supply,out}$ always are positive, the equation can be reduced to:

$$\dot{m}_{recycled} = min\big(\dot{m}_{return,in}, \dot{m}_{supply,out} - ctrl_\tau \cdot \dot{m}_{supply,out}\big)$$

So, if the control signal is 1, there is no recirculation of air in the mixing box.

Entering supply air:

$$\dot{m}_{supply,in} = \dot{m}_{supply,out} - \dot{m}_{recycled}$$

$$h_{supply,in} = f\big(T_{supply,in}, x_{supply,in}\big) \qquad Use\ psychrometric\ chart/Mollier\ diagram$$

Leaving return air:

$$\dot{m}_{return,out} = \dot{m}_{return,in} - \dot{m}_{recycled}$$

$$h_{return,out} = f\big(T_{return,out}, x_{return,out}\big) \qquad Use\ psychrometric\ chart/Mollier\ diagram$$

Leaving supply air:

$$x_{supply,out} = \min\left(\begin{array}{c} \dfrac{\dot{m}_{supply,in} \cdot x_{supply,in} + \dot{m}_{recycled} \cdot x_{return}}{\dot{m}_{supply,out}}, \\ 0.62198 \cdot \dfrac{p_{sat}\big(T_{supply,out}\big) \cdot RH_{supply,out}}{p_{supply,out} - p_{sat}\big(T_{supply,out}\big) \cdot RH_{supply,out}} \end{array}\right)$$

where

$$p_{sat} = e^{\frac{C_1}{T} + C_2 + C_3 T + C_4 T^2 + C_5 T^3 + C_6 T^4 + C_7 \ln(T)}$$

for temperatures below zero, and

$$p_{sat} = e^{\frac{C_8}{T} + C_9 + C_{10} T + C_{11} T^2 + C_{12} T^3 + C_{13} \ln(T)}$$

for temperatures above zero. $C_1 - C_{13}$ are given as [55]:

C1	-5674.5359	C6	-0.9484024E-12	C11	0.41764768E-4
C2	6.3925247	C7	4.1635019	C12	-0.14452093E-7
C3	-0.9677843E-2	C8	-5800.2206	C13	6.4559673
C4	0.62215701E-6	C9	1.3914993		
C5	0.20747825E-8	C10	-0.04860239		

Appendix D – IDA ICE air-to-air heat exchanger

Model equations:

($\dot{m}$ [kg/s], $\dot{V}_\eta$ [m^3/s], ρ [kg/m^3], T [°C], x [kg/kg], h [J/kg], $\dot{Q}$ [W])

Calculation of modified effectiveness, η':

If

$$\frac{\left|\dot{m}_{return} - \dot{m}_{supply}\right|}{\max\left(\dot{m}_{return}, \dot{m}_{supply}\right)} < 0.001$$

then

$$\eta' = \max\left(0.0001, \frac{1}{1 + \frac{0.5\left(\dot{m}_{supply} + \dot{m}_{return}\right)}{\dot{V}_\eta \cdot \rho_a \cdot \frac{\eta}{1-\eta}}}\right)$$

else

$$exp = e^{-\frac{\dot{V}_\eta \cdot \rho_a \cdot \frac{\eta}{1-\eta}}{\dot{m}_{supply}}\left(1 - \frac{\dot{m}_{supply}}{\dot{m}_{return}}\right)}$$

$$\eta' = \max\left(0.0001, \frac{(1-exp)}{1 - \frac{\dot{m}_{supply}}{\dot{m}_{return}} \cdot exp}\right)$$

Calculation of maximum heat transfer:

If wet cooling of return airflow

$$\dot{Q}_{max} = \min\left(\begin{matrix}\dot{m}_{supply}\left(h\left(T_{return,in}, x_{supply,in}\right) - h\left(T_{supply,in}, x_{supply,in}\right)\right), \\ \dot{m}_{return}\begin{pmatrix} h\left(T_{return,in}, x_{return,in}\right) - h\left(T_{supply,in}, x_{return,dew\ point}\right) \\ +\left(x_{return,in} - x_{return,dew\ point}\right) c_{p,water} T_{supply,in} \end{pmatrix}\end{matrix}\right)$$

If both supply side and return side are dry

$$\dot{Q}_{max} = \min\left(\dot{m}_{supply}, \dot{m}_{return}\right) \cdot \left(h\left(T_{return,in}, x_{supply,in}\right) - h\left(T_{supply,in}, x_{supply,in}\right)\right)$$

Available heat transfer:

$$\dot{Q}_{available} = \eta' \cdot \dot{Q}_{max}$$

Based on the available heat transfer, an attainable leaving supply air temperature is calculated. This temperature is used to find the new leaving supply air temperature and absolute humidity. The actual heat transfer is then given by:

If wet cooling of return airflow

$$\dot{Q}_{actual} = \dot{m}_{supply}\left(h\left(T_{supply,out}, x_{supply,out}\right) - h\left(T_{supply,in}, x_{supply,in}\right)\right) - \left(x_{supply,in} - x_{supply,out}\right)c_{p,water}\max\left(T_{supply,out}, T_{supply,dew\ point}\right)$$

If both supply side and return side are dry

$$\dot{Q}_{actual} = \dot{m}_{supply}\left(h\left(T_{supply,out}, x_{supply,out}\right) - h\left(T_{supply,in}, x_{supply,in}\right)\right)$$

Appendix E – IDA ICE fan

Model equations:

(p [Pa], $\dot{m}$ [kg/s], $\dot{V}$ [m^3/s], ρ [$kg/m3$], T [°C], x [kg/kg], $\dot{Q}$ [W])

Fan pressure rise:

$$dp = dp_{max} \cdot ctrl^2$$

Volume flow:

$$\dot{V} = \frac{\dot{m}_a}{\rho(T_{in}, x_{in})}$$

Fan power:

$$\dot{Q}_{fan} = \frac{\dot{V}_{rated}}{1000} \cdot dp_{max} \cdot \frac{\left(0.147 + \left(0.9506 - 0.0998 \cdot \frac{\dot{V}}{\dot{V}_{rated}}\right)\left(\frac{\dot{V}}{\dot{V}_{rated}}\right)\right)\left(\frac{\dot{V}}{\dot{V}_{rated}}\right)}{\eta_{tot}}$$

Outlet temperature:

$$T_{out} = T_{in} + \frac{\dot{Q}_{fan} \cdot \eta_{motor}}{c_{p,air}\dot{m}_a}$$

Appendix F – IDA ICE heating coil

Model equations:

($\dot{m}$ [kg/s], T [°C], x [kg/kg], $\dot{Q}$ [W])

Capacity rate of air:

$$C_{air} = \dot{m}_a\left(c_{p,air} + x \cdot c_{p,vapor}\right)$$

Capacity rate of water:

$$C_{water} = \dot{m}_{water} c_{p,water}$$

Minimum capacity rate:

$$C_{min} = \min\left(C_{air}, C_{water}\right)$$

Maximum capacity rate:

$$C_{max} = \max\left(C_{air}, C_{water}\right)$$

Capacity ratio:

$$C_{ratio} = \frac{\mathrm{C_{min}}}{\mathrm{C_{max}}}$$

Number of transfer units:

$$NTU = \frac{UA}{C_{min}} \ (UA\ calculated\ from\ the\ rated\ input\ parameters)$$

Based on the heat exchanger configuration, the heat transfer effectiveness is calculated as a function of NTU and C_{ratio}:

$$\eta = f(NTU, C_{ratio})$$

Maximum possible heat transfer:

$$\dot{Q}_{max} = C_{min}(T_{water,in} - T_{air,in})$$

Heat transfer rate:

$$\dot{Q} = \eta \cdot \dot{Q}_{max}$$

Outlet temperatures:

$$T_{air,out} = T_{air,in} + \frac{\dot{Q}}{C_{air}},\ T_{water,out} = T_{water,in} + \frac{\dot{Q}}{C_{water}}$$

Appendix G – IDA ICE boiler

Model equations:

($\dot{m}$ [kg/s], T [°C], p [Pa], $\dot{Q}$ [W])

Required useful power to satisfy outlet temperature setpoint:

$$\dot{Q}_{req} = \max\left(0, \dot{m}_{in} c_{p,water}\left(T_{out,set} - T_{in}\right)\right.$$

Delivered heating power:

$$\dot{Q}_{heating} = \min\left(\dot{Q}_{req}, \dot{Q}_{max}\right)$$

Pump power:

$$\dot{Q}_{pump} = \frac{P_{set,max} \cdot \dot{m}}{\rho_{water} \eta_{pump}}$$

Used heating power:

$$\dot{Q}_{used} = \frac{\dot{Q}_{heating}}{\eta_{boiler}}$$

Appendix H – IDA ICE liquid temperature controller (PMTMultiT)

Model equations:

($\dot{m}$ [kg/s], T [°C])

Mass flow rate from boiler:

$$\dot{m}_{heat} = \dot{m}_{heat,max} \cdot ctrl$$

Returned pool water (not heated):

$$\dot{m}_{return} = \dot{m}_{circ} - \dot{m}_{heat}$$

Temperature of water sent to pool ($T_{heat} = boiler\ setpoint\ temperature$) :

$$T_{out} = \frac{\dot{m}_{heat} T_{heat} + \dot{m}_{return} T_{in}}{\dot{m}_{circ}}$$

Appendix I – IDA ICE tank model

Model equations:

($\dot{m}$ [kg/s], $\dot{Q}$ [W], T [°C], V [m³], ρ [kg/m³], $n = \#\ inlet\ streams = \#\ outlet\ streams$)

Mass balance:

$$\sum_{i=1}^{n} \dot{m}_{in}[i] = \sum_{i=1}^{n} \dot{m}_{out}[i]$$

Energy balance:

$$\sum_{i=1}^{n} \dot{Q}_{in}[i] = \sum_{i=1}^{n} \left(\dot{m} c_p T\right)_{in}[i]$$

$$\sum_{i=1}^{n} \dot{Q}_{out}[i] = \sum_{i=1}^{n} \dot{m}_{out}[i] \cdot c_{p,tank} T_{tank}$$

$$\frac{dQ_{tank}}{dt} = \frac{\left(\rho V c_p\right)_{tank} dT_{tank}}{dt}$$

$$\frac{dQ_{tank}}{dt} = \sum_{i=1}^{n} \dot{Q}_{out}[i] - \sum_{i=1}^{n} \dot{Q}_{in}[i]$$

Appendix J – IDA ICE pool model

Model equations:

($\dot{m}$ [kg/s], $\dot{Q}$ [W], T [°C], p [Pa], A [m²])

Heat transfer through basin (positive direction is into the pool in IDA ICE):

$$\dot{Q}_{bottom} = h_c A_{bottom}(T_{bottom} - T_{pool})$$

$$\dot{Q}_{walls} = h_c A_{walls}(T_{walls} - T_{pool})$$

Heat balance:

$$\rho V c_{p,water} \frac{dT_{pool}}{dt} = \dot{Q}_{bottom} + \dot{Q}_{walls} + \dot{Q}_{zone} + \dot{m}_{circ} c_{p,water}(T_{in} - T_{pool})$$

where $\dot{Q}_{zone}$ is the heat transfer from the zone (positive direction towards the pool in IDA ICE).

Evaporation rate

$$\dot{m}_{evap} = 4 \cdot 10^{-5} A_{pool}(p_w - p_a) F_a \ (ASHRAE\ equation)$$

Appendix K – Activity log

All the activity that is either observed or logged by the users are given here. For the periods where the activity is not registered, the activity is estimated in accordance with the corresponding activity in the previous or following week. Both the registered and estimated activity is compared with the water level in the balance tank, to obtain the exact time periods of occupied pool. These periods differ slightly from the logged data beneath (minutes). An activity level of 1, 2 or 3 refers to a low, medium, or high activity level, respectively.

February 26, 2020

Time period	Number of people in the pool	Activity level
08:30 – 09:30	7	2
09:40 – 10:30	17	3
10:30 – 11:30	8	1
12:00 – 12:45	17	2-3
12:50 – 13:40	8	1
14:00 – 14:50	8	2

February 27, 2020

Time period	Number of people in the pool	Activity level
08:30 – 09:25	11	3
10:45 – 11:30	10	2
13:00 – 13:45	10	2
14:20 – 14:50	15	3

February 28, 2020

Time period	Number of people in the pool	Activity level
08:30 – 09:30	9	2
10:40 – 11:05	16	2-3
11:29 – 11:45	21	1
11:45 – 12:00	21	3
12:05 – 12:15	21	1
12:15 – 12:45	21	2
13:00 – 13:45	8	1-2

March 2, 2020

Time period	Number of people in the pool	Activity level
08:30 – 09:45	9	2
10:00 – 10:45	21	2-3
11:10 – 12:00	8	2

12:40 – 13:15	11	1
14:15 – 14:45	11	1-2
19:30 – 20:30	7	1-2
21:00 – 22:00	3	1-2

March 3, 2020

Time period	Number of people in the pool	Activity level
08:30 – 09:30	8	1
09:40 – 10:29	17	3
10:38 – 10:45	4	1
10:45 – 11:15	8	1
11:15 – 11:30	8	2
12:00 – 13:00	16	2
14:00 – 14:45	12-13	3
17:00 – 18:20	4	2-3
19:25 – 20:30	11	2

March 4, 2020

Time period	Number of people in the pool	Activity level
08:32 – 09:30	9	2-3
09:45 – 10:30	18	2-3
10:35 – 11:40	12	1
12:10 – 12:50	16	2
12:55 – 13:45	11	2

March 5, 2020

Time period	Number of people in the pool	Activity level
08:33 – 09:35	11	1
09:50 – 10:30	21	2-3
10:35 – 11:25	10	2
12:00 – 12:40	17	1
12:57 – 13:50	6	1
17:10 – 18:30	7	2-3

March 6, 2020

Time period	Number of people in the pool	Activity level
08:30 – 09:30	9	1
10:30 – 11:05	18-23	3
13:00 – 13:46	4	1-2-3
16:30 – 17:05	6	3
17:05 – 17:40	1	1
17:50 – 18:25	4	2
18:25 – 19:00	6	3

March 10, 2020

Time period	Number of people in the pool	Activity level
09:30 – 10:30	23	3
12:00 – 13:00	22	3
17:00 – 18:30	5	3

March 11, 2020

Time period	Number of people in the pool	Activity level
10:30 – 11:40	10	2
12.50 – 13:50	8	2

Appendix L – Thermography

Transition between external walls and ceiling (for a dark purple color the surface temperature is 15.6°C. Photo: Ole Smedegård):

External wall showing thermal bridges at the studs (for a dark purple color the surface temperature is 16.8°C. Photo: Ole Smedegård)

Vegard Skinnes

Validation of dynamic models of the thermal systems of swimming pools

NTNU
Norwegian University of
Science and Technology